Modeling population dynamics and species interactions in a changing climate

Darwin Scott Rinnan

A dissertation
submitted in partial fulfillment of the
requirements for the degree of

Doctor of Philosophy

University of Washington

2018

Reading Committee:

Joshua Lawler, Chair

Mark Kot

Trevor Branch

Program Authorized to Offer Degree:
Quantitative Ecology and Resource Management

University of Washington

Abstract

Modeling population dynamics
and species interactions
in a changing climate

Darwin Scott Rinnan

Chair of the Supervisory Committee:
Associate Professor Joshua Lawler
School of Environmental and Forest Sciences

Many species are expected to undergo significant distributional shifts in response to changes in climate. This adaptive response can impact population dynamics in many ways, including decreasing reproductive fitness, limiting dispersal, shrinking habitat, and exposing organisms to new competition from invasive species. What determines the successful persistence of a population exposed to climate change? In this dissertation I address different aspects of this fundamental question in three chapters.

In the first chapter, I focus on the challenges of modeling asymmetric dispersal. I use a spatially explicit integro-difference equation (IDE) to model a population whose habitat is shifting due to climate change, and demonstrate its equivalence to a stationary IDE model with asymmetric dispersal behavior. The cumulative effects of population dispersal in space and time have been described with some success by Van Kirk and Lewis's average dispersal success approximation (Van Kirk and Lewis, 1997), but this approximation has been demonstrated to perform poorly when applied to asymmetric dispersal. I provide a comparison of different characterizations of dispersal success and demonstrate how to accurately approximate the effects of asymmetric dispersal with a method known as geometric symmetrization. I apply these

different methods to a variety of IDE population models with asymmetric dispersal, and I examine the methods' effectiveness in approximating key ecological traits of the models, such as the critical patch size and the critical speed of climate change for population persistence. I show that the method using geometric symmetrization performs considerably better than other approximations for a variety of models and across a wide range of parameter values.

In the second chapter, I examine a coupled system of IDEs that models two species competing for the same resources in a shifting habitat. I determine under what conditions the two populations can coexist and the criteria for persistence in a changing climate. I demonstrate how the speed of climate change can shift the stable-state solution of the population model from mutual coexistence to a single species outcompeting the other and how these effects can be mitigated by niche differentiation, with the potential for habitat considered inhospitable to one species to provide refuge for the other. I illustrate this model with a simulated population of native bull trout (*Salvelinus confluentus*) experiencing competition from invasive brook trout (*S. fontinalis*) as their river habitat warms due to climate change. Based on current climate projections, this simulation suggests that bull trout are likely to disappear from the study area by 2080, with brook trout expanding their range in the absence of competition.

In the third chapter, I describe a new type of model that combines climate-envelope modeling with IDEs to utilize the strengths of both correlative and process-based modeling. I apply this framework to a case study of the American pika (*Ochotona princeps*), a small montane mammal that is widely recognized as threatened by climate change, and compare this with both a traditional climate-envelope model and an IDE. The results suggest that climate-envelope models alone can substantially underestimate the impacts of climate change, but the predictions of integro-difference models can be considerably improved by incorporating the modeled climate envelope.

TABLE OF CONTENTS

LIST OF FIGURES

LIST OF TABLES

ACKNOWLEDGMENTS

I have accrued an enormous debt of gratitude during my time in graduate school. Acknowledging the people who have helped me along the way scarcely even begins to pay back what I owe, but it's a start.

First and foremost, my advisors, Josh Lawler and Mark Kot, have provided me with a great deal of academic guidance, emotional and financial support, encouragement, and opportunity. They also granted a surprising amount of latitude for me to define my own research topics and goals, to which I am incredibly grateful. The rest of my committee, Trevor Branch, Janneke Hille Ris Lambers, and Laura Prugh, contributed a breadth of insight and perspective, and our discussions were extremely influential in determining the shape and scope of this dissertation.

My graduate program, QERM, has been nothing less than a second home and family to me. I am thankful for their faith in my potential, for their financial support, and for the opportunity to pursue my educational goals. Both the old and new program directors, Loveday Conquest and Tim Essington, and secretaries, Joanne Besch and Erica Owens, have done a fantastic job of demonstrating their commitment to the success and wellbeing of their students. I will wield my new soup spoon fondly.

A number of other departments and programs across campus have welcomed me as a part of their community as well, including the School of Environmental and Forest Sciences, the School of Aquatic and Fishery Sciencies, and the Program on Climate Change. These connections have helped me appreciate the interdisciplinary nature of my research and the broader academic context in which it fits. The Dead Elk Society, SAFS T.G.I.T., Burke trivia nights, and PCC's Friday Harbor retreats

have all brought much-needed levity to my graduate experience.

I am confident that I would not have been able to complete this work without a lively, colorful, caring, and all around wonderful social network to support me. I can't name everyone, but particular gratitude extends to my QERM cohort, Aneesh Hariharan, Melissa Muradian, Kiva Oken, Adam Pope, Christine Stawitz, and Kelsey Vitense: together we forged a bond in fire. Additional thanks go to fellow QERMies Cole Monnahan, Ian Fraser, Elliot Koontz, Lee Cronin-Fine, and Austin Phillips; fellow Lawler labmates Caitlin Littlefield, Ben Ditbrenner, and Rosemary Pazdral; SEFS students Deborah Nemens, Russell Kramer, and Laurel Peelle; SAFS students Bill Matsubu and Melanie Davis; Biology student Alexandra Hart; and Mechanical Engineering student Alex Soloway.

Finally, an endless amount of gratitude goes to my family, who has given me their unhesitating support in every step of the way: Mom and Dad, for shaping me into the person I am; my sisters, Alystra and Amy, for everything we've been through together; my beautiful child, Ezra, for all of the inspiration and motivation you have provided me to make the world you grow up in a better place; Grandma, for your unceasing kindness and faith in me; Grandpa, for teaching me how to be caring through action, not just words; my nephews, Jimmy, Eamon, and Alder, for all the awesome fun you are; and Jess and Jared for the understanding, patience, and all the indirect help you've provided that has made it possible for me to pursue my education.

Life takes teamwork. Thus far, I've had the extraordinarily good fortune to have the best community on my side that a person could ask for. To everyone who has helped me get to where I am today, I thank you. I look forward to returning the favor in any way I can, and paying it forward to others in kind.

DEDICATION

— to Grandpa —

I think you'd be proud.

INTRODUCTION

Climate change is a crisis of global scale that poses a significant threat to many species, populations, and ecosystems (Thomas et al., 2011; Field et al., 2014). At its worst, climate change will drive some species to extinction (Stanton et al., 2015); indeed, this appears to have already occurred for several species of amphibians (Pounds et al., 2006). Many different factors contribute to species vulnerability to climate change, including population size, reproduction rate, dispersal ability, and sensitivity to phenological changes, as well as extrinsic factors such as the potential for habitat loss, dependence on sympatric species, and climate-change driven shifts in community structure (Lawler et al., 2009; Traill et al., 2010; Pearson et al., 2014).

It has been demonstrated that species distributions at the continental scale are in part driven by climate processes (Pearson and Dawson, 2003). As their environment changes, species can respond quickly by dispersal, or through slower processes such as phenotypic plasticity or evolutionary changes. Poleward shifts have been observed in many species distributions in response to warming temperatures (Parmesan et al., 1999; Hickling et al., 2006; Sorte and Thompson, 2007); shifts in elevation have been observed in others (Wilson et al., 2005; Chen et al., 2011b).

Many different methods have been developed to model species responses to climate change: extinction risk due to climate change has been quantified using life history and spatial habitat characteristics (Pearson et al., 2014; Stanton et al., 2015); vulnerability assessments combine trait-based species data with future projections of climate (Thomas et al., 2011; Young et al., 2012; Foden et al., 2013a); species distribution models correlate environmental conditions with species presence to predict how distributions will change with the climate (Hall, 2000; Manel et al., 2001; Guisan

et al., 2002; Prasad et al., 2006; Cutler et al., 2007); deterministic models measure the ability to keep pace with climate change by modeling biological processes such as growth and dispersal (Carey, 1996; Brännström and Sumpter, 2005; Zhou and Kot, 2011). Deciding which model to employ in what circumstances can be a difficult task: each come with their own assumptions, advantages and disadvantages, and can often yield different results (Lawler et al., 2006; Pagel and Schurr, 2012). Many of these models are computationally expensive, require specialized knowledge of species traits, and can be difficult to employ efficiently across a large number of species.

Historically, methods for modeling populations and their responses to climate change have fallen into two different camps: correlative approaches and mechanistic approaches. With population modeling in a changing climate as the primary focus of this dissertation, I will now provide a brief survey of some of the more popular modeling methods.

0.1 Correlative models

The most common and popular method to modeling climate-related impacts on habitat is with correlative models that establish a statistical relationship between a species' presence and the environmental conditions in which it is found. By quantifying the environmental niche of a species, these models are able to describe potential future habitat using future projections of environmental conditions. These are known by several different names, including species distribution models, climate-envelope models, and environmental niche models, but all operate on the same basic principles. There are many approaches to climate-envelope modeling, which collectively span a spectrum of model complexity. Choosing the right approach is typically guided by the format and quality of the input data, as well as the goals of the modeler. Generalized linear models and generalized additive models provide an approach that is statistically straightforward and easy to understand (Guisan et al., 2002; Leathwick et al., 2006). If the modeler's goal is inference rather than prediction, ecological niche

factor analysis provides a straightforward characterization of how predictor variables influence habitat suitability (Hirzel et al., 2002; Basille et al., 2008). Several more sophisticated methods have more recently been developed, likely as a consequence of concurrent increases in computational power and advances in machine learning. Random forests, for example, are an excellent choice for binary classification of suitable/unsuitable habitat from presence/absence data (Cutler et al., 2007; Evans et al., 2011). Maximum entropy, by contrast, offers a more reliable approach for presence-only data and has a high degree of predictive accuracy (Phillips et al., 2004; Elith et al., 2011; Merow et al., 2013). Other choices include artificial neural networks (Lek and Guégan, 1999; Olden and Jackson, 2002) and boosted regression trees (Araújo and New, 2007; Elith et al., 2008).

Faced with this overwhelming diversity of modeling options, several authors have conducted meta-analyses that compare model performance and predictive power, with random forests and maximum entropy approaches generally demonstrating the most accuracy and reliability (Hijmans and Graham, 2006; Lawler et al., 2006; Zhang and Li, 2017).

0.2 Process-based models

Process-based models (also referred to as mechanistic models) offer a considerably different approach. These focus on explicitly modeling the ecological and biological processes that are believed to shape and determine population size. In this dissertation I am primarily concerned with spatially-explicit models, which are used to describe how ecological processes affect distribution and location over time. Reaction-diffusion models are frequently used to model growth and dispersal when time is modeled as a continuous variable (Pease et al., 1989; Berestycki et al., 2009), and integro-difference models when time is modeled discretely (Kot et al., 1996; Zhou and Kot, 2011; Harsch et al., 2014). Leroux et al. (2013) offer an excellent review of the different types of mechanistic approaches available to model spatial spread under climate change, and

Harsch et al. (2017) provides a more detailed review of the uses of integro-difference models in climate change ecology.

0.3 The murky area in between

One common criticism of SDMs is their lack of realism: describing the relationship between a species and its environment using only statistical correlations ignores all of the ecological and physiological processes that constrain the distributions of populations. The importance of ecological process has been well established (Araujo and Guisan, 2006; Buckley et al., 2010; Sinclair et al., 2010). By not accounting for dispersal ability, for example, SDMs fail to provide any insight into a species' ability to successfully colonize new areas. As such, SDMs can greatly underestimate species vulnerability to climate change.

An increasing amount of recent research has attempted to bridge the gap between correlative and process-based models. Because of the diversity of biological and ecological processes that can be modeled, however, there is no single best approach to accomplishing this goal. The choice of approach is generally guided by the nature of the data, the scale of the study, the complexity of the process, and the goals of the modeler. Carey (1996), for example, used a cellular automaton to model distributional changes due to dispersal in a changing habitat. Midgley et al. (2006) incorporated dispersal limitations into SDMs to model expected changes in biodiversity of flowering plants on the western coast of South Africa. Keith et al. (2008) introduced a model that combined SDMs with stochastic population dynamics and modeled the persistence of two different hypothetical varieties of shrubs. Rickebusch et al. (2008) accounted for the effects of changes in CO_2 concentration on transpiration and water availability in alpine tree species and examined the impact on future predictions of tree distributions. Kearney and Porter (2009) demonstrated how to use biophysical traits of species to determine its environmental niche, which then applied SDM methods to map and forecast habitat changes. Morin and Thuiller (2009) pro-

vided a direct comparison between future predictions of correlative and mechanistic population models for 15 species of North American trees. Pagel and Schurr (2012) used a Bayesian approach to integrate an SDM with spatial population dynamics.

0.4 Incorporating species interactions

Many studies have utilized species distribution models (SDMs) to predict changes in biodiversity by modeling ecological communities as a sum of their constituent parts, without accounting for the importance of community structure and relationships between species (Thomas et al., 2004; Araújo et al., 2006; Lawler et al., 2009). SDMs have also been criticized in their lack of ability to model relationships between species, however, and the importance of accounting for interspecific interactions has been well established (Araujo and Guisan, 2006; Araújo and Luoto, 2007; HilleRisLambers et al., 2013; Wisz et al., 2013). Interspecific competition, for example, can have significant effects on the success and spread of species (Connell, 1983; Dunson and Travis, 1991; Davis et al., 1998). Shifting into new habitat often involves competition with species that have already established themselves. Climate change is also predicted to increase the amount and intensity of biological invasions by invasive species (Thuiller et al., 2007; Vilà et al., 2007).

More recent advances in modeling approaches have focused on addressing this shortcoming, and a new field of joint species distribution modeling has emerged, with every bit as much variety in methodology (Gilman et al., 2010; Guisan and Rahbek, 2011; Clark et al., 2014; Pollock et al., 2014; Thorson et al., 2015). Additional progress has been made on modeling interactions from a mechanistic approach (Hosono, 1998; Potapov and Lewis, 2004; Adler et al., 2007).

0.5 Research goals

In this dissertation I address some of the challenges and deficiencies associated with correlative and mechanistic population modeling in a changing climate. The research

questions I attempt to answer may be succinctly stated as thus:

1. How does dispersal behavior affect population persistence in a changing climate?

2. How does interspecific competition affect persistence, and when is coexistence possible?

3. How can the mechanistic biological processes of population growth and dispersal be integrated with correlative species distribution modeling?

4. How do future predictions of persistence from an integrated correlative/process-based model compare with the predictions of models that are purely correlative or process-based?

In Chapter 1 I compare a variety of techniques for approximating the criteria for persistence of populations that are moving due to climate change, and I develop a useful metric for quantifying the effects of asymmetric dispersal. In Chapter 2 I use the techniques of Chapter 1 to explore a coupled system of integro-difference equations that model two species competing for the same resources under climate change, show how the effects of climate change can change the expected outcome of the competitive population dynamics, and establish persistence and coexistence criteria for each species. In Chapter 3 I demonstrate how to incorporate more biological and ecological realism into traditional species distribution modeling techniques by combining an integro-difference population model with a traditional SDM. I illustrate how, by explicitly accounting for species growth rate and dispersal ability, this approach can yield more geographically realistic predictions. I discuss several ways in which this model can be generalized, including using the competition model from Chapter 2 to create a hybrid correlative/mechanistic joint species distribution model.

For each chapter, I will provide a brief motivation, followed by a model formulation, a description of methods, a model illustration, an interpretation of results, and

a discussion. I have striven to establish some overarching themes to this dissertation. Each chapter is designed to build on the preceding chapter in a natural, intuitive, and straightforward fashion. Lastly, I provide a conclusion that reexamines the results in the broader context of this dissertation and its research goals.

One brief editorial note: this dissertation makes use of both a singular and a plural first-person voice, and this is quite intentional. Where I use the singular voice I describe concrete actions that I did for the sake of my research and this dissertation. The plural voice refers to both you, the reader, and myself, and is used in places where I develop theory and explore mathematical arguments. In this context, please feel free to imagine me as your tour guide leading you through my work. Math is always more enjoyable with good company.

I invite you now to dive into my work with the same enthusiasm with which it was approached. And to be clear, my enthusiasm was considerable.

Chapter 1

THE DISPERSAL SUCCESS AND PERSISTENCE OF SPECIES WITH ASYMMETRIC DISPERSAL

1.1 Introduction

Dispersal — defined by Trakhtenbrot et al. (2005) as the movement of organisms, their propagules, or their genes away from the source population — can have a profound effect on the persistence and spread of populations through space and time. Spatial population models commonly describe the dispersal by means of a dispersal kernel $k(x, y)$, a probability density function that reflects the likelihood of moving from the location y to the point x in a single time step. Dispersal kernels have been derived from observations of dispersal events for a variety of populations and species, including trees (Clark et al., 1999; Nathan and Muller-Landau, 2000), plants (Willson, 1993), birds (Veit and Lewis, 1996), and fish (Rodríguez, 2010). Dispersal is often represented as a symmetric process, under the assumption that dispersal in any direction is equally likely (Vuilleumier and Possingham, 2006).

A clear and consistent pattern throughout the literature, however, suggests that biological dispersal is a fundamentally *asymmetric* spatial process: asymmetric dispersal due to wind patterns have been observed in fungal pathogens (Rieux et al., 2014), lichen spores (Werth et al., 2006), and tree pollen (Austerlitz et al., 2007); ocean currents play a similar role in affecting the dispersal of marine organisms (Byers and Pringle, 2006), and stream currents for aquatic insects (Lutscher et al., 2010); population persistence in a habitat shifting due to climate change can be characterized by asymmetric dispersal (Zhou and Kot, 2011; Bouhours and Lewis, 2016); elevational asymmetries in dispersal have been observed in a variety of montane habitats (Will-

son and Traveset, 2000). Indeed, asymmetric dispersal seems to be the rule rather than the exception. Although many researchers readily acknowledge the significance of the possible effects of asymmetric dispersal, it appears uncommon for asymmetric dispersal to be explicitly incorporated into spatial population models, likely due to the mathematical complexity involved, or a simple lack of data.

The concept of *average dispersal success* (ADS) has proven to be a useful tool for addressing many of the issues that arise from a scarcity of dispersal data and model complexity. Van Kirk and Lewis (1997) defined a population's average dispersal success S across a patch of habitat Ω as

$$S = \frac{1}{\Omega} \int_{\Omega} \int_{\Omega} k(x, y)\, dx\, dy, \tag{1.1}$$

the spatially-averaged probability of remaining in Ω after dispersal, assuming that the individual begins in Ω. Alternatively, this can be interpreted as the proportion of individuals beginning in Ω that remain in Ω after dispersing. ADS distinguishes individuals that disperse "locally" (i.e., within the habitat patch) from those that disperse "farther away" (i.e., outside the habitat patch), and in doing so, provides a tool for relating field data collected at a regional scale to population dynamics at a larger scale (Fagan and Lutscher, 2006). Dispersal success has been used to address a variety of questions in conservation ecology such as reserve network design in marine systems (Baskett et al., 2007), metapopulation dynamics (Fagan and Lutscher, 2006), and population dynamics of caterpillars (Hughes et al., 2015) and stream insects (Vasilyeva et al., 2016).

As defined in (1.1), however, ADS has its limitations. In particular, Van Kirk and Lewis (1997) explored S only in the context of symmetric dispersal. Although they suggested a method for generalizing S to asymmetric kernels, this method has nonetheless been shown to provide an increasingly poor approximation of the effects of dispersal for increasingly asymmetric kernels (Reimer et al., 2015). This limitation

is unfortunate, because a great deal of insight might be gleaned from studying the consequences of asymmetric dispersal, and, given the ubiquity of the phenomenon, an accurate, generalizable method that quantifies asymmetric dispersal success would apply to a much a wider variety of ecological processes and issues of considerable current interest.

One such issue is the effect of climate change on population persistence. A large number of species are expected to be unable to keep pace with the speed at which their suitable habitat is shifting due to the effects of climate change (Chen et al., 2011b; Schloss et al., 2012). Fewer individuals are able to successfully disperse at higher climate velocities, which leads to fewer individuals that are able to successfully reproduce. In theory, beyond a certain critical speed, the population cannot persist. Zhou and Kot (2011) demonstrated how an asymmetric shifted dispersal kernel can represent the effects of a habitat shifting due to climate change. Another related concept is the threshold of habitat size necessary for persistence. If a population's habitat is too small, individuals cannot reproduce rapidly enough to offset the loss of individuals through dispersal, and the population will eventually die out. Ensuring that the amount of available habitat is sufficient to sustain a population through time is essential for successful reserve design. ADS is ill-suited to address the question of critical climate speed, and can only address critical habitat size if dispersal is assumed to be symmetric.

In this chapter I demonstrate how to adapt ADS to more accurately reflect the consequences of asymmetric dispersal in an integro-difference population model. In Section 1.2 I introduce integro-difference equations (IDEs) and discuss their criteria for population persistence. In Section 1.3 I motivate dispersal success in both a mathematical and biological context, and explore Van Kirk and Lewis (1997)'s original definition S in (1.1), and a modification $\widehat{S}$ proposed by Reimer et al. (2015) that weights the integrand of S by population density. In Section 1.4 I introduce and formalize the method of geometric symmetrization, a technique that uses a result

of linear algebra to address the issue of asymmetric kernels (Kot and Phillips, 2015). Finally, in Section 1.5 I apply these three approaches to IDEs with asymmetric dispersal, and explore how each method can be used to estimate the model's critical patch size, critical shift speed, and average population density at equilibrium, and how these estimates compare with one another. The majority of this paper uses shifted kernels to illustrate asymmetric dispersal, but the theory I develop extends to other types of asymmetric kernels as well, which I explicitly show in subsection 1.5.4.

1.2 Persistence criteria and integro-difference equations

The persistence of populations can often be characterized as an eigenvalue problem (Leslie, 1945; Caswell, 2001). A simple matrix population model, for example, is written as

$$\mathbf{n}_{t+1} = \mathbf{M}\mathbf{n}_t, \tag{1.2}$$

where $\mathbf{n}_t$ is a vector of population densities of different life stages, and $\mathbf{M}$ is a matrix that describes the rates of transition from one life stage to another. The associated eigenvalue equation of (1.2) is

$$\lambda\mathbf{u} = \mathbf{M}\mathbf{u}. \tag{1.3}$$

Persistence (and growth) of the population will occur when the dominant eigenvalue $\lambda_{\max}$ of $\mathbf{M}$ is greater than 1, and the population will collapse when $\lambda_{\max}$ is less than 1.

Integro-difference equations (IDEs), by comparison, use a spatially-explicit approach to model a population as

$$N_{t+1}(x) = \int_0^L k(x,y) f[N_t(y)]\, dy, \tag{1.4}$$

with population $N_t(x)$ at location x and time t, growth function $f[N_t(y)]$, and dispersal kernel $k(x,y)$. Since most choices of dispersal and growth functions make

IDEs analytically intractable, it is not usually possible to obtain an analytic steady-state solution, and we are unaware of any such examples in the literature (although Zhou and Kot (2011) outline a scheme for approximating one example of an IDE with a separable kernel). Instead, various approximation methods are commonly employed. Assuming no Allee effects, and homogeneous and symmetric dispersal such that $k(x, y) = k(|x - y|)$, the corresponding eigenvalue equation of (1.4) can be approximated by

$$\lambda u(x) = R_0 \int_0^L k(x - y)u(y)\, dy, \tag{1.5}$$

with R_0 the net reproductive rate given by $R_0 = f'(0)$, eigenvalue λ and corresponding eigenfunction $u(\bar{x})$ (Kot and Schaffer, 1986). Again, the dominant eigenvalue $\lambda_{\max}$ of the integral operator of (1.5) determines persistence: for $\lambda_{\max} > 1$, the population will persist, and for $\lambda_{\max} < 1$ the population will die out.

Zhou and Kot (2011) studied the persistence of a population in a habitat shifting in space due to climate change, described by the IDE

$$N_{t+1}(x) = \int_{ct}^{L+ct} k(x, y) f[N_t(y)]\, dy, \tag{1.6}$$

with associated eigenvalue problem

$$\lambda u(\bar{x}) = R_0 \int_0^L k(\bar{x} + c - \bar{y})u(\bar{y})\, d\bar{y}, \tag{1.7}$$

where c is the speed of climate change, and $\bar{x} = x - ct$ and $\bar{y} = y - ct$. This equation is an example of the type of eigenvalue problem of primary concern in this paper. An equivalent formulation can be derived from the stationary IDE in (1.4) assuming a shifted kernel $k(x + c - y)$, and for other types of asymmetric kernels as we will later see. For the remainder of this paper I will drop the bars on $\bar{x}$ and $\bar{y}$ for notational convenience when referencing (1.7).

More recently, Kot and Phillips (2015) explored methods for approximating $\lambda_{\max}$

of (1.7), and found that in certain cases,

$$\lambda_{\max} \approx \lambda_S \equiv \frac{R_0}{L} \int_0^L \int_0^L k(x + c - y)\, dx\, dy \tag{1.8}$$

$$= R_0 S, \tag{1.9}$$

where S is the average dispersal success in (1.1). This reflects a similar approximation Lutscher and Lewis (2004) derived for stage-structured populations.

To a first-order approximation, (1.9) demonstrates how ADS succinctly relates to population persistence: the net reproductive rate must be greater than $1/S$ for the population to persist. I note, however, that our kernel has become asymmetric due to the spatial shift by c. Since I have asserted that S provides a poor approximation in the case of asymmetric dispersal, we might expect λ_S to diverge from the true value of $\lambda_{\max}$ for increasing c, and Kot and Phillips (2015) indeed provide examples in support of our expectations.

I will now provide a brief discussion of ADS, before demonstrating how it can be modified to better capture the effects of asymmetric dispersal.

1.3 Average dispersal success

I begin by establishing some basic terminology, following the notational conventions of Van Kirk and Lewis (1997) and Lutscher and Lewis (2004). The *dispersal kernel* $k(x, y)$ is a probability density function that describes the likelihood of an individual dispersing from the location y to the location x by the next time step.

The *dispersal success function* $s(y)$ describes the probability that an individual starting at location y will settle within the domain Ω by the next time step, given by

$$s(y) \equiv \int_\Omega k(x, y)\, dx. \tag{1.10}$$

Conversely, the *redistribution function* $r(y)$ reflects the probability that an individual

Table 1.1: Discrete-time growth functions and dispersal kernels considered in this paper. (Adapted from Reimer et al. (2015).)

Growth functions		
Beverton-Holt	$N_{t+1} = \frac{R_0 N_t}{1+\frac{R_0-1}{K}N_t}$	Compensatory (Beverton and Holt, 1957)
Logistic	$N_{t+1} = N_t + rN_t\left(1-\frac{N_t}{K}\right)$	Overcompensatory (May and Oster, 1976)
Ricker	$N_{t+1} = N_t \exp\left[r\left(1-\frac{N_t}{K}\right)\right]$	Overcompensatory (Ricker, 1954)
Dispersal kernels		
Shifted Gaussian	$k(x,y) = \frac{1}{\sqrt{2\pi\sigma^2}}\exp\left(-\frac{(x+c-y)^2}{2\sigma^2}\right)$	(Lutscher et al., 2005; Kot and Phillips, 2015)
Shifted Laplace	$k(x,y) = \frac{1}{2b}\exp\left(-\frac{\lvert x+c-y\rvert}{b}\right)$	(Lutscher et al., 2005; Kot and Phillips, 2015)
Shifted Cauchy	$k(x,y) = \left[\pi\gamma\left(1+\left(\frac{x+c-y}{\gamma}\right)^2\right)\right]^{-1}$	(Lutscher et al., 2005)
Asymmetric Laplace	$k(x,y) = \begin{cases} A\exp(a_1(x-y)), & x \le y \\ A\exp(a_2(x-y)), & x > y \end{cases}$	(Lutscher et al., 2005)

starting within the domain Ω will successfully disperse to location y by the next time step, given by

$$r(y) \equiv \int_\Omega k(y,x)\,dx. \tag{1.11}$$

When the kernel is symmetric we have $k(x,y) = k(y,x)$, and so $r(y) = s(y)$.

Finally, the *average dispersal success* is the spatial average of the dispersal success function, defined by

$$S \equiv \frac{1}{|\Omega|}\int_\Omega s(y)\,dy = \frac{1}{|\Omega|}\int_\Omega\int_\Omega k(x,y)\,dx\,dy, \tag{1.12}$$

where $|\Omega|$ represents the size of the domain.

The value of S reflects the proportion of a population in Ω that will remain in Ω after a single dispersal event, assuming that the population was initially distributed uniformly throughout Ω. This uniformity is implicit in the fact that all locations in Ω are weighted equally in the spatial average of the dispersal success function $s(y)$ or redistribution function $r(y)$. This naturally invites the question of how to quantify

the average dispersal success of a population that is heterogeneously distributed in Ω. Reimer et al. (2015) defined the *modified average dispersal success* $\widehat{S}$, which weighs the dispersal success function by the distribution of individuals in Ω as predicted by $r(y)$, given by

$$\widehat{S} \equiv \frac{1}{|\Omega|} \int_{\Omega} \frac{r(y)}{S} s(y)\, dy. \tag{1.13}$$

The value of $\widehat{S}$ reflects the proportion of individuals that will remain in Ω after a single dispersal event, assuming an initial distribution in Ω of $r(y)$.

Under the right conditions, the solution of a population model will converge to an equilibrium. In a spatial population model with symmetric dispersal, this equilibrium often closely resembles $s(y)$ (Van Kirk and Lewis, 1997); dispersal success is greatest at the center of Ω and lowest at its edges, and individuals will end up distributed in Ω accordingly. Provided a sufficient growth rate to replenish the proportion of the population that is lost due to dispersal outside Ω, the population will stay at this equilibrium indefinitely. As such, when the kernel $k(x, y)$ is symmetric, we may reasonably use S and $\widehat{S}$ to approximate the persistence of a population over time. When $k(x, y)$ is asymmetric, however, individuals disperse with a directional bias, and (by assumption) this bias is persistent through time, affecting each generation equally, and propagating with each successive dispersal event. In this scenario, we might expect that S and $\widehat{S}$ fail to reflect population persistence, since the long-term population equilibrium might be quite different than the population after the first or second dispersal events (Reimer et al., 2015).

Kot and Phillips (2015) described a method for approximating the effects of one such class of asymmetric dispersal kernels, the shifted kernel $k(x, y) = k(x + c - y)$, using geometric symmetrization to construct a symmetric kernel with the same qualitative properties as $k(x, y)$. As we will see, this method can be used to provide a lower bound on the proportion of individuals remaining in Ω at population equilibrium. In the following section I outline the method, beginning with some relevant results from

linear algebra.

1.4 Geometric symmetrization

Schwenk (1986) identified a nonnegative, symmetric $m \times m$ matrix $\mathbf{G}$ with dominant eigenvalue $\rho(\mathbf{G})$ that provides a lower bound for the dominant eigenvalue of a nonnegative, asymmetric matrix $\mathbf{A}$. The *geometric symmetrization* $\mathbf{G}$ of $\mathbf{A}$ is defined by the property

$$\mathbf{G} \circ \mathbf{G} = \mathbf{A} \circ \mathbf{A}^T, \tag{1.14}$$

where $\circ$ is the Hadamard product symbolizing element-wise multiplication, so that element $g_{ij} = g_{ji} = \sqrt{a_{ij}a_{ji}}$ is the geometric mean of a_{ij} and a_{ji}. In particular, Schwenk found that

$$\rho(\mathbf{G}) \leq \rho(\mathbf{A}). \tag{1.15}$$

A simple proof of this inequality can be found in Alpin and Merikoski (2010).

For a symmetric matrix $\mathbf{G}$, the Rayleigh quotient

$$R(\mathbf{G}, \mathbf{u}) \equiv \frac{\mathbf{u}^T\mathbf{G}\mathbf{u}}{\mathbf{u}^T\mathbf{u}} \tag{1.16}$$

is equal to $\rho(\mathbf{G})$ when $\mathbf{u}$ is the eigenvector associated with the dominant eigenvalue of $\mathbf{G}$; for all other $\mathbf{u}$, the Rayleigh quotient will be less than $\rho(\mathbf{G})$. Kolotilina (1993) used this property to propose a simple, easily calculable lower bound for $\rho(\mathbf{G})$, given by

$$\frac{\mathbf{e}^T\mathbf{G}\mathbf{e}}{m} \leq \rho(\mathbf{G}) \leq \rho(\mathbf{A}), \tag{1.17}$$

where $\mathbf{e} = (1, \ldots, 1)^T$, a vector of ones with length m.

Schwenk's and Kolotilina's results are relevant to us for two reasons. First, we can approximate an asymmetric dispersal kernel with a nonnegative, asymmetric matrix, a common approach for numerical analysis. Kot and Phillips (2015) detail one such method for discretizing $k(x, y)$ into an $m \times m$ matrix $\mathbf{K}$. Applying this discretization

to (1.7) yields the eigenvalue problem

$$\lambda \mathbf{u} = R_0 \mathbf{K} \mathbf{u}. \tag{1.18}$$

Second, the Rayleigh quotient approximation of $\rho(\mathbf{A})$ can likewise be used to approximate $\rho(R_0\mathbf{K})$, which is precisely the dominant eigenvalue we desire to describe persistence. Hence, these results provide us with a simple method for estimating the eigenvalue that determines persistence in a population with asymmetric dispersal.

I will now formalize the notion of geometric symmetrization for a continuous kernel $k(x, y)$, beginning by defining the *geometric success function* $G(y)$ as

$$G(y) \equiv \int_\Omega \sqrt{k(x, y)k(y, x)}\, dx. \tag{1.19}$$

When $k(x, y)$ is symmetric, $G(y) = s(y) = r(y)$, since $k(x, y) = k(y, x)$ implies that $\sqrt{k(x, y)k(y, x)} = k(x, y)$. As $k(x, y)$ becomes increasingly asymmetric, $s(y)$ and $r(y)$ diverge from one another, and $G(y)$ diverges from both (Figure 1.1). Averaging $G(y)$ over Ω gives us the geometric symmetrization of the average dispersal success S, defined as

$$GS \equiv \frac{1}{|\Omega|} \int_\Omega G(y)\, dy = \frac{1}{|\Omega|} \int_\Omega \int_\Omega \sqrt{k(x, y)k(y, x)}\, dx\, dy. \tag{1.20}$$

Kot and Phillips (2015) observed that GS is the continuous form of the Rayleigh quotient in (1.17), i.e.,

$$GS = \lim_{m\to\infty} \frac{\mathbf{e}^T \mathbf{G} \mathbf{e}}{m} = \frac{\int_\Omega \int_\Omega \sqrt{k(x, y)k(y, x)}\, dx\, dy}{\int_\Omega 1\, dy} \tag{1.21}$$

$$= \frac{1}{|\Omega|} \int_\Omega \int_\Omega \sqrt{k(x, y)k(y, x)}\, dx\, dy, \tag{1.22}$$

where m is again the number of discrete points in Ω and with the elements of $\mathbf{G}$ given

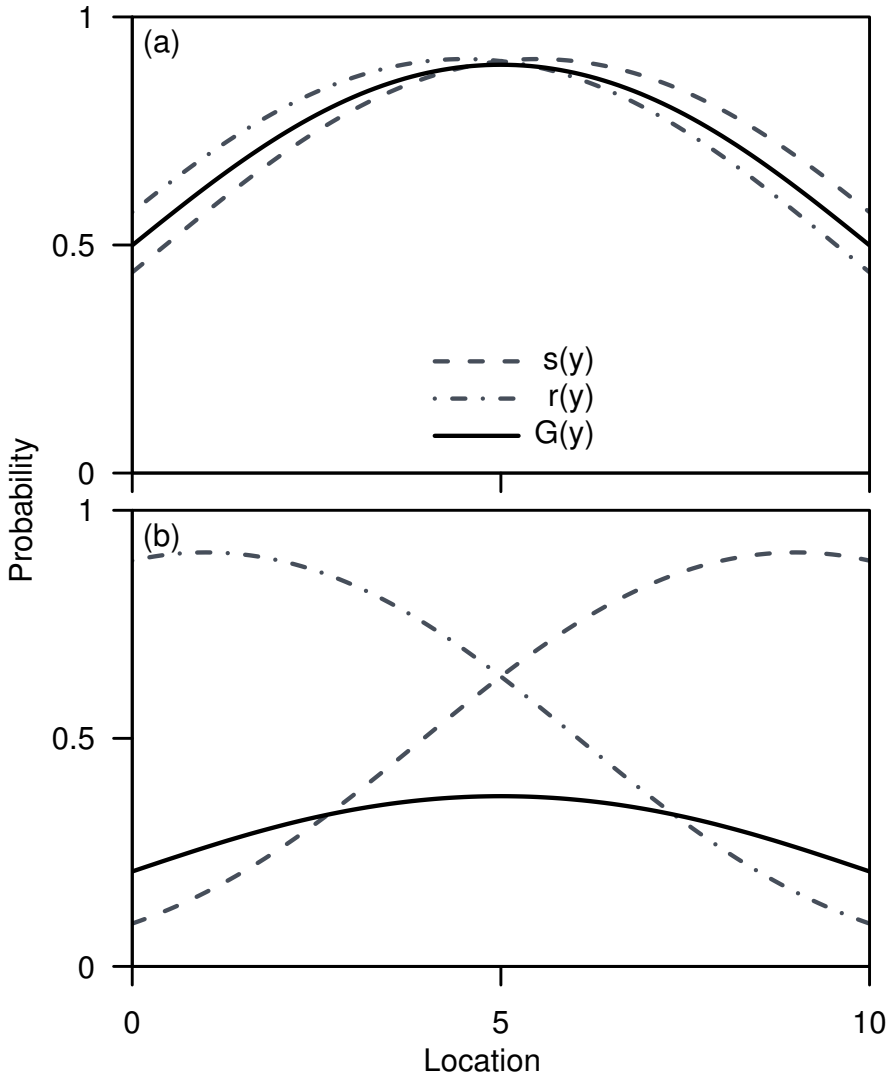

Figure 1.1: Dispersal success function $s(y)$, redistribution function $r(y)$, and geometric success function $G(y)$ of a shifted Gaussian kernel with $\sigma = 3$ on the domain $\Omega = [0, 10]$ for varying c. In (a), $c = 0.5$, and $s(y)$ and $r(y)$ are relatively close in value in Ω. In (b), $c = 4$, and $s(y)$ and $r(y)$ diverge from one another. S is the spatial average of $s(y)$ (equivalently, $r(y)$) across Ω, whereas GS is the spatial average of $G(y)$.

Table 1.2: Dispersal success approximations considered in this paper.

Average dispersal success	S	(2.17)	Proportion of individuals staying in patch after single dispersal event (Van Kirk and Lewis, 1997)
Modified S	$\widehat{S}$	(1.13)	Weights S by population density (Reimer et al., 2015)
Geometric symmetrization of S	G_nS	(1.30)	Proportion of individuals staying in patch after dispersal event at equilibrium (Kot and Phillips, 2015)

by $g_{ij} = \sqrt{k_{ij}k_{ji}}$. This observation, along with Kolotilina's result in (1.17), guarantees that GS provides a lower-bound approximation of the dominant eigenvalue of (1.6).

How might we interpret the value of GS biologically? If we begin with an initial population N_0 uniformly distributed across Ω, then the spatial distribution of individuals after one time step is described by $r(y)$, and the average dispersal success S reflects the proportion $P_1 = N_1/N_0$ of population left in Ω after one time step. Similarly, the modified average dispersal success $\widehat{S}$ reflects the proportion of population left in Ω after one time step assuming an initial distribution of $r(y)$, or, equivalently, the ratio $P_2 = N_2/N_1$ of populations between the first and second time steps. Repeating the dispersal process over multiple time steps yields the sequence $P_3, P_4, P_5, ...$ As $t \to \infty$, eventual extirpation occurs if $P_t \to 0$. If the population converges to an equilibrium, then the sequence is bounded below by GS. Thus, we can interpret GS as an estimate of the proportion of individuals that remain in Ω after dispersal when the population has reached equilibrium. If the population dies out, then $GS = 0$; if $GS > 0$, then the population is able to persist.

To illustrate this, I simulated the process of repeated dispersal on a patch of length $L = 10$. I began with a population $N_0(x)$ of $N_0 = 1\,000\,000$ individuals distributed uniformly across $\Omega = [0, 10]$. Dispersal distances were randomly drawn from a shifted Gaussian kernel (see Table 1.1) with $\sigma = 2$, and added to $N_0(x)$ to simulate dispersal. P_1 was then calculated as the proportion of individuals left inside of Ω after the dispersal event. The locations of the individuals that dispersed successfully (i.e., stayed inside the patch) were then randomly resampled to replace

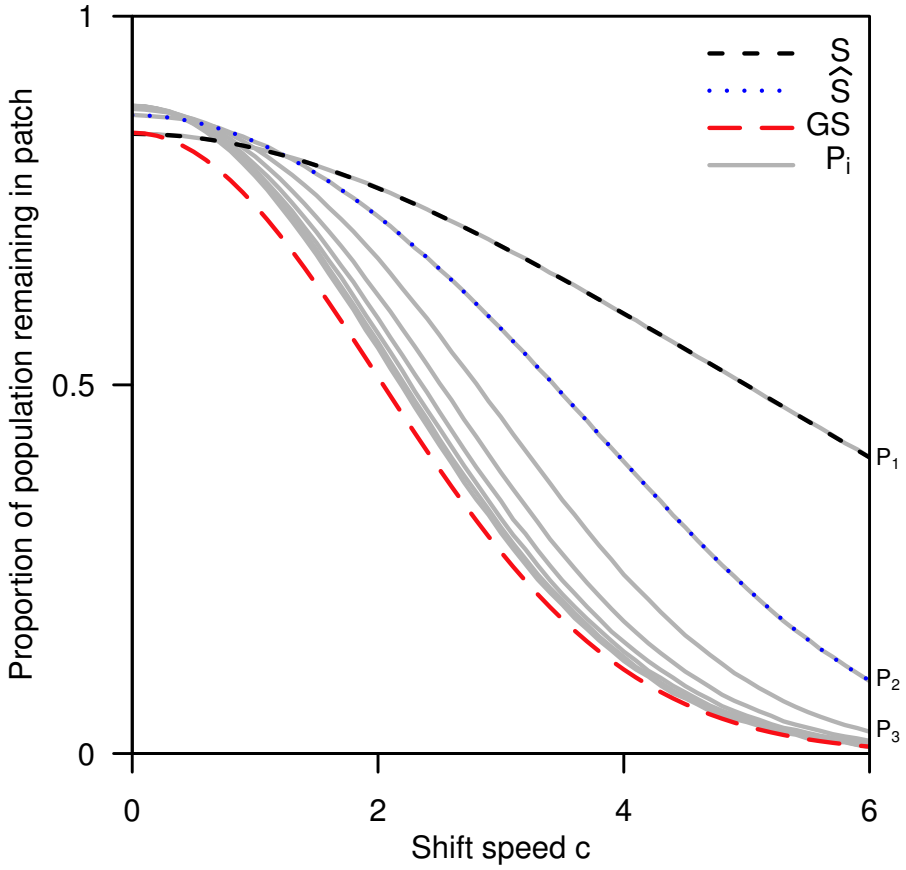

Figure 1.2: The proportions of eight generations of individuals remaining in a patch of length 10, assuming shifted Gaussian dispersal with $\sigma = 2$, averaged over 100 simulations for each value of c. Each simulation began with initial population $N_0 = 1\,000\,000$ distributed randomly and uniformly across Ω. After dispersal, each generation was bootstrapped back to the initial population size, providing a sufficient growth rate to repeat the process of dispersal indefinitely. The proportion remaining after the first time step $P_1 = N_1/N_0$ is indistinguishable from the average dispersal success S. The ratio of populations between the first and second time step $P_2 = N_2/N_1$ is indistinguishable from the modified average dispersal success $\widehat{S}$. The sequence of population ratios between each successive time step $P_3, P_4, P_5, \ldots$ approaches the geometric symmetrization GS of S.

the number of individuals lost due to dispersal, to give a new population $N_1(x)$, such that the population stayed constant (i.e., $N_0 = N_1$). Resampling allowed the process of dispersal to be iterated indefinitely without running out of individuals, while capturing the desired sequence of population ratios $P_1, P_2, P_3, \ldots$ that reflect the population losses due to dispersal at each time step. I replicated this process for 61 different shift speeds ranging from $c = 0$ to $c = 6$. A comparison of the proportion of individuals remaining in the patch for the first eight time steps and the values of S, $\widehat{S}$, and GS can be seen in Figure 1.2.

Returning to the mathematical discussion, I note that Kolotilina (1993) further proposed a sequence of lower bounds that improve the approximation of $\rho(\mathbf{A})$, given by

$$\frac{\mathbf{e}^T\mathbf{G}\mathbf{e}}{m} \leq \left(\frac{\mathbf{e}^T\mathbf{G}_2\mathbf{e}}{m}\right)^{1/2} \leq \cdots \leq \left(\frac{\mathbf{e}^T\mathbf{G}_{2^k}\mathbf{e}}{m}\right)^{2^{-k}} \leq \rho(\mathbf{A}), \tag{1.23}$$

where $\mathbf{G}_n$ is the geometric symmetrization of $\mathbf{A}^n$, such that $(g_n)_{ij} = \sqrt{a^n_{ij}a^n_{ji}}$, with a^n_{ij} the ij-th element of $\mathbf{A}^n$. It can likewise be seen that

$$\lim_{m\to\infty}\left(\frac{\mathbf{e}^T\mathbf{G}_n\mathbf{e}}{m}\right)^{n^{-1}} = \left(\frac{\int_\Omega\int_\Omega \sqrt{k^n(x,y)k^n(y,x)}\,dx\,dy}{\int_\Omega 1\,dy}\right)^{n^{-1}} \tag{1.24}$$

$$= \left(\frac{1}{|\Omega|}\int_\Omega\int_\Omega \sqrt{k^n(x,y)k^n(y,x)}\,dx\,dy\right)^{n^{-1}}, \tag{1.25}$$

where $k^n(x,y)$ is the *nth iterated kernel* of $k(x,y)$ (Zabreyko et al., 2013), defined recursively such that

$$k^1(x,y) = k(x,y), \tag{1.26}$$

$$k^n(x,y) = \int_\Omega k(x,z)k^{n-1}(z,y)\,dz. \tag{1.27}$$

The iterated kernel $k^n(x,y)$ is analogous to the iterated dispersal matrix $\mathbf{K}^n$. The

second iterated kernel $k^2(x,y)$ of the shifted Laplace kernel, for example, is

$$k^2(x,y) = \frac{1}{4b^2}\int_0^L e^{-\frac{|x+c-z|}{b}} e^{-\frac{|z+c-y|}{b}}\,dz \tag{1.28}$$

$$= \frac{1}{8b}\left(2e^{-s} + 2se^{-s} - e^{-\left(\frac{x+y}{b}\right)} - e^{-\left(\frac{2L-x-y}{b}\right)}\right), \tag{1.29}$$

with $s = \left|\frac{x+2c-y}{b}\right|$.

We may now generalize the formula for GS in (1.20) to

$$G_nS \equiv \left(\frac{1}{|\Omega|}\int_\Omega\int_\Omega \sqrt{k^{2^n}(x,y)k^{2^n}(y,x)}\,dx\,dy\right)^{2^{-n}}, \tag{1.30}$$

which provides increasingly tight lower bounds of the dominant eigenvalue of (1.6) for increasing n. I note that GS defined in (1.20) is equivalent to G_0S in (1.30); for the remainder of this chapter I will use the notation GS to refer to G_0S, and G_nS to refer to any value of n other than $n = 0$. For many parameter values, G_0S provides a perfectly adequate approximation of dispersal success.

In the next section, I will demonstrate that GS is a far more useful tool for describing the effects of asymmetric dispersal than either Van Kirk and Lewis' average dispersal success S or Reimer's modified $\widehat{S}$ (see Table 1.2 for reference).

1.5 Applications to integro-difference models

Consider the integro-difference equation

$$N_{t+1}(x) = \int_\Omega k(x,y)f[N_t(y)]\,dy, \tag{1.31}$$

and assume that $k(x,y)$ is asymmetric. With geometric symmetrization in hand, we are now equipped with a blueprint for constructing a symmetric kernel $\sqrt{k(x,y)k(y,x)}$ from $k(x,y)$. Furthermore, under certain assumptions on f and $k(x,y)$ (Zhou and

Kot, 2011), we know that the persistence criteria of

$$N_{t+1}(x) = \int_\Omega \sqrt{k(x,y)k(y,x)} f[N_t(y)]\, dy. \tag{1.32}$$

will be close in value to the persistence criteria of (1.31). Although these two equations utilize different kernels, their dominant eigenvalues are approximately equal, which determines the criteria for population persistence. Finally, we have a simple method for approximating $\lambda_{\max}$ for (1.31), given by

$$\lambda_{\max} \approx \lambda_{GS} \equiv \frac{R_0}{|\Omega|} \int_\Omega \int_\Omega \sqrt{k(x,y)k(y,x)}\, dx\, dy \tag{1.33}$$

$$= R_0 GS, \tag{1.34}$$

which can be used to better understand how different model parameters relate to persistence. To illustrate, I turn again to shifted kernels of the form $k(x,y) = k(x + c - y)$.

1.5.1 Approximating the critical speed c^*

The critical speed c^* beyond which the population can no longer persist corresponds to the bifurcation value of $\lambda_{\max} = 1$; when $c > c^*$, $\lambda_{\max} < 1$, and the population will die out.

For some dispersal kernels, the formulae for the various dispersal success approximations are simple enough to solve analytically. The shifted Laplace kernel (Table 1.1), for example, can be plugged into (2.17) to get

$$S = \begin{cases} 1 - \frac{c}{L} - \frac{be^{-c/b}}{L} + \frac{be^{-L/b}}{L} \cosh\left(\frac{c}{b}\right), & c < L, \\ \frac{be^{-c/b}}{L}\left(\cosh\left(\frac{L}{b}\right) - 1\right), & c \geq L. \end{cases} \tag{1.35}$$

Likewise, (1.20) gives

$$GS = \begin{cases} \frac{1}{L}\left[be^{-L/b} + e^{-c/b}\left(L - c - b + \frac{cL}{b} - \frac{c^2}{2b}\right)\right], & c < L, \\ \frac{1}{2b}e^{-c/b}L, & c \geq L. \end{cases} \tag{1.36}$$

Using the approximation of $\lambda_{\max} \approx \lambda_S = R_0 S$ in (1.9), we can substitute (1.35) into (1.9) and set $\lambda_S = 1$ to get

$$1 = R_0\left[1 - \frac{c^*}{L} - \frac{be^{-c^*/b}}{L} + \frac{be^{-L/b}}{L}\cosh\left(\frac{c^*}{b}\right)\right]. \tag{1.37}$$

From this we can derive an expression for R_0 in terms of c^* and the model parameters L and b,

$$R_0 = \frac{L}{L - c^* - be^{-c^*/b} + e^{-L/b}\cosh\frac{c^*}{b}}, \tag{1.38}$$

assuming that $c^* < L$. Similarly, the formula for λ_{GS} in (1.34) for GS implies

$$R_0 = \frac{L}{be^{-L/b} + e^{-c^*/b}\left(L - c^* - b + \frac{c^*L}{b} - \frac{c^{*2}}{2b}\right)}. \tag{1.39}$$

Applying L'Hôpital's rule to (1.39) as $L \to \infty$, this equation predicts limiting curves of

$$R_0 = \frac{e^{c^*/b}}{1 + \frac{c^*}{b}}. \tag{1.40}$$

For a given growth rate R_0, this curve approximates the invasion speed p^* of an IDE with an infinite domain, described parametrically in Kot et al. (2004) as

$$p^* = \frac{2ub^2}{1 - u^2b^2}, \tag{1.41}$$

$$R_0 = \left(1 - u^2b^2\right)\exp\left(\frac{2u^2b^2}{1 - u^2b^2}\right), \tag{1.42}$$

as can be seen in Figure 1.3.

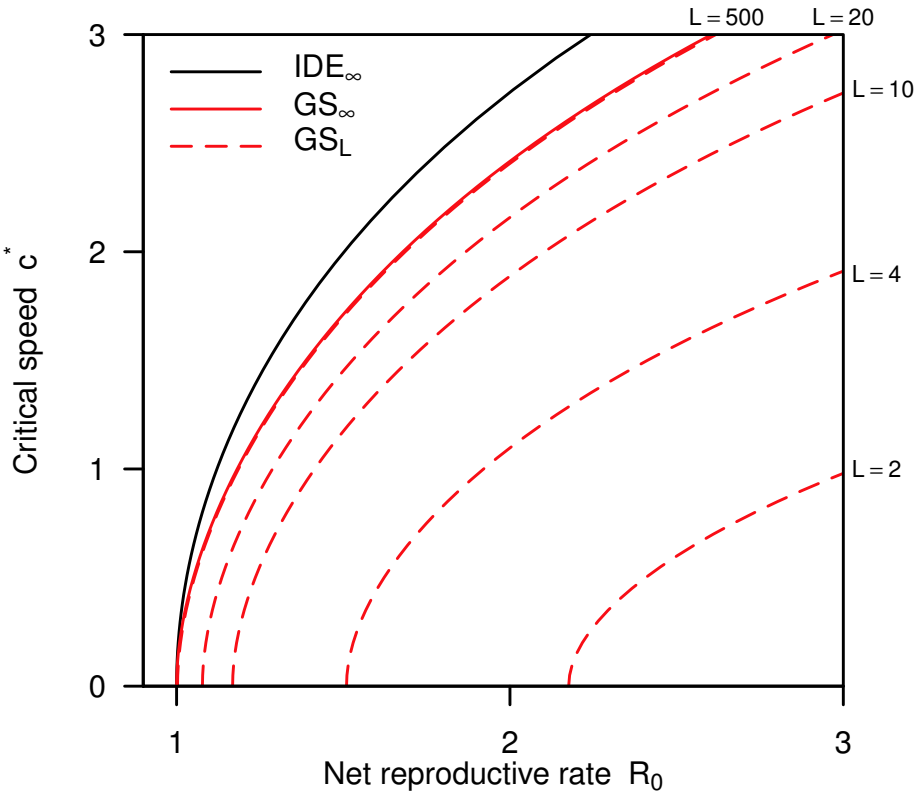

Figure 1.3: Critical speed curves GS_L for a shifted Laplace kernel with $b = 1.44$ predicted using GS (dashed red lines) for a variety of domain sizes, compared with the invasion speed IDE_∞ on an infinite domain predicted by (1.41) and (1.42) (solid grey line) and the approximation GS_∞ of the invasion speed on an infinite domain provided by (1.40) (solid red line).

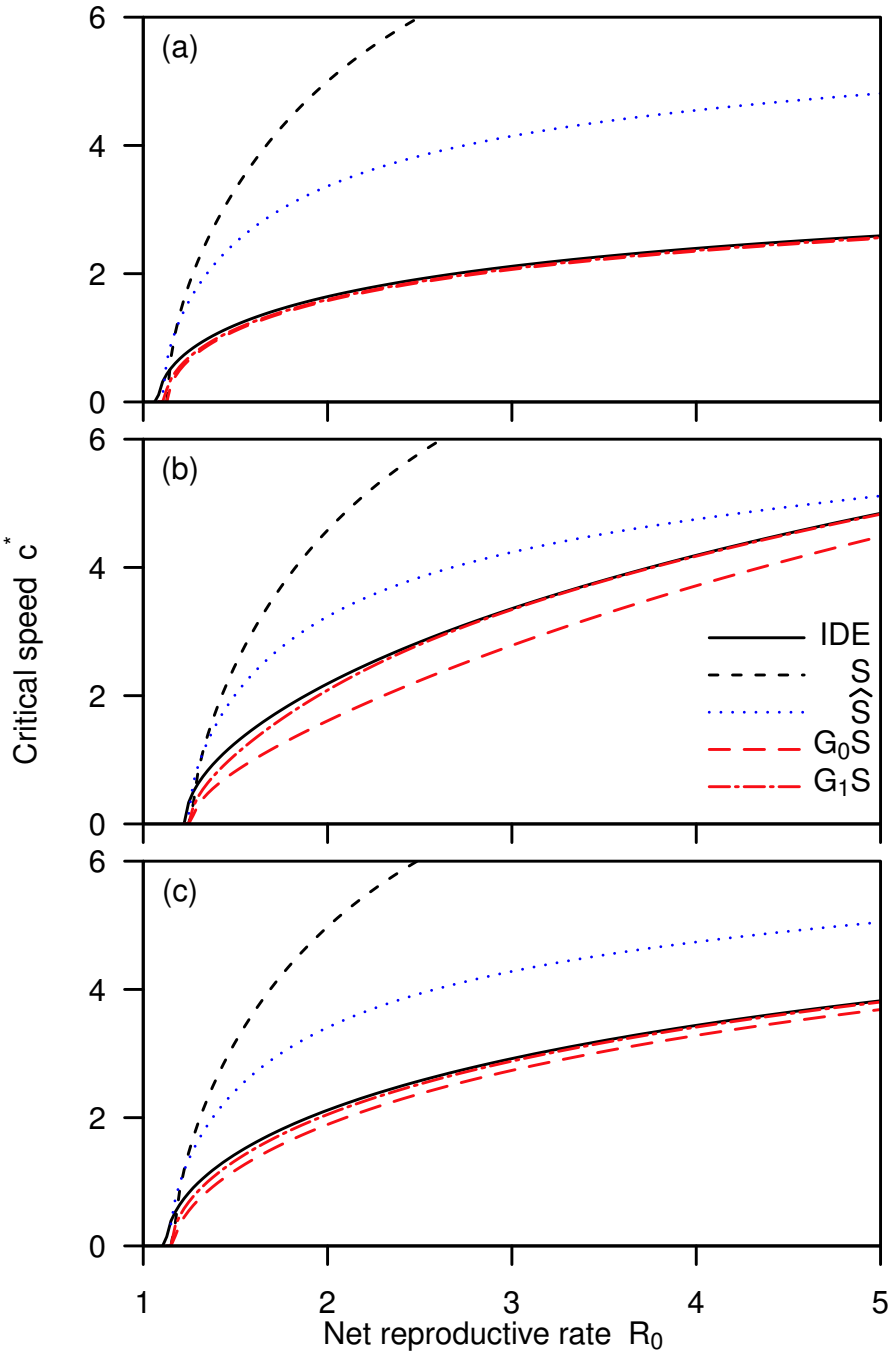

Figure 1.4: Numerical approximations of critical speed curves for (a) a shifted Gaussian kernel with $\sigma = 1.48$, (b) a shifted Cauchy kernel with $\gamma = 1$, and (c) a shifted Laplace kernel with $b = 1.44$, and with $L = 10$.

For kernels less amenable to analytic evaluation, it remains quite straightforward to use numerical optimization to solve $1 = R_0 S$, and likewise, the corresponding equations for $\widehat{S}$ and GS. To illustrate, I numerically calculated c^* for IDEs discretized at $m = 101$ points on a patch of length 10, using R's `optimize` function (R Core Team, 2017) to minimize the quantity

$$|\rho(R_0 \mathbf{K}) - 1| \tag{1.43}$$

for different values of R_0, and compared this critical speed curve with the critical speed curves derived by minimizing

$$|R_0 S - 1|, \tag{1.44}$$

$$|R_0 \widehat{S} - 1|, \tag{1.45}$$

$$|R_0 G_n S - 1|, \tag{1.46}$$

for S, $\widehat{S}$, and $G_n S$, respectively, for various R_0, with increasingly accurate estimates of $\lambda_{\max}$ provided by $G_n S$ for increasing n. Figure 1.4 compares the results for three different shifted kernels, using dispersal parameters $\sigma = 1.48$ (Gaussian), $\gamma = 1$ (Cauchy), $b = 1.44$ (Laplace) so that each kernel has the same median absolute deviation when $c = 0$ (Rousseeuw and Croux, 1993). Figure 1.4 shows that $G_0 S$ more closely approximates the critical speed curve of a numerically approximated IDE of the form found in (1.6) for the chosen parameter values than S or $\widehat{S}$, and this approximation can be considerably improved with $G_1 S$. These patterns are consistently observable across a wide range of parameter values.

All other parameters being equal, $G_n S$ also correctly predicts higher critical speeds for kernels with higher kurtosis κ, a measure of the "fatness" of tails. (Although the Cauchy distribution does not have finite kurtosis on an unbounded domain, its kurtosis is finite on the bounded domain $\Omega = [0, L]$.) In contrast, kurtosis does not

Table 1.3: Different estimates of the critical speed c^* of an IDE with $L = 100$, $R_0 = 1.8$, $\sigma = 2 \cdot 1.48$ (Gaussian), $\gamma = 2$ (Cauchy), and $b = 2 \cdot 1.44$ (Laplace). c^* increases with the kurtosis of the kernel.

	numeric	S	$\widehat{S}$	G_0S	G_1S	G_2S
Gaussian	3.2	40.0	30.8	3.1	3.2	3.2
Laplace	4.9	40.0	30.8	4.1	4.5	4.7
Cauchy	12.6	40.0	30.4	4.3	8.1	12.2

appear to have a significant effect on estimates of c^* derived with S or $\widehat{S}$. Table 1.3 compares estimates of c^* for an IDE with $L = 100$, $R_0 = 1.8$, and $\sigma = 2 \cdot 1.48$ (Gaussian), $\gamma = 2$ (Cauchy), and $b = 2 \cdot 1.44$ (Laplace). These estimates illustrate how long-distance dispersal can influence persistence: the Gaussian kernel ($\kappa = 3$ for $c = 0$) has the thinnest tails of the three, signifying a low probability of long-distance dispersal events, and hence has the smallest critical speed. The Cauchy kernel ($\kappa \approx 15$ for $c = 0$) has the fattest tails of the three, meaning that long-distance dispersal events are much more likely, making it possible for the population to persist at much higher shift speeds. The Laplace distribution ($\kappa = 6$ for $c = 0$) falls somewhere in between.

1.5.2 Approximating the critical domain size L^*

Just as equations (1.35) and (1.36) enabled us to explore the relationship between the intrinsic growth rate R_0 and the critical speed c^*, so may they help us determine the critical domain size L^*. We use equations (1.38) and (1.39) to plot L^* as a function of c for various values of R_0 (Figure 1.5).

Again, the same numerical techniques used for solving $1 = R_0S$ (and the corresponding equations for $\widehat{S}$ and G_nS) for c^* apply just as readily to solving $1 = R_0S$ for L^*. Minimizing (1.43) for different values of c yields a critical domain size curve, and minimizing (1.44), (1.45), (1.46) similarly yield critical domain size curves as a function of S, $\widehat{S}$, and G_nS, respectively. Figure 1.5 compares these critical domain size

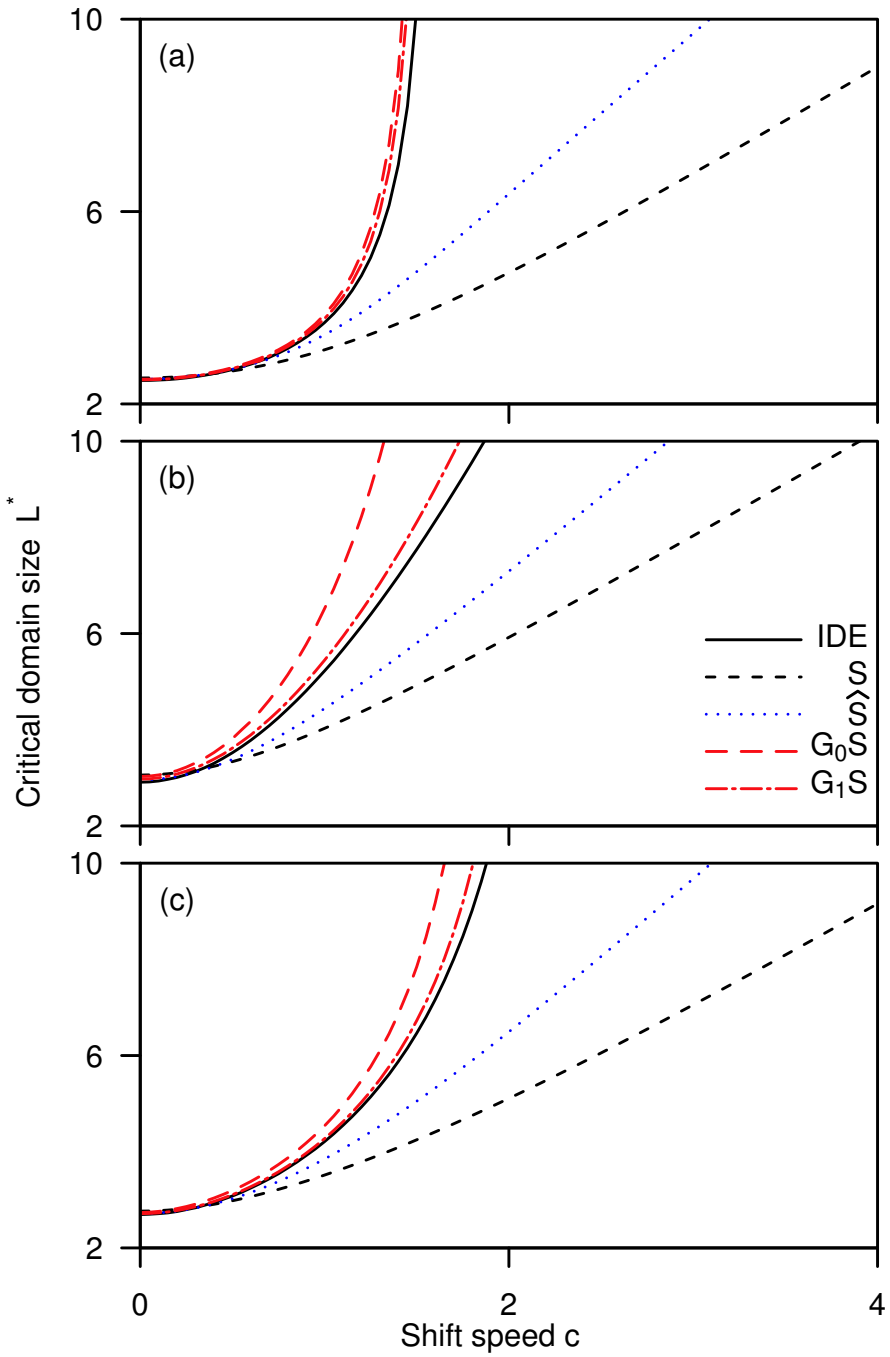

Figure 1.5: Numerical approximations of critical domain size for a shifted Gaussian kernel with $\sigma = 1.48$, a shifted Cauchy kernel with $\gamma = 1$, and a shifted Laplace kernel with $b = 1.44$, and with $R_0 = 1.8$.

curves for three different shifted kernels, again using dispersal parameters $\sigma = 1.48$ (Gaussian), $\gamma = 1$ (Cauchy), $b = 1.44$ (Laplace), and with $R_0 = 1.8$. As with critical speed in Figure 1.4, Figure 1.5 illustrates that G_1S most closely approximates the critical domain size curve of the numerically approximated IDE for the chosen parameter values, and this can be observed for other parameter values as well.

1.5.3 Approximating mean population density at equilibrium

Let us assume that (1.31) has a nontrivial equilibrium solution $N^*(x)$ such that

$$N^*(x) = \int_\Omega k(x,y) f[N^*(y)]\, dy. \tag{1.47}$$

By applying ADS to (1.47), we can approximate the effects of $k(x,y)$ with S by averaging the cumulative effects of dispersal over the domain. This method reduces the equilibrium solution of the IDE to its spatial average, which can then be used to describe persistence more explicitly. This technique is detailed in Lutscher and Lewis (2004), but I outline the process here.

We begin by averaging the population distribution $N_t(x)$ over the spatial domain, denoted as

$$\overline{N}_t \equiv \frac{1}{|\Omega|} \int_\Omega N_t(x)\, dx. \tag{1.48}$$

Applying this average to both sides of (1.31) yields

$$\frac{1}{|\Omega|} \int_\Omega N_{t+1}(x)\, dx = \frac{1}{|\Omega|} \int_\Omega \int_\Omega k(x,y) f[N_t(y)]\, dx\, dy. \tag{1.49}$$

The first-order Taylor expansion of f about $\overline{N}_t$ is

$$f[N_t(x)] \approx f[\overline{N}_t] + f'[\overline{N}_t]\big(N_t(x) - \overline{N}_t\big). \tag{1.50}$$

If the difference between the nonzero equilibrium $N^*(x)$ and the spatial average $\overline{N}_t$

of $N_t(x)$ is small, i.e., if the spatial average $\overline{N}_t$ is close to equilibrium, then we may neglect the linear term in (1.50) and approximate f by

$$f[N_t(x)] \approx f[\overline{N}_t]. \tag{1.51}$$

Substituting (1.51) into (1.49) yields

$$\frac{1}{|\Omega|}\int_\Omega N_{t+1}(x)\,dx \approx f[\overline{N}_t]\frac{1}{|\Omega|}\int_\Omega\int_\Omega k(x,y)\,dx\,dy, \tag{1.52}$$

which implies that $\overline{N}_t$ changes over time as

$$\overline{N}_{t+1} \approx S\cdot f[\overline{N}_t]. \tag{1.53}$$

In this manner we may approximate an IDE by averaging over space, which separates the dispersal kernel and growth function into individual, more digestible components. In the case of a Beverton-Holt growth curve (Table 1.1), the spatial average of the nontrivial equilibrium solution of (1.31) is approximated by

$$\overline{N_S^*} = \frac{K(SR_0-1)}{R_0-1}. \tag{1.54}$$

(Note the similarities between this and the fixed point of the nonspatial Beverton-Holt model, $N^* = \frac{K(R_0-1)}{R_0-1} = K$.) Similarly, the spatial averages of the logistic and Ricker growth functions are approximated by

$$\overline{N_S^*} = \frac{SK(1+r)-K}{Sr}, \tag{1.55}$$

and

$$\overline{N_S^*} = K\left(\frac{\log S}{r}+1\right), \tag{1.56}$$

respectively.

As we've already seen in other examples, approximations derived using S do not extend well to the case of asymmetric dispersal. Indeed, it is quite easy to verify that (1.54), (1.55), and (1.56) can substantially overestimate the mean equilibrium $\overline{N^*(x)}$ of an IDE with asymmetric dispersal. We may, however, derive similar estimates of $\overline{N^*(x)}$ in terms of GS by applying similar reasoning to the integro-difference model

$$N_{t+1}(x) = \int_\Omega \sqrt{k(x,y)k(y,x)} f[N_t(y)]\, dy. \tag{1.57}$$

Following the same process as before, $\overline{N}$ now changes over time as

$$\overline{N}_{t+1} \approx GS \cdot f[\overline{N}_t]. \tag{1.58}$$

This yields the estimates

$$\overline{N^*_{GS}} = \frac{K(GSR_0 - 1)}{R_0 - 1}, \tag{1.59}$$

$$\overline{N^*_{GS}} = \frac{GSK(1+r) - K}{GSr}, \tag{1.60}$$

$$\overline{N^*_{GS}} = K\left(\frac{\log GS}{r} + 1\right), \tag{1.61}$$

for the spatial averages of the Beverton-Holt, logistic, and Ricker growth functions, respectively. Similar estimates may also be found approximating the equilibrium $\overline{N^*_{\widehat{S}}}$ in terms of $\widehat{S}$.

Why might we expect (1.57) to have similar average population densities as (1.31) at equilibrium? To answer this question, we consider the kernel $k(x,y)$, and note that

$$k(x,y) = \sqrt{k(x,y)k(x,y)} \tag{1.62}$$

$$= \sqrt{k(x,y)k(y,x) + k(x,y)\Big(k(x,y) - k(y,x)\Big)}. \tag{1.63}$$

Assuming the quantity $k(x,y)\big(k(x,y) - k(y,x)\big)$ is small, then applying the linear

approximation

$$\sqrt{x+\epsilon} \approx \sqrt{x} + \frac{1}{2\sqrt{x}}\epsilon \tag{1.64}$$

to (1.63) yields

$$k(x,y) \approx \sqrt{k(x,y)k(y,x)} + \frac{1}{2}\sqrt{\frac{k(x,y)}{k(y,x)}}\Big(k(x,y) - k(y,x)\Big) \tag{1.65}$$

$$\approx \sqrt{k(x,y)k(y,x)}. \tag{1.66}$$

Thus, (1.57) can be seen as a lower order approximation of (1.31). For shifted kernels, the quantity $k(x,y) - k(y,x)$ should be small for smaller values of c, since $k(x,y) \approx k(y,x)$ when $k(x,y)$ is close to symmetric. For larger values of c we already know that (1.57) has approximately identical persistence criteria as (1.31), so we should expect the two to have similar population densities as c approaches the critical speed c^*, and equal densities for $c \geq c^*$. In this regard, we may reasonably expect that (1.59), (1.60), and (1.61) provide more accurate estimates of mean population density for increasing c than (1.54), (1.55), and (1.56).

In fact, we may further improve these estimates by calculating one more iteration of the integro-difference equation in (1.31). Taking $\overline{N^*_{GS}}$ as our estimate of $N^*(x)$, we get

$$N^*(x) = \int_\Omega k(x,y) f[N^*(x)]\, dy \tag{1.67}$$

$$\approx \int_\Omega k(x,y) f[\overline{N^*_{GS}}]\, dy \tag{1.68}$$

$$= \int_\Omega k(x,y) \frac{\overline{N^*_{GS}}}{GS}\, dy \tag{1.69}$$

$$= \frac{\overline{N^*_{GS}}}{GS} \int_\Omega k(x,y)\, dy. \tag{1.70}$$

Recognizing the integral in (1.70) as the redistribution function $r(x)$ from (1.11),

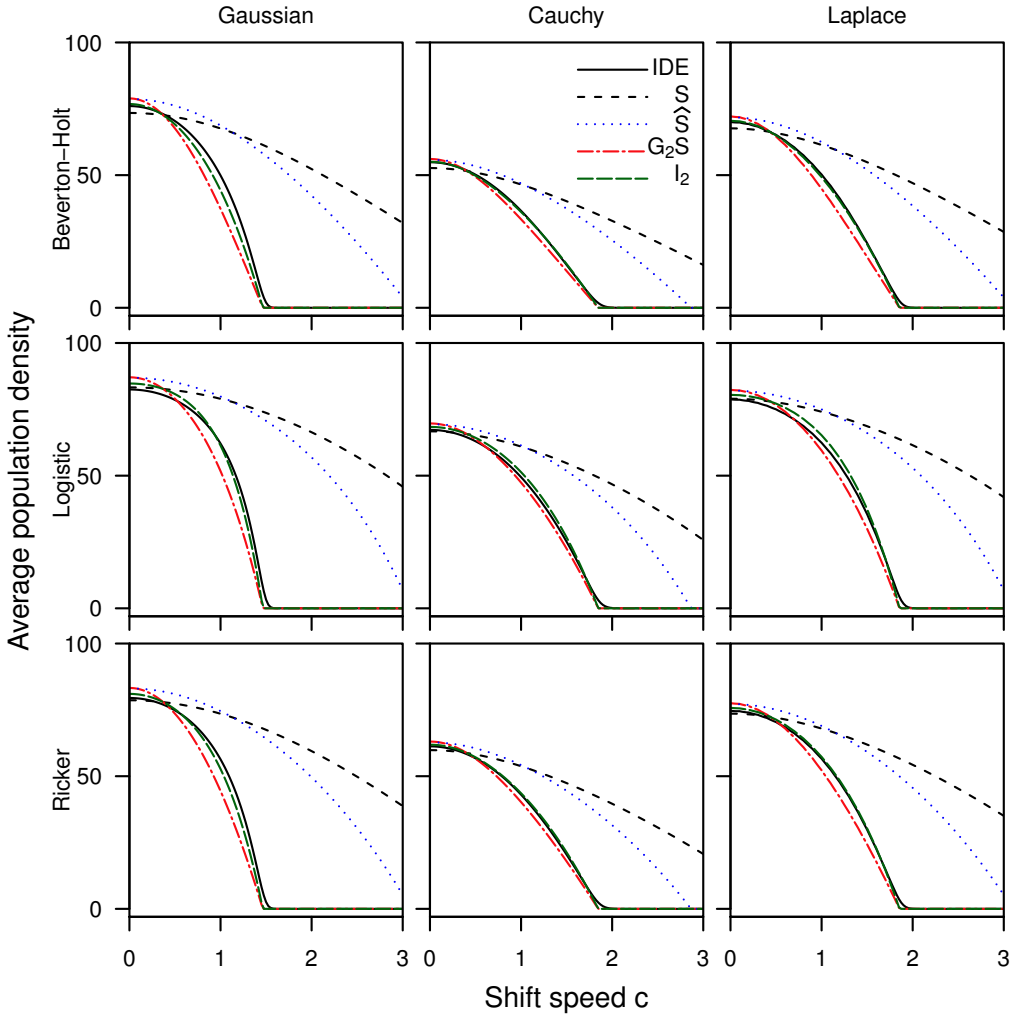

Figure 1.6: A comparison of the spatial averages of the nontrivial equilibrium solutions of an IDE with a variety of growth functions and a variety of shifted dispersal kernels, with $L = 10, K = 100$, $R_0 = 1.8$ (Beverton-Holt), $r = 0.8$ (logistic) and $r = \log(1.8)$ (Ricker), and $\sigma = 1.48$ (Gaussian), $\gamma = 1$ (Cauchy), and $b = 1.44$ (Laplace).

we infer

$$N^*(x) \approx \frac{\overline{N^*_{GS}}}{GS} r(x). \tag{1.71}$$

This equation is similar in form to the *redistribution approximation* described by Lutscher and Lewis (2004), defined in terms of S as

$$N^*(x) \approx \frac{\overline{N^*}}{S} r(x). \tag{1.72}$$

Finally, averaging (1.71) across the domain yields the estimate

$$\overline{N^*(x)} \approx \frac{\overline{N^*_{GS}}}{GS} \int_\Omega r(x)\, dx \tag{1.73}$$

$$= \frac{S}{GS} \overline{N^*_{GS}}. \tag{1.74}$$

We denote the approximation in (1.74) as $\overline{N^*_I}$, or more generally for G_nS as

$$\overline{N^*_{I_n}} = \frac{S}{G_nS} \overline{N^*_{G_nS}}. \tag{1.75}$$

Figure 1.6 shows estimates of the spatial average of the nontrivial equilibrium solution $\overline{N^*_S}$, $\overline{N^*_{\widehat{S}}}$, $\overline{N^*_{G_2S}}$, and $\overline{N^*_{I_2}}$ for a variety of growth functions, dispersal kernels, and shift speeds. I quantified the accuracy of these estimates for two different domain sizes using the root-mean-square error (RMSE) between each estimate and the spatial average of the numerically calculated IDE equilibrium solution, calculated for equally-spaced values of c ranging from $c = 0$ to $c = c^*_{all}$, the smallest value of c for which all four estimates predicted extinction. $\overline{N^*_{I_2}}$ provided the lowest RMSE in all but one scenario (Table 1.4), suggesting that it is the most accurate approximation of the four.

Figure 1.7 illustrates a more extreme example of Figure 1.6, considering a shifted Cauchy distribution with $L = 100$, $R_0 = 1.8$, and $\gamma = 2$. In this case, patch size is considerably larger than the mean dispersal distance, but the fatter tails of the

Table 1.4: Root-mean-square error between the spatial average of the numerically-calculated IDE equilibrium solution and various approximations of the spatial average. Each approximation was calculated for m equally-spaced values from $c = 0$ to $c = c^*_{all}$, the smallest value of c for which all four estimates predicted extinction. Lowest values are in bold.

Scenario				**Root-mean-square error**			
L	Dispersal	Growth	m	$\overline{N^*_S}$	$\overline{N^*_{\widehat{S}}}$	$\overline{N^*_{G_2S}}$	$\overline{N^*_{I_2}}$
10	Gaussian	BH	89	32.5	24.6	4.7	**2.2**
		Logistic		41.6	31.3	4.5	**1.8**
		Ricker		37.0	28.0	4.6	**1.9**
	Cauchy	BH	79	18.4	13.1	1.5	**0.3**
		Logistic		26.1	18.4	1.4	**1.1**
		Ricker		22.1	15.6	1.5	**0.5**
	Laplace	BH	89	25.9	18.2	2.6	**0.5**
		Logistic		34.5	24.1	2.4	**1.5**
		Ricker		30.1	21.1	2.5	**0.6**
100	Gaussian	BH	90	54.0	48.4	9.3	**8.1**
		Logistic		62.6	55.3	8.3	**6.8**
		Ricker		58.4	51.9	8.8	**7.5**
	Cauchy	BH	89	40.6	33.7	11.1	**7.4**
		Logistic		49.7	40.9	9.2	**4.6**
		Ricker		45.1	37.3	10.3	**6.0**
	Laplace	BH	90	52.6	46.8	8.9	**7.2**
		Logistic		61.3	53.8	7.6	**5.4**
		Ricker		57.0	50.3	8.3	**6.3**

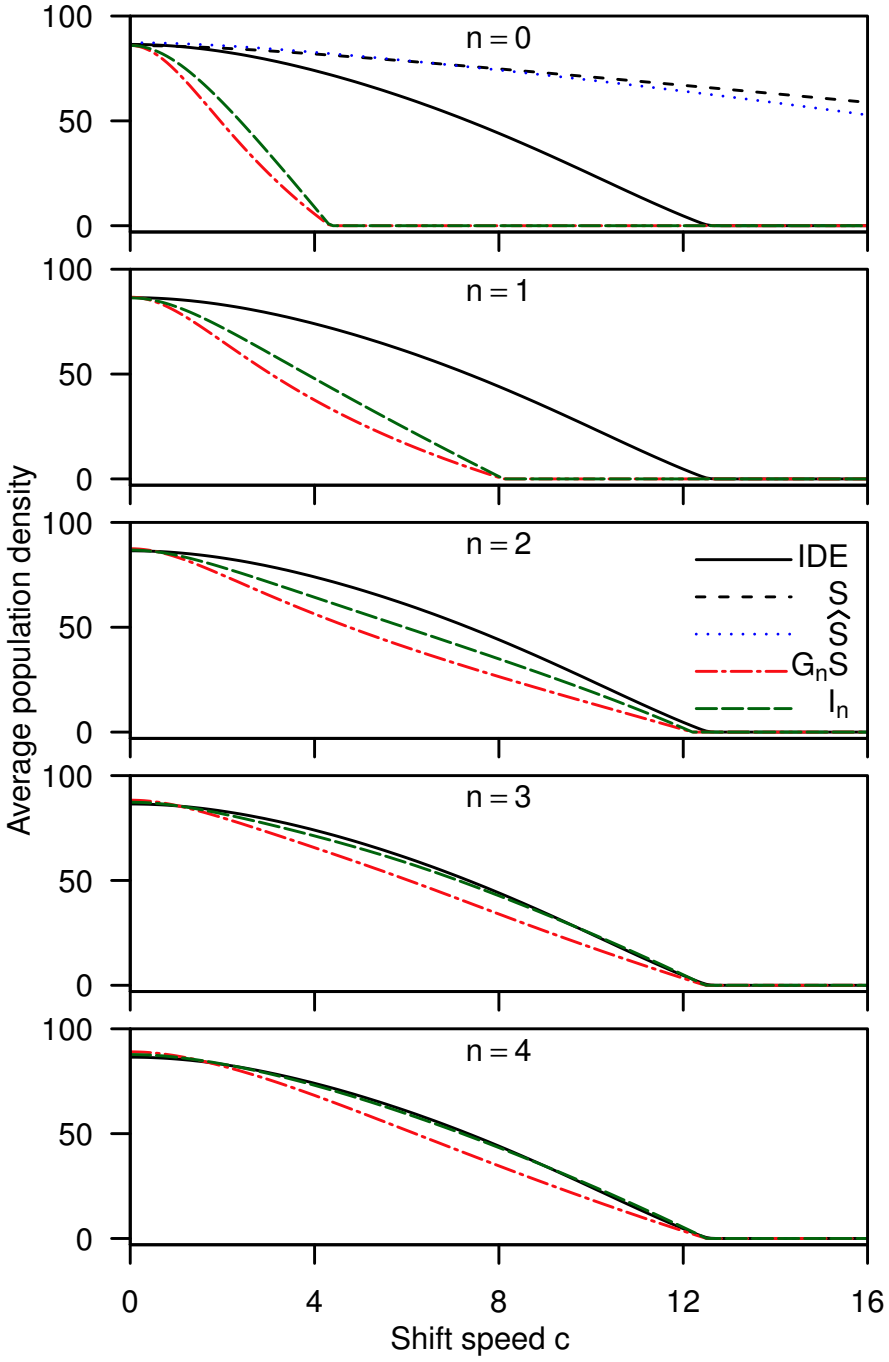

Figure 1.7: A comparison of estimates of the spatial averages of population at equilibrium derived from G_nS and I_n for increasing values of n, assuming Beverton-Holt dynamics with $R_0 = 1.8$, a shifted Cauchy kernel with $\gamma = 2$, and $L = 100$. As n increases, G_nS and I_n provide increasingly accurate estimates of $\overline{N^*(x)}$. The top panel includes estimates based on S and $\widehat{S}$ for comparison, but these estimates do not change with n.

Cauchy distribution makes long-distance dispersal events more likely, and the critical speed c^* for persistence is considerably higher than for kernels with thinner tails (see Table 1.3). Figure 1.7 shows how estimates of the mean population at equilibrium based on G_nS and I_n improve for increasing n. Although G_nS and I_n significantly underestimate $\overline{N^*(x)}$ for $n = 0$, these estimates are considerably improved for $n = 1$, and quite respectable for $n = 2$. By $n = 3$, $\overline{N^*_{I_3}}$ is almost indistinguishable from $\overline{N^*(x)}$.

1.5.4 Other types of asymmetry

So far I have explored asymmetric dispersal primarily in the context of climate change, examining Zhou and Kot (2011)'s integro-difference model with shifted kernels, but there are several other possible mechanisms through which asymmetric dispersal can arise. Advection can act upon individuals in the form of wind, ocean, or stream currents (Lutscher et al., 2005), or the diffusion process itself may be biased in a particular direction due to physiological or morphological constraints (Levin et al., 2003). I will now demonstrate how the various metrics of dispersal success can be applied to a dispersal kernel subject to advection.

Lutscher et al. (2005) used a partial differential equation modeling the individual movement of aquatic insects in a stream habitat to derive a modified Laplace kernel that accounts for advection. This asymmetric Laplace kernel is given by

$$k(x,y) = \begin{cases} A\exp(a_1(x-y)), & x \le y, \\ A\exp(a_2(x-y)), & x > y, \end{cases} \tag{1.76}$$

where $a_{1,2} = v/2D \pm \sqrt{v^2/4D^2 + \alpha/D}$, with D the diffusion constant, $v \ge 0$ the advection velocity, and α a constant settling rate, and where $A = a_1a_2/(a_2 - a_1) = \alpha/\sqrt{v^2 + 4\alpha D}$, which ensures that $k(x,y)$ integrates to 1. The advection velocity v is analogous to the shift speed c in the shifted Laplace, and the quantity $\sqrt{\frac{D}{\alpha}}$ is

analogous to the shape parameter b. In a similar fashion, the shifted Gaussian and shifted Cauchy can be seen as specific cases of the more general formulae

$$k(x,y) = \frac{1}{\sqrt{4\pi\alpha D}} \exp\left(-\frac{(x+\alpha v - y)^2}{4\alpha D}\right) \tag{1.77}$$

and

$$k(x,y) = \left[\frac{\pi\gamma}{\alpha}\left(\alpha^2 + \left(\frac{x+\alpha v - y}{\gamma}\right)^2\right)\right]^{-1}, \tag{1.78}$$

respectively, with $2\alpha D = \sigma^2$ and $\alpha = 1$ (Reimer et al., 2015).

The average dispersal success of the asymmetric Laplace is

$$S = \frac{A(e^{-a_1 L} + a_1 L - 1)}{L{a_1}^2} - \frac{A(a_2 L - e^{a_2 L} + 1)}{L{a_2}^2}, \tag{1.79}$$

and the geometric symmetrization of S is

$$GS = \frac{2A}{B} + \frac{2A}{B^2 L}\left(e^{-BL} - 1\right), \tag{1.80}$$

where $B = \frac{a_1 - a_2}{2}$. We note that Reimer et al. (2015) provides a formula for $\widehat{S}$ for the asymmetric Laplace, which we will not reproduce here.

We may once again use these formulae to calculate the critical domain size L^* or the critical advection velocity v^*. Substituting (1.79) into $\lambda_S = R_0 S$ and setting $\lambda_S = 1$ yields

$$R_0 = \frac{L{a_1}^2{a_2}^2}{A(e^{-a_1 L} + a_1 L - 1) - A(a_2 L - e^{a_2 L} + 1)}. \tag{1.81}$$

Similarly, substituting (1.80) into $\lambda_{GS} = R_0 GS$ and setting $\lambda_{GS} = 1$ yields

$$R_0 = \frac{B^2 L}{2A\left(BL + e^{-BL} - 1\right)}. \tag{1.82}$$

Comparisons of estimates of L^* and v^* can be seen in Figure 1.8.

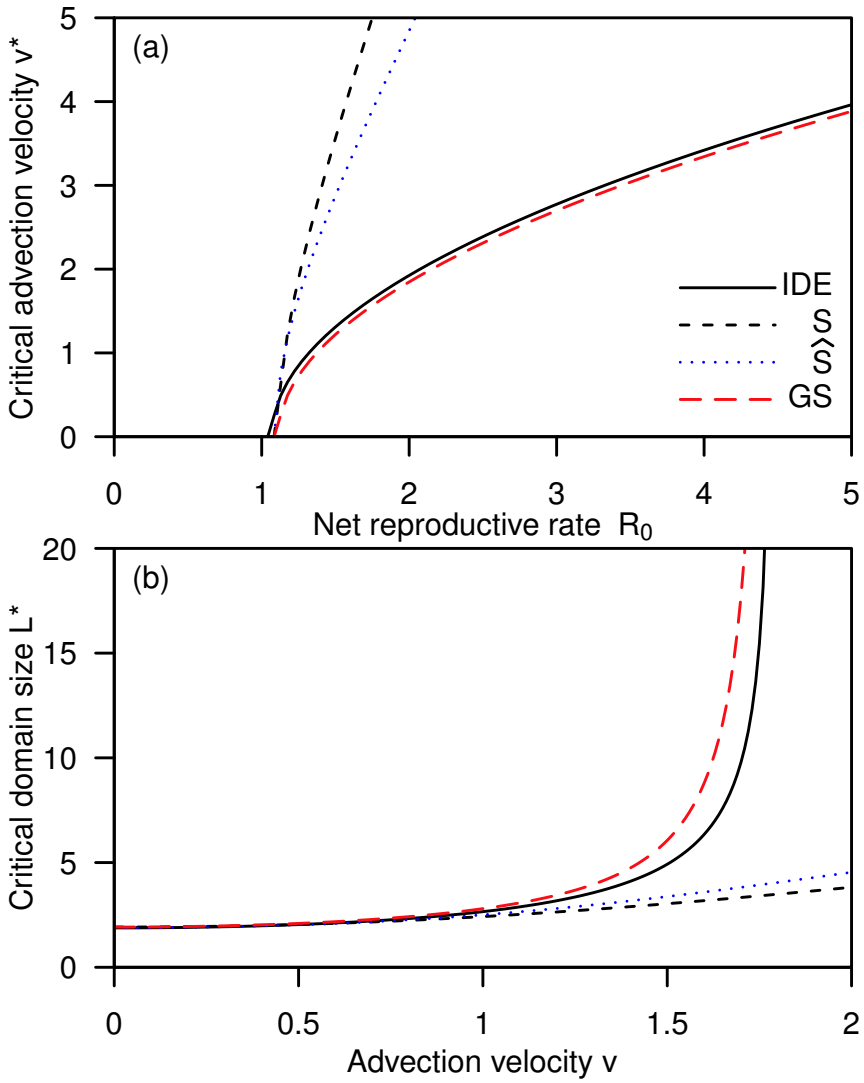

Figure 1.8: Approximations of (a) the critical advection velocity v^* of an IDE with $\alpha = 1$, $D = 1$, and $L = 10$, and (b) the critical domain size L^* of an IDE with $R_0 = 1.8$ and an asymmetric Laplace dispersal kernel with $\alpha = 1$, $D = 1$.

1.6 Discussion

Dispersal is a complicated process. Dispersal takes place at the scale of the individual, and is inevitably influenced by a multitude of factors that affect the individual, such as habitat heterogeneity in both space and time, and demographic and environmental stochasticity. Modeling dispersal at the scale of the individual necessitates tracking each individual through time and space, but this method is often constrained by computational power, and this limitation grows with model complexity (Snyder, 2003). In many situations, it behooves us to focus our efforts on modeling emergent population properties that result from the aggregate effects of individual dispersal. At the expense of granularity, modeling cumulative population behavior greatly simplifies the task of understanding how process affects pattern (Rahmandad and Sterman, 2008). Average dispersal success is one such example of an emergent property, describing the aggregate effects of dispersal within a population over the course of a generation, and, asymptotically, population persistence.

In addition to the distinction between modeling the individual vs. modeling the population is the contrast in using numerical analysis or analytic methods to obtain results. One of the benefits of the analytic approach is that an analytic solution can often more succinctly illuminate the relationships between a model's components. In the fortuitous (and admittedly rare) circumstance of possessing an analytic solution to an IDE model, one can see precisely how a population scales with the tweaking of a parameter or the value of a variable. Of course, many (if not most) integro-difference equations do not lend themselves kindly to analytic approaches, and numerical methods are more common (Zhou and Kot, 2011). Prudent and judicious applications of analytic approximations, however, provide us another way forward. By averaging the spatial aspects of integro-difference equations, we found a family of approximations of the dominant eigenvalue that determines population persistence. This sacrifice of spatial explicitness is of little consequence if we are not concerned with *where* individuals

are in space, but simply that they *are*.

The benefits of such approximations are further evident in the simplicity of equations such as

$$\lambda_{\max} \approx R_0 G_n S \tag{1.83}$$

in (1.34). The integro-difference equation of Zhou and Kot (2011) in (1.6) is a convolution of the growth and dispersal processes, and (to paraphrase one of the authors) generates a nasty eigenvalue problem (Kot and Phillips, 2015). In contrast to this nastiness, (1.83) elegantly decouples the growth and dispersal components, and in doing so, illuminates how dispersal success and growth rate each relate to population persistence. Moreover, this approximation appears to be quite accurate.

I highlighted the fact that dispersal is, more often than not, an asymmetric process. With asymmetric dispersal, the aggregate effects of individual dispersal events appear as a bias for the population to move in a certain direction, be it in latitude, elevation, slope, along ocean currents, or stream flow. Any such metric that hopes to meaningfully quantify a population's dispersal through space and time must account for this asymmetry. I asserted that the original definition of average dispersal success in Van Kirk and Lewis (1997) does not adequately reflect the effects of asymmetric dispersal, but I explored how to address this shortcoming using geometric symmetrization.

One benefit of the average dispersal success S is that it can be estimated experimentally through observation of population dispersal without explicit knowledge of $k(x, y)$. This is due to its simple ecological interpretation as the proportion of individuals remaining after a single dispersal event. I provided a similar interpretation of GS as the proportion of individuals remaining after dispersal when the population is at equilibrium. This suggests that GS can also be estimated experimentally without knowledge of $k(x, y)$ through repeated observation of population dispersal events over time, thus providing a practical method for inferring persistence criteria from

empirical data.

It is also worth acknowledging the importance of long-distance dispersal events in determining the rates and extents of population spread. Dispersal events are frequently observed at distances and frequencies greater than those predicted by a normal distribution, and kernels fit to observation data are typically characterized by fatter tails (Nathan et al., 2003). Kot et al. (1996) demonstrated how long-distance dispersal can affect the rate of spread of a population of fruit flies; fat-tailed kernels have likewise been proposed as a solution to Reid's Paradox, concerning the disparity between predicted and observed rates of tree repopulation in Northern Britain after the last ice age (Clark et al., 1998). In my analysis I demonstrated that geometric symmetrization can be used to accurately describe the characteristics of an IDE with a Cauchy dispersal kernel, the prototypical example of a fat-tailed kernel. Supporting similar conclusions in Lutscher et al. (2005), Table 1.3 and Figure 1.7 showed shifted kernels with higher kurtosis result in populations persisting at greater shift speeds, because there is a higher probability that some individuals will be able to disperse quite far, thus preserving the population. These results suggest that the effects of long-distance dispersal can indeed be captured by dispersal success approximations.

There are, of course, some caveats to my methods that are worth discussing. I used geometric symmetrization to quantify the asymptotic persistence of a population, but there are situations in which asymptotic behavior may be misleading. Transient population dynamics can sometimes imply extinction even when asymptotic dynamics suggest persistence (Caswell, 2007). Caution is therefore appropriate when using geometric symmetrization to predict persistence.

There are many types of population models that I have not explored here in the context of geometric symmetrization. Integro-difference equations come in many different flavors, including ones that account for Allee effects (Wang et al., 2002), heterogeneous habitat (Van Kirk and Lewis, 1997), and stage structure of populations (Harsch et al., 2014). Van Kirk and Lewis (1997) used the average dispersal success S

to analyze an IDE on a network of patches and Lutscher and Lewis (2004) applied S to a stage-structured matrix population model; Reimer et al. (2015) recreated similar models for both of these scenarios and compared model performance to those using Reimer's modified $\widehat{S}$. I have not yet pursued these avenues with GS, but have no reason to believe that it would not continue to outperform S and $\widehat{S}$ in a shifting habitat or in the presence of advection. These models and others would benefit from further analysis.

Finally, our comparison of dispersal success characterizations is by no means complete, as there are many different ways to quantify dispersal success, and there are likely many as yet undiscovered methods that are worth exploring. Anticipating future efforts, I suggest that any meaningful definition of dispersal success should necessarily have three fundamental characteristics: a biological interpretation, a mathematical justification, and adherence to the principle of parsimony.

There are many examples in the literature of dispersal success being applied to ecological issues, but it is worthwhile to revisit these studies in the context of climate change. Fagan and Lutscher (2006) provide an eloquent argument for the usefulness of the average dispersal success in reserve network design, but Araújo et al. (2004) demonstrated that reserve selection methods are inadequate for ensuring the long-term persistence of species due to the effects of climate change. Hughes et al. (2015) demonstrated how dispersal success can model host-parasitoid interactions in a fragmented habitat, but there is considerable evidence to suggest that species interactions can be strongly influenced by climate change (Harrington et al., 1999; Hance et al., 2006). Cobbold et al. (2005) used the average dispersal success to quantify how parasitism affects the critical patch size of the forest tent caterpillar, but Potapov and Lewis (2004) found that the critical patch size of a species can increase as the rate of climate change increases. Clearly, the effects of climate change should not be ignored. Zhou and Kot (2011) demonstrated how climate change can be represented with a shifted dispersal kernel, and this framework continues to be developed and explored

(Harsch et al., 2014; Phillips and Kot, 2015; Bouhours and Lewis, 2016).

Spatially-explicit population models help elucidate the relationship between a population and its environment, and have proven to be quite useful for modeling biological processes such as growth and dispersal. Average dispersal success helps describe the aggregate population-level pattern of individual dispersal events, and geometric symmetrization enables us to describe the aggregate effects of asymmetric dispersal with a much greater degree of confidence in the approximations than other currently known methods. Moving forward, I heartily encourage using this method to incorporate asymmetric dispersal processes into spatially-explicit population models.

1.7 Note

An edited version of this chapter has been published as:

Rinnan (2018). The dispersal success and persistence of populations with asymmetric dispersal. *Theoretical Ecology*, 11(1), 55-69. doi:10.1007/s12080-017-0348-x

Chapter 2

POPULATION PERSISTENCE IN THE FACE OF CLIMATE CHANGE AND COMPETITION: A BATTLE ON TWO FRONTS

2.1 Introduction

Climate change is having substantial impacts on species around the globe, and these impacts are expected to increase dramatically over the coming century (Thomas et al., 2011; Field et al., 2014). The effects can be seen at virtually every scale, from the individual and micro-habitat (Broitman et al., 2009) to the population level (Pearson and Dawson, 2003). Dispersal is a common species adaptation to climate change: poleward shifts have been observed in many species distributions in response to warming temperatures (Parmesan et al., 1999; Hickling et al., 2006; Sorte and Thompson, 2007), and shifts to higher elevations have been observed in others (Wilson et al., 2005; Chen et al., 2011b). Similar shifts in latitude and depth have been observed in marine species (Perry et al., 2005; Pinsky et al., 2013).

Interspecific competition can, however, curtail the movement and spread of populations, as shifting into new habitat often involves competing with species that are already established (Dunson and Travis, 1991; Davis et al., 1998). Although the importance of accounting for biotic interactions when modeling the effects of climate change on species has been well documented (Araújo and Luoto, 2007; Van der Putten et al., 2010; Urban et al., 2012), there is a notable deficit of modeling tools available to accomplish this, in part due to a lack of theoretical foundation on which to build (Gilman et al., 2010). Recent advances in modeling techniques have begun to address the gap between the assumptions of species distribution models and community

ecology theory (Pollock et al., 2014; Harris, 2015; Thorson et al., 2015), but these methods all use statistical approaches that ignore how biological traits and processes such as dispersal ability, growth rate, and niche breadth all contribute to population survival.

Here I describe a spatially-explicit, mechanistic competition model that incorporates aspects of climate change, while explicitly accounting for important ecological processes such as population growth, dispersal ability, and competition strength. I derive approximations of persistence criteria for each species, and demonstrate the accuracy of the approximations. Finally, I illustrate the model with two species of competing trout, using observed stream temperature data and future climate projections for the Salmon River in central Idaho.

2.2 Methods

2.2.1 Models

Interspecific competition has been well-studied through deterministic models such as the continuous-time Lotka-Volterra competition model (Cosner and Lazer, 1984), or its discrete-time analogue, the Leslie-Gower model (Leslie and Gower, 1958), and the dynamics of these systems have been thoroughly described. The Lotka-Volterra model has been used to study the effects of climate change on vegetation patterns (Jesse, 1999; Svirezhev, 2000). The Leslie-Gower model has been used to model a variety of competitive systems, including flour beetles (Park, 1948), plant assemblages (Levine and Rees, 2002; Adler et al., 2007), and fish (AlSharawi and Rhouma, 2009), but I am unaware of any examples in the literature that explicitly incorporate climate change into the modeling framework.

The Leslie-Gower model,

$$M_{t+1} = \frac{\lambda_m M_t}{1 + \alpha_m M_t + \beta_m N_t}, \tag{2.1}$$

$$N_{t+1} = \frac{\lambda_n N_t}{1 + \alpha_n N_t + \beta_n M_t}, \tag{2.2}$$

quantifies the populations of two univoltine species M and N, with $\alpha_m = (\lambda_m - 1)/K_m$, $\alpha_n = (\lambda_n - 1)/K_n$, where K_m and K_n represent the carrying capacities of species M and N, and β_m, β_n correspond to the strengths of competition between M and N.

Equations (2.1) and (2.2) have four fixed points, denoted as

$$L_0 = (0, 0), \tag{2.3}$$

$$L_M = \left(\frac{\lambda_m - 1}{\alpha_m}, 0 \right), \tag{2.4}$$

$$L_N = \left(0, \frac{\lambda_n - 1}{\alpha_n} \right), \tag{2.5}$$

$$L_B = \left(\frac{\alpha_n(\lambda_m - 1) - \beta_m(\lambda_n - 1)}{\alpha_m\alpha_n - \beta_m\beta_n}, \frac{\alpha_m(\lambda_n - 1) - \beta_n(\lambda_m - 1)}{\alpha_m\alpha_n - \beta_m\beta_n} \right). \tag{2.6}$$

L_B is asymptotically stable (Leslie and Gower, 1958) when

$$\frac{\lambda_n - 1}{\alpha_n} < \frac{\lambda_m - 1}{\beta_m} \tag{2.7}$$

and

$$\frac{\lambda_m - 1}{\alpha_m} < \frac{\lambda_n - 1}{\beta_n}, \tag{2.8}$$

and stability of this fixed point corresponds to coexistence of the two species. Defining

$$x = \frac{\beta_m\beta_n}{\alpha_m\alpha_n}, \qquad y = \frac{\beta_m(\lambda_n - 1)}{\alpha_n(\lambda_m - 1)}, \tag{2.9}$$

we may summarize four possible scenarios:

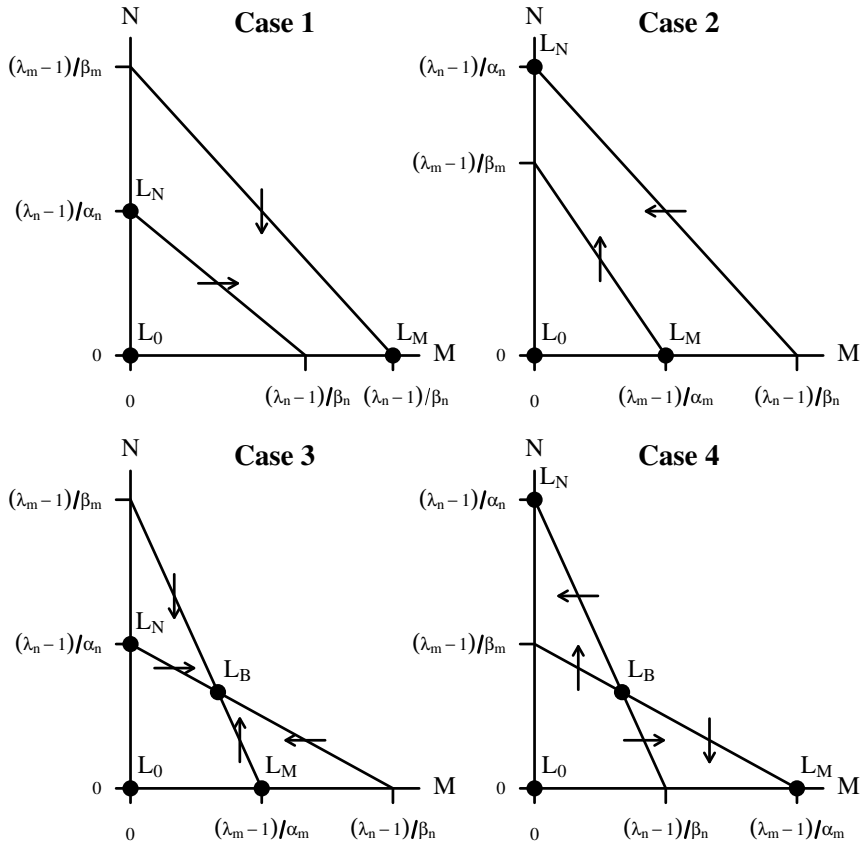

Figure 2.1: Phase portraits of the four possible scenarios of the Leslie-Gower model. Each portrait shows the fixed points, nullclines (i.e., zero-growth isoclines), and directions of trajectories crossing the nullclines.

Case 1:	$y < x$, $y < 1$,	M persists, N does not
Case 2:	$x < y$, $y > 1$,	N persists, M does not
Case 3:	$x < y < 1$,	both M and N persist
Case 4:	$1 < y < x$,	either M or N persists, depending on initial conditions

The phase portraits of these scenarios are illustrated in Figure 2.1.

Integro-difference equations (IDEs), by contrast, offer a spatially-explicit approach to population modeling, describing a population density $N_t(x)$ as a function of the cumulative effects of growth and dispersal at the previous time step, written as

$$N_{t+1}(x) = \int_{\Omega} k(x,y) f[N_t(y)]\, dy, \tag{2.10}$$

where $N_t(x)$ is the population density in generation t at location x, Ω is the spatial domain, f is the recruitment or growth function, and $k(x,y)$ is the dispersal kernel of the species that reflects the likelihood of moving from a location y to a location x. IDEs have recently been used to describe the effects of climate-related habitat shifts (Zhou and Kot, 2011; Kot and Phillips, 2015; Bouhours and Lewis, 2016).

Using the Leslie-Gower competition model to describe the growth phase of our two species yields a system of integro-difference equations, given by

$$M_{t+1}(x) = \int_{\Omega_m} \frac{k_m(x,y)\lambda_m M_t(y)}{1+\alpha_m M_t(y) + \beta_m N_t(y)}\, dy, \tag{2.11}$$

$$N_{t+1}(x) = \int_{\Omega_n} \frac{k_n(x,y)\lambda_n N_t(y)}{1+\alpha_n N_t(y) + \beta_n M_t(y)}\, dy, \tag{2.12}$$

where $k_m(x,y), k_n(x,y)$ are the dispersal kernels of species M and N as in Equation (2.10), the parameters $\lambda_m, \lambda_n, \alpha_m, \alpha_n, \beta_m, \beta_n$ are as in Equations (2.1) and (2.2).

I define the domains Ω_i such that $\Omega_i = [L_{i_1}+ct, L_{i_2}+ct]$ is a length of climatically suitable habitat for species i, and c represents the speed at which the habitat is shifting due to climate change (Zhou and Kot, 2011), which I assume here is constant. I further assume that dispersal probability depends only on the distance between locations x and y, which allows us to write the dispersal kernels as difference kernels, i.e., $k_i(x,y) = k_i(x-y)$. Finally, I will only consider cases in which $\Omega_m \cap \Omega_n \neq \emptyset$, so that interaction between the two populations is possible.

2.2.2 Habitat

I outline three different representations of habitat, with increasing model complexity. I begin with the simplest case, with two species occupying the same stationary patch.

Model 1: a stationary patch of habitat

Let us represent habitat as a stationary patch of length L, so that $\Omega_m = \Omega_n = [0,\, L]$ and $c = 0$. This yields the system

$$M_{t+1}(x) = \int_0^L \frac{k_m(x-y)\lambda_m M_t(y)}{1 + \alpha_m M_t(y) + \beta_m N_t(y)}\, dy, \tag{2.13}$$

$$N_{t+1}(x) = \int_0^L \frac{k_n(x-y)\lambda_n N_t(y)}{1 + \alpha_n N_t(y) + \beta_n M_t(y)}\, dy, \tag{2.14}$$

or, more succinctly,

$$M_{t+1}(x) = \int_0^L k_m(x-y) f[M_t(y), N_t(y)]\, dy, \tag{2.15}$$

$$N_{t+1}(x) = \int_0^L k_n(x-y) g[M_t(y), N_t(y)]\, dy. \tag{2.16}$$

If the populations are able to coexist over time, then we may expect each population to eventually settle at a stable distribution. I will denote the limiting distributions of M and N as $M^*(x)$ and $N^*(x)$, respectively. Without specifying kernels k_m and k_n, it is not possible to find an explicit solution for this system. Instead, I will derive approximations of the average population densities $\overline{M^*}$ and $\overline{N^*}$ of $M^*(x)$ and $N^*(x)$, which I will in turn use to approximate persistence criteria.

Van Kirk and Lewis (1997) defined the average dispersal success S of a population on a domain Ω as

$$S = \frac{1}{|\Omega|} \int_\Omega \int_\Omega k(x,y)\, dy\, dx, \tag{2.17}$$

where $|\Omega|$ represents the length of Ω. This approximation averages across the spatial

aspects of the kernel to give a number that reflects the proportion of propagules that stay inside the domain after a single dispersal event. I will use (2.17) to simplify (2.15) and (2.16), reducing the spatial population densities to their means.

I begin by averaging the populations $M_t(x), N_t(x)$ over the patch of habitat, which I denote as

$$\overline{M}_t = \frac{1}{L}\int_0^L M_t(x)\,dx, \tag{2.18}$$

$$\overline{N}_t = \frac{1}{L}\int_0^L N_t(x)\,dx. \tag{2.19}$$

Applying this average to both sides of (2.15) and (2.16) yields

$$\frac{1}{L}\int_0^L M_{t+1}(x)\,dx = \frac{1}{L}\int_0^L\int_0^L k_m(x-y)f[M_t(y),N_t(y)]\,dy\,dx, \tag{2.20}$$

$$\frac{1}{L}\int_0^L N_{t+1}(x)\,dx = \frac{1}{L}\int_0^L\int_0^L k_n(x-y)g[M_t(y),N_t(y)]\,dy\,dx. \tag{2.21}$$

If the respective differences between the nonzero equilibriums $M^*(x), N^*(x)$ and the spatial averages $\overline{M}_t, \overline{N}_t$ of $M_t(x), N_t(x)$ are small, then the first terms of the Taylor expansions of f and g about $\overline{M}_t, \overline{N}_t$ suggest that

$$f[M_t(y),N_t(y)] \approx f[\overline{M}_t,\overline{N}_t], \tag{2.22}$$

$$g[M_t(y),N_t(y)] \approx g[\overline{M}_t,\overline{N}_t]. \tag{2.23}$$

(See Lutscher and Lewis (2004) for a more thorough treatment of this approximation). Substituting these approximations into (2.20) and (2.21) yields

$$\frac{1}{L}\int_0^L M_{t+1}(x)\,dx \approx f\left[\overline{M}_t,\overline{N}_t\right]\frac{1}{L}\int_0^L\int_0^L k_m(x-y)\,dy\,dx, \tag{2.24}$$

$$\frac{1}{L}\int_0^L N_{t+1}(x)\,dx \approx g\left[\overline{M}_t,\overline{N}_t\right]\frac{1}{L}\int_0^L\int_0^L k_n(x-y)\,dy\,dx, \tag{2.25}$$

which simplifies to

$$\overline{M}_{t+1} \approx S_m \cdot f\Big[\overline{M}_t, \overline{N}_t\Big], \tag{2.26}$$

$$\overline{N}_{t+1} \approx S_n \cdot g\Big[\overline{M}_t, \overline{N}_t\Big], \tag{2.27}$$

where S_m, S_n are the average dispersal success of species M and N, respectively. More explicitly, we have

$$\overline{M}_{t+1} \approx \frac{S_m \lambda_m \overline{M}_t}{1 + \alpha_m \overline{M}_t + \beta_m \overline{N}_t}, \tag{2.28}$$

$$\overline{N}_{t+1} \approx \frac{S_n \lambda_n \overline{N}_t}{1 + \alpha_n \overline{N}_t + \beta_n \overline{M}_t}. \tag{2.29}$$

This system has four fixed points at

$$P_0 = (0, 0), \tag{2.30}$$

$$P_M = \left(\frac{S_m \lambda_m - 1}{\alpha_m}, 0\right), \tag{2.31}$$

$$P_N = \left(0, \frac{S_n \lambda_n - 1}{\alpha_n}\right), \tag{2.32}$$

$$\begin{aligned} P_B = {} & (M^*, N^*) \\ = {} & \left(\frac{\alpha_n(S_m\lambda_m - 1) - \beta_m(S_n\lambda_n - 1)}{\alpha_m\alpha_n - \beta_m\beta_n}, \right. \\ & \left. \frac{\alpha_m(S_n\lambda_n - 1) - \beta_n(S_m\lambda_m - 1)}{\alpha_m\alpha_n - \beta_m\beta_n}\right) \end{aligned} \tag{2.33}$$

P_B is asymptotically stable when

$$\frac{S_n \lambda_n - 1}{\alpha_n} < \frac{S_m \lambda_m - 1}{\beta_m} \tag{2.34}$$

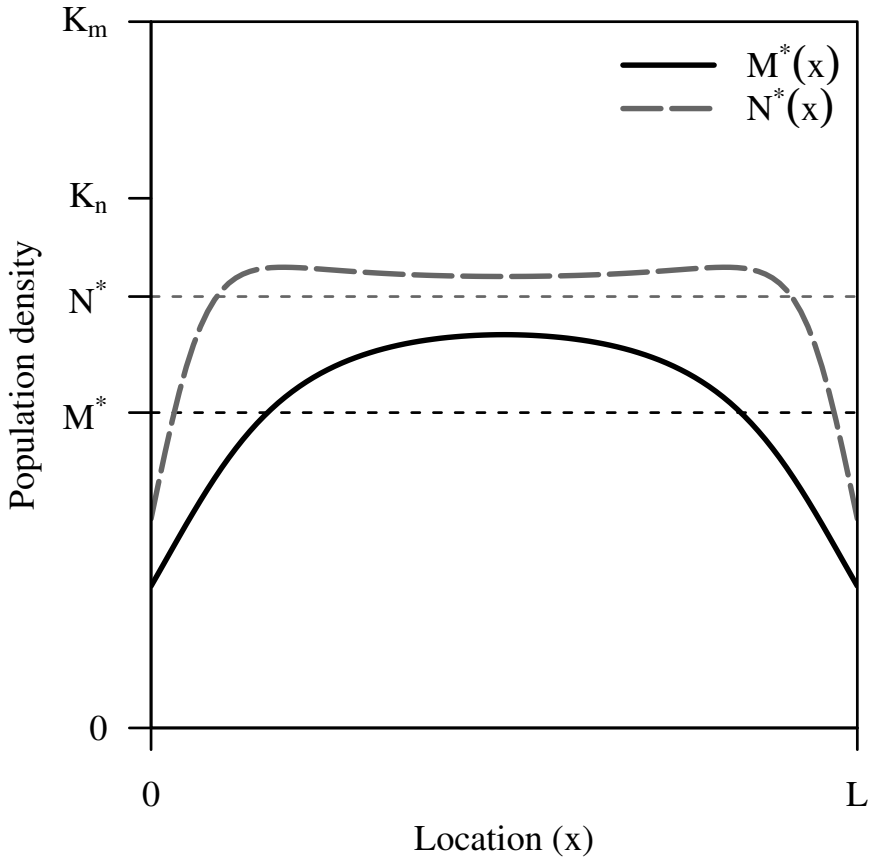

Figure 2.2: Equilibrium distributions $M^*(x)$ (black) and $N^*(x)$ (grey) of (2.15) and (2.16) with $\lambda_1 = 2.2$, $\lambda_2 = 2.5$, $K_m = 80$, $K_n = 60$, $\beta_m = 0.1$, $\beta_n = 0.005$, and assuming Gaussian dispersal kernels for $k_m(x-y)$, $k_n(x-y)$ with $\sigma_m = 1$ and $\sigma_n = 0.5$. Approximations M^* and N^* in (2.33) provide estimates of the average population densities.

and

$$\frac{S_m\lambda_m - 1}{\alpha_m} < \frac{S_n\lambda_n - 1}{\beta_n}, \tag{2.35}$$

which is similar in form to the conditions of stability for the nontrivial fixed point of the Leslie-Gower model described in (2.7) and (2.8), but with the addition of the dispersal success parameters S_m and S_n. A proof of the stability of P_B is offered in Appendix I.

An illustration of mutual stable coexistence can be seen in Figure 2.2. Although species M has a higher carrying capacity ($K_m = 80$) than species N ($K_n = 60$), N has a higher rate of reproduction ($\lambda_n = 2.5$) and a stronger competitive edge ($\beta_n = 0.005$) than M ($\beta_m = 0.01$), both of which contribute to N having a higher average population density than M across the patch of habitat.

Model 2: a shifting patch of habitat

In this scenario, I consider two species occupying the same patch, which is now moving at a constant speed c, so that $\Omega_m = \Omega_n = [ct,\, L + ct]$. This yields the equations

$$M_{t+1}(x) = \int_{ct}^{L+ct} k_m(x-y) f[M_t(y), N_t(y)]\, dy, \tag{2.36}$$

$$N_{t+1}(x) = \int_{ct}^{L+ct} k_n(x-y) g[M_t(y), N_t(y)]\, dy. \tag{2.37}$$

If we wish to discuss persistence of the populations in the patch, it is useful to reparameterize our model to the reference frame of the moving patch rather than absolute location. Substituting $\overline{x} = x - ct$, $\overline{y} = y - ct$ into (2.36) and (2.37) and

shifting by c gives us

$$M_{t+1}(\overline{x}) = \int_0^L k_m(\overline{x} + c - \overline{y}) f[M_t(\overline{y}), N_t(\overline{y})]\, d\overline{y}, \tag{2.38}$$

$$N_{t+1}(\overline{x}) = \int_0^L k_n(\overline{x} + c - \overline{y}) g[M_t(\overline{y}), N_t(\overline{y})]\, d\overline{y}. \tag{2.39}$$

For the remainder of this paper I will drop the bars on $\bar{x}$ and $\bar{y}$ for notational convenience when referring to a shifting patch of habitat, with the understanding that x and y refer to locations in the shifting domain.

From the perspective of the patch, it is now apparent that kernels k_m, k_n become increasingly asymmetric with increasing c. Unfortunately, Van Kirk and Lewis (1997)'s average dispersal success approximation S in (2.17) does not provide accurate approximations of asymmetric kernels (Rinnan, 2018b). Rinnan (2018b) defined the geometric symmetrization of the average dispersal success as

$$GS = \frac{1}{|\Omega|} \int_\Omega \int_\Omega \sqrt{k(x + c - y)k(y + c - x)}\, dx\, dy, \tag{2.40}$$

and demonstrated that an IDE with kernel $k(x+c-y)$ has similar persistence criteria to an IDE with the symmetric kernel $\sqrt{k(x + c - y)k(y + c - x)}$. As a result, GS can be used in place of S to more accurately determine the persistence criteria of populations modeled with asymmetric dispersal. (It is worth noting that, in Model 1, GS could have been used in place of S as well, since $GS = S$ when $c = 0$.)

Applying GS to (2.38) and (2.39) and using similar methods of approximation as

in Model 1, we get

$$G_0 = (0, 0), \tag{2.41}$$

$$G_M = \left(\frac{GS_m\lambda_m - 1}{\alpha_m}, 0 \right), \tag{2.42}$$

$$G_N = \left(0, \frac{GS_n\lambda_n - 1}{\alpha_n} \right), \tag{2.43}$$

$$G_B = \left(\frac{\alpha_n(GS_m\lambda_m - 1) - \beta_m(GS_n\lambda_n - 1)}{\alpha_m\alpha_n - \beta_m\beta_n}, \right. \\ \left. \frac{\alpha_m(GS_n\lambda_n - 1) - \beta_n(GS_m\lambda_m - 1)}{\alpha_m\alpha_n - \beta_m\beta_n} \right). \tag{2.44}$$

Approximation (2.44) is nearly identical to the fixed point approximation (2.33) in Model 1, but G_B is now implicit functions of the shift speed c, since GS_m, GS_n are themselves functions of c, as shown in (2.40).

Following Leslie and Gower (1958), I find it helpful to define some parameters to simplify our notation a bit. First, let p, q be given by

$$p = \frac{GS_m\lambda_m - 1}{\alpha_m}, \tag{2.45}$$

$$q = \frac{GS_n\lambda_n - 1}{\alpha_n}, \tag{2.46}$$

which can be thought of as penalized carrying capacities that account for population loss due to dispersal. Note that if $GS_m = 1$, for example, indicating all individuals staying inside the patch after dispersal, then $p = (\lambda_m - 1)/\alpha_m = K_m$. Second, we define u and v such that

$$u = \frac{\beta_m\beta_n}{\alpha_m\alpha_n}, \tag{2.47}$$

$$v = \frac{\beta_m(GS_n\lambda_n - 1)}{\alpha_n(GS_m\lambda_m - 1)}, \tag{2.48}$$

where u can be seen as the ratio of the strengths of interspecific competition to in-

traspecific competition. v is more difficult to interpret intuitively, but will nonetheless prove useful for deriving persistence criteria, as we shall see. For now, I will rewrite the fixed points more succinctly as

$$G_0 = (0, 0), \tag{2.49}$$

$$G_M = (p, 0), \tag{2.50}$$

$$G_N = (0, q), \tag{2.51}$$

$$G_B = \left(p\left(\frac{1-v}{1-u}\right), q\left(\frac{1-u/v}{1-u}\right)\right). \tag{2.52}$$

Model 3: overlapping patches of shifting habitat

In this scenario each species has its own specialized habitat niche with some degree of overlap, allowing for interaction between the two populations. I denote the patches of habitat by

$$\Omega_m = [L_{m_1} + ct, L_{m_2} + ct], \tag{2.53}$$

$$\Omega_n = [L_{n_1} + ct, L_{n_2} + ct], \tag{2.54}$$

with $\Omega_m \cap \Omega_n \neq \emptyset$. I further assume that both habitats are shifting at the same rate c. The locations where the habitats do not overlap can now provide locations of possible refuge for each species, i.e., patches without competition from the other species (see Figure 2.3).

The growth functions f and g can now be written piecewise, so that

$$f[M_t(y), N_t(y)] = \begin{cases} \frac{\lambda_m M_t(y)}{1+\alpha_m M_t(y)}, & L_{m_1} < y \leq L_{n_1}, \\ \frac{\lambda_m M_t(y)}{1+\alpha_m M_t(y)+\beta_m N_t(y)}, & L_{n_1} < y \leq L_{m_2}, \end{cases} \tag{2.55}$$

$$g[M_t(y), N_t(y)] = \begin{cases} \frac{\lambda_n N_t(y)}{1+\alpha_n N_t(y)+\beta_n M_t(y)}, & L_{n_1} < y \leq L_{m_2}, \\ \frac{\lambda_n N_t(y)}{1+\alpha_n N_t(y)}, & L_{m_2} < y \leq L_{n_2}. \end{cases} \tag{2.56}$$

The system may now be rewritten as a disjoint sum of IDEs. In the example illustrated in 2.3, this takes the form

$$M_{t+1}(x) = \int_{L_{m_1}}^{L_{n_1}} \frac{k_m(x+c-y)\lambda_m M_t(y)}{1+\alpha_m M_t(y)}\, dy + \int_{L_{n_1}}^{L_{m_2}} \frac{k_m(x+c-y)\lambda_m M_t(y)}{1+\alpha_m M_t(y)+\beta_m N_t(y)}\, dy \tag{2.57}$$

$$N_{t+1}(x) = \int_{L_{n_1}}^{L_{m_2}} \frac{k_n(x+c-y)\lambda_n N_t(y)}{1+\alpha_n N_t(y)+\beta_n M_t(y)}\, dy + \int_{L_{m_2}}^{L_{n_2}} \frac{k_n(x+c-y)\lambda_n N_t(y)}{1+\alpha_n N_t(y)}\, dy, \tag{2.58}$$

where once again x and y represent locations from the frame of reference of the moving habitats.

I will make use of a basic property of integrals to rewrite GS_m, GS_n as disjoint sums as well. For an integrable function $f(x, y)$, define

$$F = \frac{1}{L}\int_0^L \int_0^L f(x,y)\, dx\, dy, \tag{2.59}$$

$$F_1 = \frac{1}{a}\int_0^a \int_0^L f(x,y)\, dx\, dy, \tag{2.60}$$

$$F_2 = \frac{1}{(L-a)}\int_a^L \int_0^L f(x,y)\, dx\, dy. \tag{2.61}$$

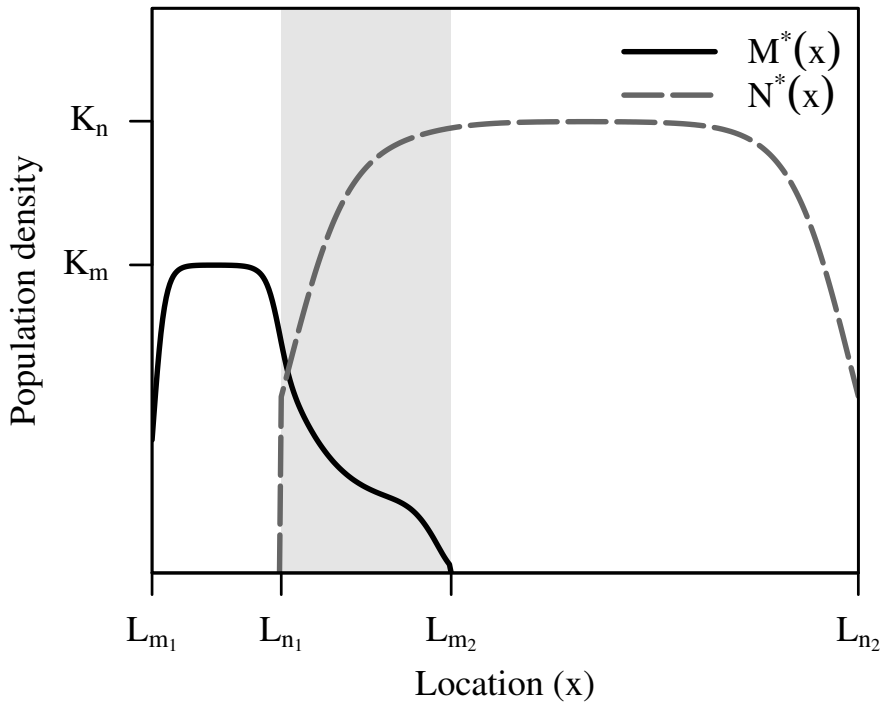

Figure 2.3: An illustration of equilibrium distributions $M^*(x)$ and $N^*(x)$ of Model 3 in Equations (2.57) and (2.58). The shaded area of the figure shows the region of habitat overlap where the two species interact. Outside of the shaded area, each species has patches of habitat that provide refuge from competition.

It follows that

$$F = \frac{a}{aL}\int_0^a \int_0^L f(x,y)\,dx\,dy + \frac{(L-a)}{(L-a)L}\int_a^L \int_0^L f(x,y)\,dx\,dy \tag{2.62}$$

$$= \frac{a}{L}F_1 + \frac{(L-a)}{L}F_2. \tag{2.63}$$

Applying (2.60) and (2.61) to $k_m(x,y)$, $k_n(x,y)$ yields

$$GS_{m_1} = \frac{1}{(L_{n_1} - L_{m_1})} \int_{L_{m_1}}^{L_{n_1}} \int_{L_{m_1}}^{L_{m_2}} f_m(x,y)\,dx\,dy, \tag{2.64}$$

$$GS_{m_2} = \frac{1}{(L_{m_2} - L_{n_1})} \int_{L_{n_1}}^{L_{m_2}} \int_{L_{m_1}}^{L_{m_2}} f_m(x,y)\,dx\,dy, \tag{2.65}$$

$$GS_{n_1} = \frac{1}{(L_{m_2} - L_{n_1})} \int_{L_{n_1}}^{L_{m_2}} \int_{L_{n_1}}^{L_{n_2}} f_n(x,y)\,dx\,dy, \tag{2.66}$$

$$GS_{n_2} = \frac{1}{(L_{n_2} - L_{m_2})} \int_{L_{m_2}}^{L_{n_2}} \int_{L_{n_1}}^{L_{n_2}} f_n(x,y)\,dx\,dy, \tag{2.67}$$

where $f_i(x,y) = \sqrt{k_i(x+c-y)k_i(y+c-x)}$. Denoting the proportions φ_m, φ_n of L_m and L_n in which interaction between the two species is possible as

$$\varphi_m = \frac{L_{m_2} - L_{n_1}}{L_m}, \tag{2.68}$$

$$\varphi_n = \frac{L_{m_2} - L_{n_1}}{L_n}, \tag{2.69}$$

I now write GS_m, GS_n as

$$GS_m = (1-\varphi_m)GS_{m_1} + \varphi_m GS_{m_2}, \tag{2.70}$$

$$GS_n = \varphi_n GS_{n_1} + (1-\varphi_n)GS_{n_2}. \tag{2.71}$$

Applying the same approximation methods as Model 2 then yields

$$\begin{aligned}\overline{M}_{t+1} = &\\ &\frac{1}{L_m}\int_{L_{m_1}}^{L_{m_2}}\int_{L_{m_1}}^{L_{n_1}} \frac{k_m(x+c-y)\lambda_m M_t(y)}{1+\alpha_m M_t(y)}\,dy + \\ &\frac{1}{L_m}\int_{L_{m_1}}^{L_{m_2}}\int_{L_{n_1}}^{L_{m_2}} \frac{k_m(x+c-y)\lambda_m M_t(y)}{1+\alpha_m M_t(y)+\beta_m N_t(y)}\,dy \qquad (2.72)\\ &\approx (1-\varphi_m)\frac{GS_{m_1}\lambda_m \overline{M}_t}{1+\alpha_m \overline{M}_t} + \varphi_m \frac{GS_{m_2}\lambda_m \overline{M}_t}{1+\alpha_m \overline{M}_t + \beta_m \overline{N}_t}, \qquad (2.73)\end{aligned}$$

and similarly,

$$\overline{N}_{t+1} \approx \varphi_n \frac{GS_{n_1}\lambda_n \overline{N}_t}{1+\alpha_n \overline{N}_t + \beta_n \overline{M}_t} + (1-\varphi_n)\frac{GS_{n_2}\lambda_n \overline{N}_t}{1+\alpha_n \overline{N}_t}. \tag{2.74}$$

Unfortunately, the coexistence equilibrium of equations (2.73) and (2.74) is prohibitively arduous to compute, and I cannot derive an explicit formula for M^* and N^* as I did with Models 1 and 2. Instead, I will make a few qualitative observations about the nature of the fixed point of interest.

First, we can see that (2.73) and (2.74) are bound above by the case of no interaction and bound below by the case of interaction across the entire domain (Model 2). Specifically, we have

$$\frac{GS_m\lambda_m \overline{M}_t}{1+\alpha_m \overline{M}_t + \beta_m \overline{N}_t} \leq \overline{M}_{t+1} \leq \frac{GS_m\lambda_m \overline{M}_t}{1+\alpha_m \overline{M}_t}, \tag{2.75}$$

$$\frac{GS_n\lambda_n \overline{N}_t}{1+\alpha_n \overline{N}_t + \beta_n \overline{M}_t} \leq \overline{N}_{t+1} \leq \frac{GS_n\lambda_n \overline{N}_t}{1+\alpha_n \overline{N}_t}. \tag{2.76}$$

These inequalities can also be shown by observing that $\frac{\partial GS_{m_1}}{\partial L_{n_1}} > 0$ and $\frac{\partial GS_{m_2}}{\partial L_{n_1}} < 0$ together imply

$$\frac{\partial M_{t+1}}{\partial L_{n_1}} = \frac{1}{L_m}\frac{GS_{m_1}\lambda_m \overline{M}_t}{1+\alpha_m \overline{M}_t}\frac{\partial GS_{m_1}}{\partial L_{n_1}} - \tag{2.77}$$

$$\frac{1}{L_m}\frac{GS_{m_2}\lambda_m \overline{M}_t}{1+\alpha_m \overline{M}_t + \beta_m \overline{N}_t}\frac{\partial GS_{m_2}}{\partial L_{n_1}} \tag{2.78}$$

$$> 0, \tag{2.79}$$

and similarly, $\frac{\partial GS_{n_1}}{\partial L_{m_2}} > 0$ and $\frac{\partial GS_{n_2}}{\partial L_{m_2}} < 0$ collectively imply $\frac{\partial N_{t+1}}{\partial L_{m_2}} > 0$.

At equilibrium, (2.75) and (2.76) become

$$\frac{GS_m\lambda_m M^*}{1+\alpha_m M^*+\beta_m N^*} \leq M^* \leq \frac{GS_m\lambda_m M^*}{1+\alpha_m M^*}, \tag{2.80}$$

$$\frac{GS_n\lambda_n N^*}{1+\alpha_n N^*+\beta_n M^*} \leq N^* \leq \frac{GS_n\lambda_n N^*}{1+\alpha_n N^*}. \tag{2.81}$$

Rearranging (2.80) and (2.81), let us denote the upper and lower bounds of M^* and N^* by the equations

$$l_m: \qquad N = \frac{GS_m\lambda_m - \alpha_m M - 1}{\beta_m}, \tag{2.82}$$

$$u_m: \qquad M = \frac{GS_m\lambda_m - 1}{\alpha_m} = p, \tag{2.83}$$

$$l_n: \qquad M = \frac{GS_n\lambda_n - \alpha_n N - 1}{\beta_n}, \tag{2.84}$$

$$u_n: \qquad N = \frac{GS_n\lambda_n - 1}{\alpha_n} = q. \tag{2.85}$$

Plotting these bounds in M, N-space, we may visualize the regions of space that satisfy (2.80) and (2.81), corresponding to values of (M^*, N^*) that result in coexistence (see Figure 2.4). In particular, we see that the two populations at equilibrium will never be larger than what each can obtain in the absence of interaction with the other.

Second, since φ_m, $\varphi_n > 0$ by assumption, (2.73) and (2.74) at equilibrium can be arranged to get

$$M^* = \frac{(GS_n\lambda_n - 1 - \alpha_n N^*)(1+\alpha_n N^*)}{\beta_n(1+\alpha_n N^* - (1-\varphi_n)GS_{n_2}\lambda_n)}, \tag{2.86}$$

$$N^* = \frac{(GS_m\lambda_m - 1 - \alpha_m M^*)(1+\alpha_m M^*)}{\beta_m(1+\alpha_m M^* - (1-\varphi_m)GS_{m_1}\lambda_m)}. \tag{2.87}$$

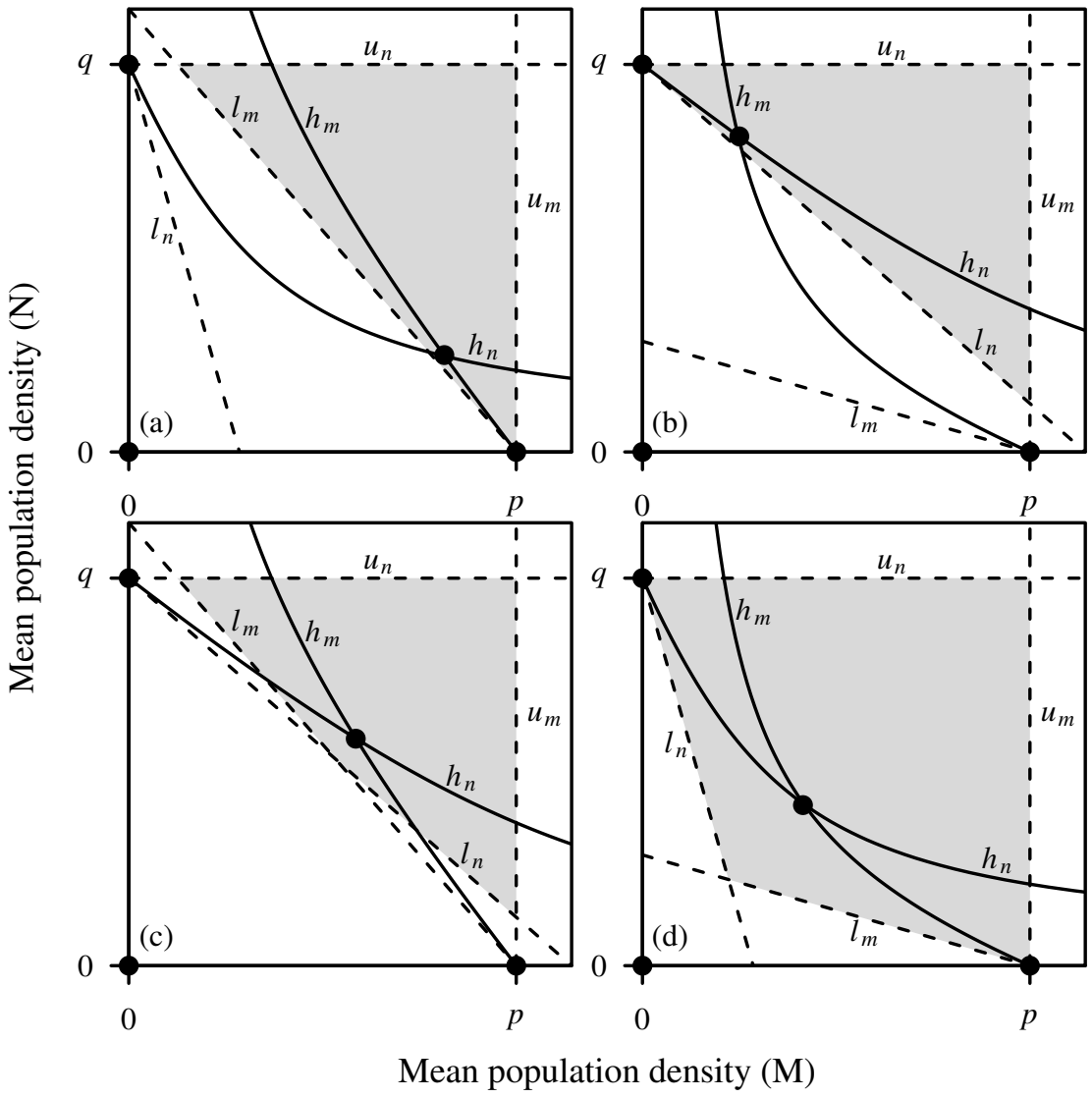

Figure 2.4: Regions of potential stability of Model 3, assuming $p, q > 0$ and (a) $v < u$, $v < 1$; (b) $u < v$, $v > 1$; (c) $u < v < 1$; and (d) $1 < v < u$. Shaded regions of M, N-space correspond to values of M and N that satisfy inequalities (2.80) and (2.81). The fixed point (M^*, N^*) is given by the intersection of the hyperbolas h_m and h_n, defined in (2.88) and (2.89), and can be located anywhere inside the shaded regions, depending on the shapes of h_m and h_n.

Rewriting these as

$$h_m : \qquad N = \frac{(GS_m\lambda_m - 1 - \alpha_m M)(1 + \alpha_m M)}{\beta_m(1 + \alpha_m M - (1 - \varphi_m)GS_{m_1}\lambda_m)}, \tag{2.88}$$

$$h_n : \qquad M = \frac{(GS_n\lambda_n - 1 - \alpha_n N)(1 + \alpha_n N)}{\beta_n(1 + \alpha_n N - (1 - \varphi_n)GS_{n_2}\lambda_n)}, \tag{2.89}$$

h_m and h_n define two hyperbolas in M, N-space, intersecting at the fixed point (M^*, N^*) (see Figure 2.4), and with asymptotes

$$a_m = \frac{(1 - \varphi_m)GS_{m_1}\lambda_m - 1}{\alpha_m}, \tag{2.90}$$

$$a_n = \frac{(1 - \varphi_n)GS_{n_2}\lambda_n - 1}{\alpha_n}. \tag{2.91}$$

2.3 Results

2.3.1 Persistence criteria

When $\Omega_m = \Omega_n$ (Models 1 and 2), there are four possible outcomes for our model: mutual extirpation, species M survives, species N survives, or mutual survival. These outcomes are summarized in Figure 2.5 and Figure 2.6.

Outcome I: mutual extirpation

Survival of species M and N depends first and foremost on their respective abilities to keep pace with the speed of climate change. When $GS_i\lambda_i < 1$, the growth rate of species i is not large enough to compensate for the population loss through dispersal and the speed of climate change, and species i will go extinct. Mutual extirpation occurs when $GS_m\lambda_m < 1$ and $GS_n\lambda_n < 1$, or equivalently, when $p < 0$ and $q < 0$, with p, q as defined in equations (2.45) and (2.46).

Outcome II: M outcompetes N

Two scenarios can lead to species M surviving over species N. In the first, we have $p > 0$, $q < 0$. Species N cannot keep pace with the speed of climate change, and dies out. This simplifies to a one-dimensional shifting habitat IDE model, with species M experiencing Beverton-Holt population growth in the absence of species N.

In the second scenario, we have $p > 0$, $q > 0$ and $u > v$, $v < 1$, with u, v as defined in equations (2.47) and (2.48). Both species can keep pace with the shifting climate, but species M will outcompete species N.

Outcome III: N outcompetes M

Again, there are two possible scenarios in which species N can survive and M cannot. In the first, $p < 0$, $q > 0$, species M cannot keep pace with the shifting habitat and species N can. In the second, $p > 0$, $q > 0$ and $u < v$, $v > 1$, and species N outcompetes species M.

Outcome IV: mutual survival

In order for mutual survival to occur, we must have $p > 0$, $q > 0$ and $u < v < 1$. In this situation, both species can keep pace with the speed of climate change, and there is a stable equilibrium for both populations at the fixed point in equation (2.44). When $p > 0$, $q > 0$ and $u > v$ and $v > 1$, this fixed point is unstable (Leslie and Gower, 1958), which will ultimately result in outcome II or III, depending on the initial population densities.

2.3.2 Effects of climate change on competition

The speed of climate change c has the capacity to change the long-term outcome of the system by shifting the equilibrium through a bifurcation. Since we have defined v as a function of both GS_m and GS_n, it is therefore implicitly a function of c.

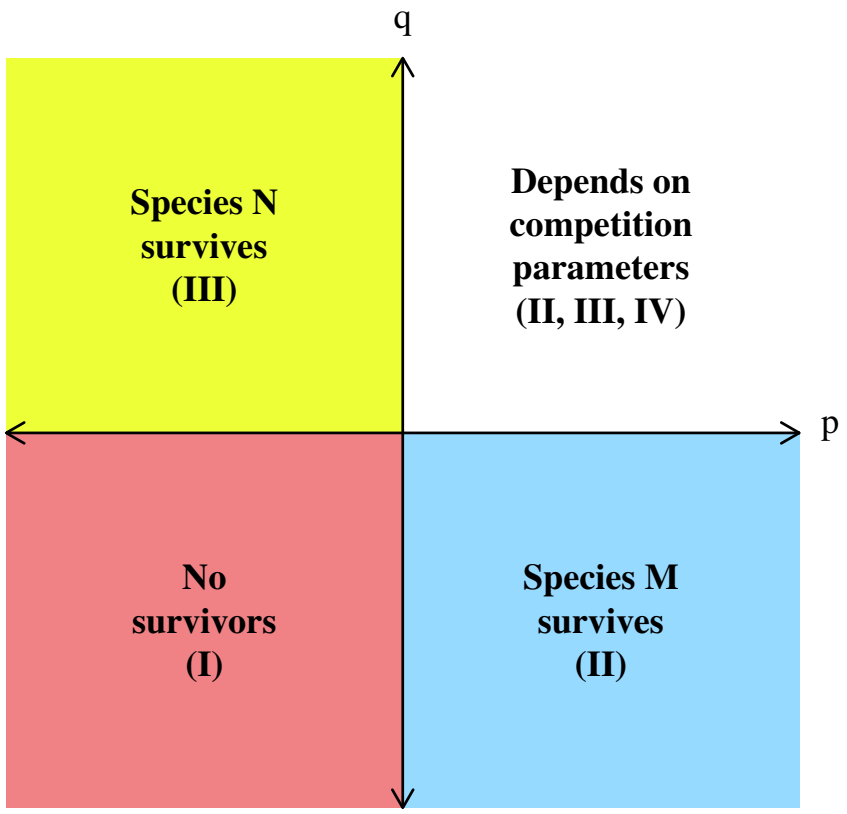

Figure 2.5: A delineation of p, q-space, illustrating the approximated outcome for Models 1 and 2. If the growth rate of a species is sufficient to replace the population lost due to the speed of climate change, then the species can survive.

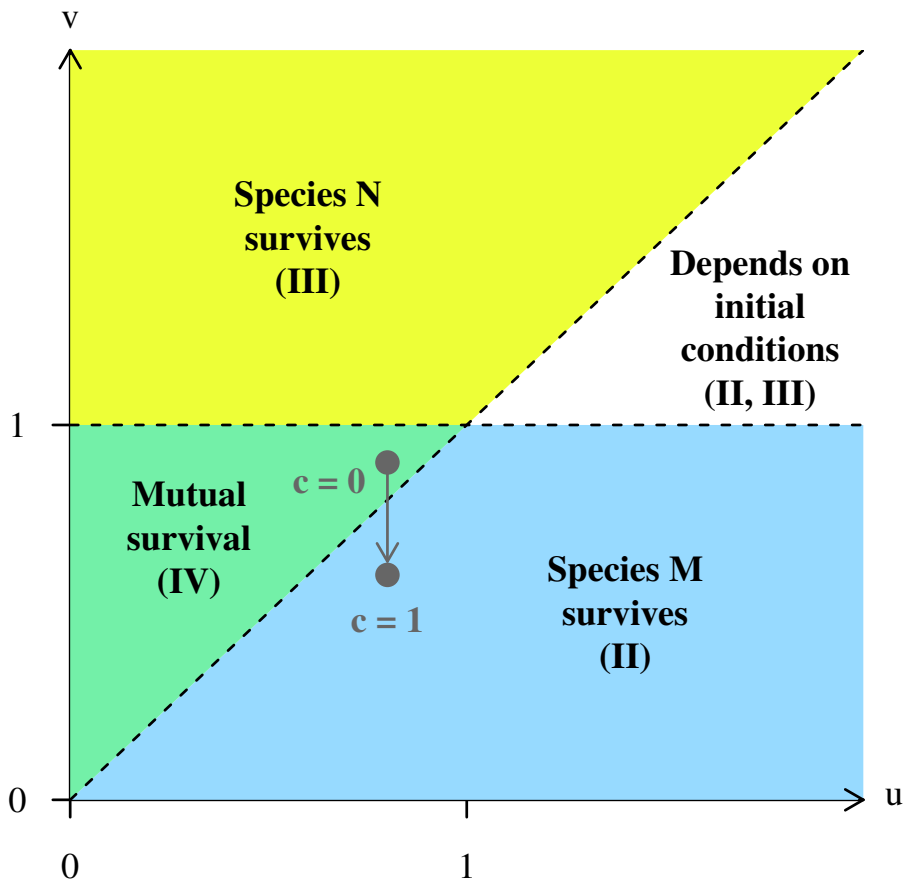

Figure 2.6: A delineation of u, v-space, illustrating the approximated outcome for Models 1 and 2, assuming $p > 0$ and $q > 0$. A hypothetical case is shown (grey) to illustrate the effects of the speed of climate change, predicting mutual survival when $c = 0$, but species M outcompeting species N when $c = 1$.

Holding all other parameters constant, as the value of c changes, the fixed point of the system may move up or down vertically parallel to the v-axis (Figure 2.6). In certain cases, it is possible for c to change the outcome from mutual survival to one species outcompeting the other. This result illustrates the compounding effects of climate change and competition: even if a species is able to keep pace with a changing climate, its capacity to compete with other species may be weakened, which may lead to qualitatively different outcomes compared to competing with the same species in a static climate.

2.3.3 Effects of refuge habitat

When a species has habitat in which they do not experience competition (Model 3), this habitat may act as a stable island for a source population, which can replenish losses incurred from competition in sufficiently nearby populations. If $\varphi_m = \varphi_n = 1$ (representing interaction between M and N across the entire domain, as in Model 2), (2.86) and (2.87) reduces to

$$M^* = \frac{GS_n\lambda_n - 1 - \alpha_n N^*}{\beta_n}, \tag{2.92}$$

$$N^* = \frac{GS_m\lambda_m - 1 - \alpha_m M^*}{\beta_m}, \tag{2.93}$$

which can be solved to get the coexistence fixed point G_B of Model 2, as expected. As the amount of refuge for species M increases (i.e., as φ_m decreases), the value of the asymptote a_m in (2.90) increases, which in turn increases the average population density at equilibrium of M. A similar pattern of behavior can be seen in N.

Figure 2.4(a) shows that in conditions that lead to M outcompeting N in Model 2 ($u > v$, $v < 1$), it is possible for M and N to coexist if there is sufficient refuge habitat for N. Figure 2.4(b) similarly shows that conditions that lead to N outcompeting M in Model 2 can result in coexistence in Model 3. Figure 2.4(d) shows that the conditions that lead to unstable coexistence in Model 2 ($1 < v < u$) may yield stable

coexistence in Model 3.

2.3.4 Accuracy

To quantify the accuracy of the persistence criteria described in subsection 2.3.1, I ran numerical simulations of Model 2 and compared the outcomes with those predicted by p, q, u, and v, with an unknown predicted outcome (either M or N surviving) when $v > 1$ and $u > v$. I generated 10,000 sets of random parameter values, with each parameter randomly drawn from a distribution that I judged to reflect biologically feasible values (see Table 2.1). I assumed Gaussian dispersal for both species. Numerical IDEs were then run for 100 time steps, using the randomly generated parameter values. If the mean densities of the resulting populations were at least one-tenth the carrying capacity of the species, then the population was recorded as persisting, and extirpated otherwise. This threshold choice will inevitably affect model performance, so I also tested a range of other threshold values. Minimum viable population size is highly context-specific, and there is no general rule of thumb that applies broadly across taxa (Traill et al., 2007). Some species may be able to recover from extremely low population densities given the chance, while others may not (Hilborn et al., 2014). Populations with low densities generally have a heightened risk of extinction, though, due to vulnerability to stochastic events (Goodman, 1987), lack of genetic diversity (Soule and Wilcox, 1980), and Allee effects (Courchamp et al., 1999).

I also tested the effects of refuge habitat by running 10,000 simulations with the same sets of parameter values as Model 2, but with an amount of overlap between the two habitats determined by random draw. I then compared the differences in observed outcomes between Models 2 and 3. All numerical simulation and analysis was conducted in R (R Core Team, 2017), and this code is provided in Appendix II.

The persistence criteria described in subsection 2.3.1 correctly predicted the outcome of Model 2 in 95.2% of the simulations. Approximately 38% of the models ended with mutual extinction, 29% with M surviving over N, 29% with N surviving over M,

Table 2.1: Parameter values and prior distributions that were used for numerical simulations of Models 2 and 3, assuming Gaussian dispersal. I assumed that $L_m = L_n$.

Growth rate	λ_m, λ_n	Exp(2) + 1
Dispersal distance	σ_m, σ_n	Lognormal(0.5, 0.5)
Intraspecific competition	α_m, α_n	Lognormal(-2, 1)
Interspecific competition	β_m, β_n	Exp($1/\alpha_i$)
Habitat size	L_m, L_n	10 - Exp(1.5)
Overlap (Model 3)	φ_m, φ_n	Uniform(0, 1)
Speed of climate change	c	Exp(1)

and 5% with mutual survival. Of the 593 unknown (M or N) or incorrectly predicted outcomes, 111 had outcomes that matched the predictions of one species outcompeting the other dependent on initial conditions; another 391 may have been attributable to the effects of transient population dynamics, with one or both species going extinct before the populations were able to reach the predicted equilibrium. Model 3 had 341% more instances of mutual survival than Model 2, due to the availability of refuge habitat. Table 2.2 compares the predicted outcomes with the observed outcomes, and provides basic summary statistics.

The choice of threshold used to define extinction had a noticeable impact on the accuracy of the model predictions (see Figure 2.7). Overall accuracy (i.e., the proportion of correctly predicted outcomes) and Cohen's Kappa (takes into account the possibility of correctly predicting outcomes by chance) were both highest around a threshold of 5% of carrying capacity K, with an accuracy of 0.962 and Kappa of 0.945. All thresholds between 1% and 16% of K had an overall accuracy and Kappa above 0.9. This suggests that model predictions will remain accurate for species with a wide range of sensitivities to low population densities.

Table 2.2: (a) Predicted vs. observed survival outcomes for 10,000 numerical simulations of Model 2. Each simulation was run for 100 time steps with a different set of randomly chosen parameter values. Bold numbers indicate agreement between model predictions and observations. Starred numbers indicate incorrect model predictions in which transient dynamics may have had an effect on the observed outcome. Predictions of "M or N" were excluded from the calculations of performance metrics. (b) Total observed outcomes for Models 2 and 3. Bold numbers indicate agreement between models, and italic numbers indicate cases in which the presence of refuge habitat resulted in mutual survival that would not otherwise occur.

(a) Model 2

Predicted survival	**Observed survival**			
	None	M	N	Both
None	**3501**	26	13	0
M	140*	**2725**	17*	18
N	124*	16*	**2752**	27
Both	5	51*	43*	**429**
M or N	2	45	66	0
Sensitivity	0.929	0.967	0.974	0.905
Specificity	0.994	0.975	0.976	0.989
Precision	0.989	0.940	0.943	0.812
Prevalence	0.381	0.285	0.286	0.048
Balanced Accuracy	0.961	0.971	0.975	0.947
Overall accuracy	0.952			
Cohen's Kappa	0.930			

(b) Observed survival

Model 3	**Model 2**			
	None	M	N	Both
None	**3710**	4	0	0
M	24	**2235**	0	0
N	38	13	**2377**	8
Both	0	*611*	*514*	**466**

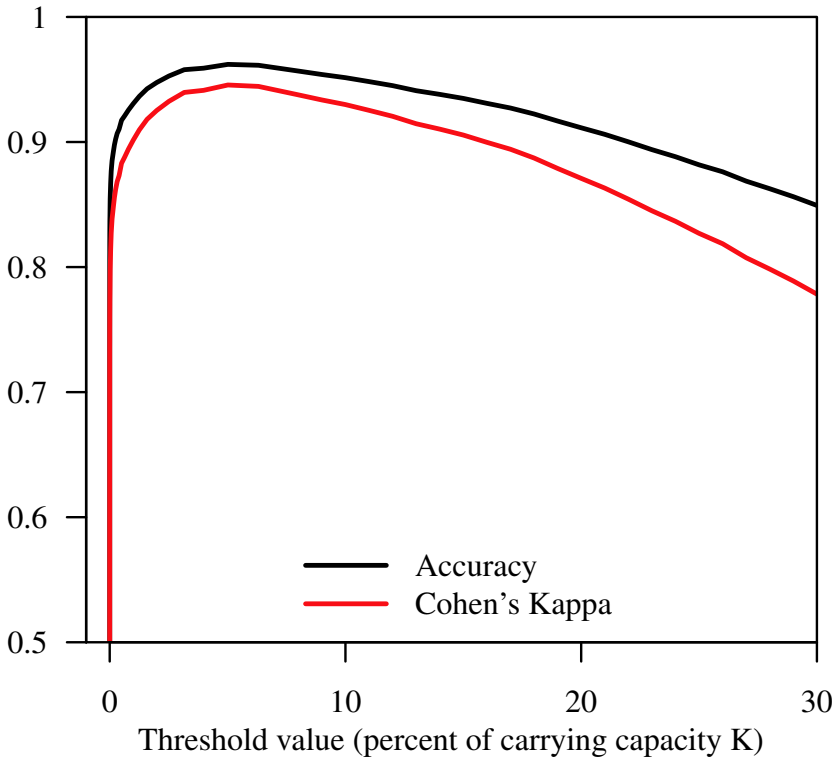

Figure 2.7: Overall accuracy (black) and Cohen's Kappa (red) of Model 2 as a function of the threshold value used to determine whether a species persisted or went extinct. Overall accuracy is calculated as the proportion of correctly predicted outcomes.

2.4 An application to populations of competing trout

I provide an illustration of Model 3 with two hypothetical populations of competing trout species, in a river that is warming due to climate change. I attempted to use realistic parameter values where possible, but I caution the reader against overinterpreting the results; this example is intended to illustrate the dynamics of species interaction and the effects of climate change, but should not be construed as a model for real populations (Real and Levin, 1991).

Bull trout (*Salvelinus confluentus*) is a salmonid that thrives in clear, cold moun-

tain streams in the Pacific Northwest. Bull trout tolerate a relatively small range of water temperatures, preferring mean summer temperatures below 13°C (US Fish and Wildlife Service and others, 2008; Isaak et al., 2015). They are currently recognized as threatened under the Endangered Species Act, due to loss and degradation of spawning habitat, increasing numbers of barriers to migration such as dams, and increasing competition from nonnative species (Nakano et al., 1998; Gunckel et al., 2002). The invasive brook trout (*S. fontinalis*) is one such species – intentionally introduced as a recreational fishing species in the late 1800s (Dunham et al., 2002) – with many similar habitat requirements as bull trout, but much more tolerant of warm water, thriving in temperatures up to 22°C (Dunham et al., 2002).

The undammed Salmon River in central Idaho provides ideal salmonid habitat, stretching 684 kilometers through sparsely populated mountainous terrain, and spanning the thermal tolerances of both species. I used the NorWeST stream temperature database downscaled to a 200m resolution to obtain a mean August stream temperature profile for 2011 and a projected future profile based on global climate model ensemble averages that represent the A1B warming trajectory for 2080s (2070-2099) (Isaak et al., 2011).

I used carrying capacities of 5.1 fish/200m and 15 fish/200m for bull and brook trout, respectively, which reflect mean population densities observed via snorkeling surveys conducted by the Idaho Department of Fish and Game (Levin et al., 2002; High et al., 2008). Growth rates of $\lambda_m = 1.09$ and $\lambda_n = 1.1$ were similarly estimated (Adams, 1999; High et al., 2008).

I modeled dispersal with Laplace kernels with mean dispersal distances of 1km for bull trout and 200m for brook trout (Hutchings and Gerber, 2002), representing populations with relatively high site fidelity. A number of studies have found success at modeling fish dispersal with mixture kernels, a linear combination of two kernels that collectively represent the sedentary and mobile dispersal processes commonly observed in stream networks (Skalski and Gilliam, 2000; Rodríguez, 2010). There

is evidence of long-distance dispersal ability in both bull and brook trout (Dunham et al., 2002; US Fish and Wildlife Service and others, 2008), but I opted not to use mixture kernels here, as this would have introduced several new parameters to the model, with no population data to support their estimation.

Competition coefficients are notoriously hard to quantify from observational field studies (Pfister, 1995); Gunckel et al. (2002) noted that bull trout appear to demonstrate a competitive advantage over the invasive brook trout when interacting directly, but Nakano et al. (1998) found no significant difference between the two. Thus, I explored model outcomes for a variety of scenarios, using 1681 ordered pairs of β_m and β_n with values ranging between 0 and 1.

I simulated populations of bull and brook trout by populating each 200m segment of the Salmon River with both species at carrying capacity for any segment that was in the thermal tolerance of each species. This gave initial population densities $m_{b0}(x)$ and $n_{b0}(x)$ (Figure 2.8a). I then allowed the populations to grow, disperse, and interact according to the dynamics specified in (2.57) and (2.58) for 100 generations with speed of climate change $c = 0$. This allowed the two populations to reach an equilibrium, minimizing the influence of potential transient dynamics. The resulting densities $m_{b100}(x)$ and $n_{b100}(x)$ (Figure 2.8b) were then used as the initial population densities $M_1(x)$ and $N_1(x)$ for the year 2011, and propagated for a period of 70 years to get $M_{70}(x)$ and $N_{70}(x)$ (Figure 2.8c) with $c = 0.0377°\text{C/yr}$, reflecting the predicted mean annual increase in temperature between 2011–2080 (Isaak et al., 2011).

In all cases, bull trout were heavily impacted by warming river temperature, displaced upstream by more than 30km. In cases where β_n was approximately less than $\frac{1}{3}\beta_m$, bull trout displayed a significant initial competitive advantage over brook trout, and brook trout were prevented from populating the river where bull trout were present. Despite this advantage, brook trout were able to maintain a population due to the downstream warmer water refuge that the bull trout could not occupy. As the river warmed and bull trout were displaced to higher elevations, the brook

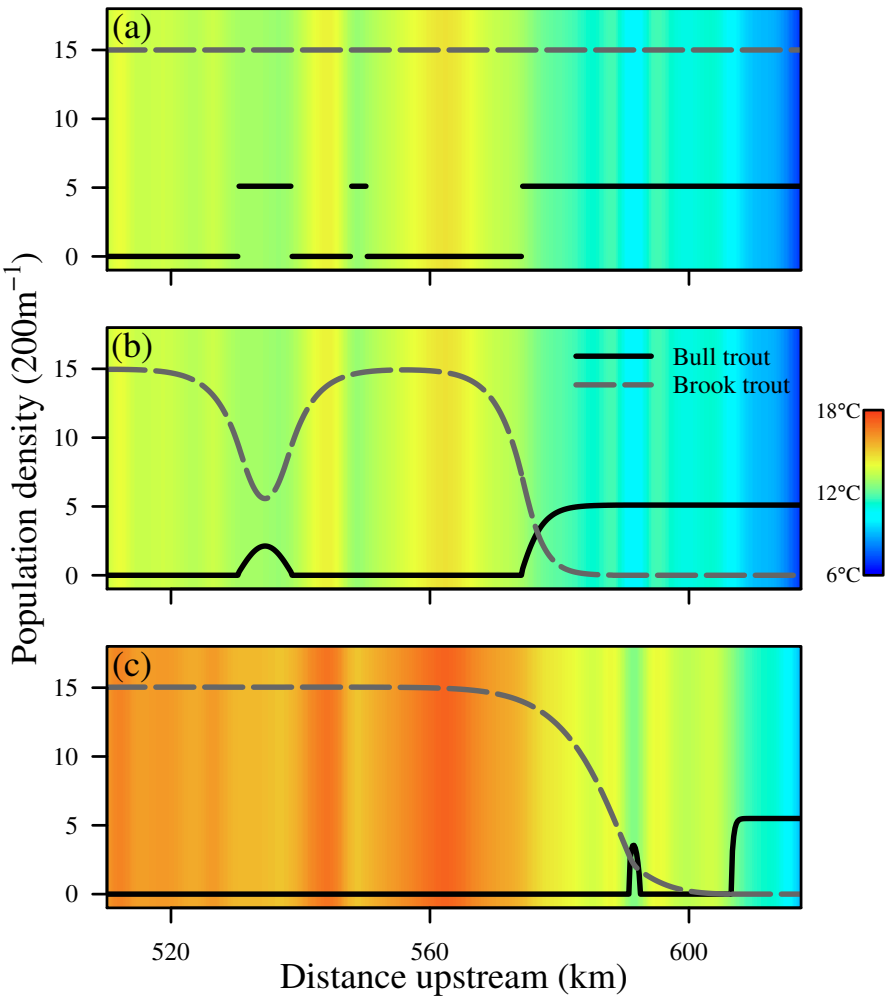

Figure 2.8: Population distributions of bull (solid) and brook (dashed) trout for competition coefficients $\beta_m = 0.08, \beta_n = 0.01$. (a) shows the initial densities $m_{b0}(x)$ and $n_{b0}(x)$ at carrying capacities $K_m = 5.1$, $K_n = 15$; (b) shows the densities $m_{b100}(x)$ and $n_{b100}(x)$ at equilibrium after 100 time steps with $c = 0$ used as initial population densities $M_1(x)$ and $N_1(x)$ beginning in 2011; (c) shows $M_{70}(x)$ and $N_{70}(x)$ for 2080, after an average warming of $c = 0.0377°$ C/yr.

trout slowly replaced them at a pace determined by their dispersal ability. When β_n was approximately greater than $\frac{1}{3}\beta_m$, brook trout were able to outcompete bull trout, and the bull trout were displaced from the river by the end of the burn-in period. Our model suggests that bull trout will likely be extirpated from the Salmon River by the beginning of the 22nd century if temperature increases continue on a similar trajectory as the 2080 projections.

2.5 Discussion

The speed of climate change c plays a critical role in the long-term stability of the two-species system. For variables u and v defined in Equations (2.47) and (2.48), u is a function of the competition parameters, whereas v is also a function of c. Given parameters such that $0 < u < 1$, different values of c could lead to species M outcompeting N, species N outcompeting M, or both persisting. In all but the simplest cases, an analytic formula for the critical speed c^* at which a species is no longer able to persist does not exist (Zhou and Kot, 2011). Rinnan (2018b) demonstrated how to approximate the critical speed of a single-species model using geometric symmetrization, and we demonstrated that this method can likewise be used to gain insight into multiple-species systems.

Although our model explicitly accounts for growth, dispersal, and competition, the mathematical representations of these processes are highly simplistic compared to the complex ecology of real-life organisms and their environment, and a number of caveats are worth mentioning.

At the continental scale, population distributions are largely determined by climate processes (Pearson and Dawson, 2003). At the scale of the individual, however, habitat selection can be strongly influenced by other processes such as spatial heterogeneity, resource availability, and environmental stochasticity. Our model delineates suitable habitat by thermal tolerances alone, but this is no doubt overly simplistic from the perspective of an individual organism. Kareiva (1982) found that habitat

heterogeneity led to different rates and patterns of dispersal in flea beetles, and there is good reason to believe that the same behavior could be found in trout species, due to their preferential selection of areas with vegetative cover or deep pools.

Similarly, our model assumes thoroughly homogeneous populations. In reality, demographic stochasticity will create different tolerances and reactions to changes in climate (Selong et al., 2001). Indeed, adaptation can be a very effective response to climate change, and adaptive processes such evolution and phenotypic plasticity likely play an equally important role as dispersal. Accounting for adaptation in this context is difficult, in large part due to its unpredictability. Phillips and Kot (2015) explored persistence in a two-dimensional moving habitat model. By imagining a specific phenotypic response to climate change as a dimension in which individuals disperse in each generation, one could conceivably use two-dimensional methods to model species dispersal in geographic space as well as phenotypic space.

Species interactions are complex and varied, and are often not simply a matter of competitive exclusion. The impacts of brook trout on bull trout populations, for example, are not just limited to resource pressures; hybridization between the two species has negatively impacted bull trout as well. Moreover, interactions are often not limited to just one competing species. Bull and brook trout are both sympatric with cutthroat trout, *Oncorhynchus clarkii*, and there is considerable evidence that brook trout have caused significant declines in cutthroat trout populations (Nakano et al., 1998; Dunham et al., 2002). The model can be generalized to accommodate hybridization or a greater number of species with a numerical modeling approach, but will likely not offer insight comparable to the analytic results we derived for the simpler two-species model. Nor or interactions constant through time and space, as the parameters β_m, β_n suggest. A more realistic model might describe competition strength as a function of habitat quality.

Finally, climate change is represented in our model as a simple linear increase in temperature. In reality, there is considerable variation in climate patterns year to year,

and decade to decade. In mountain streams, the quality of habitat is influenced by drought, snowpack, and forest fires (Isaak et al., 2010). Some amount of temperature variability could be introduced to the model by drawing values of the speed of climate change c at each time step from a specified distribution.

Although my analysis involved several approximations and simplifications, the delineation of parameter space nonetheless provides a relatively high degree of accuracy and predictive power. It is important to recognize, however, that this approach only predicts model *outcome*, and in the process, loses many interesting characteristics of the model itself. There is undoubtedly a great deal more to study regarding the size and spatial distributions of the populations themselves — as we glimpsed in the example of competing species of trout — and such a study will require an approach that preserves these properties. Fortunately, it is quite straightforward to simulate the IDE competition model explicitly, which provides useful reference and validation for any analysis.

This competition model demonstrated how simple growth, dispersal, and competition processes can give rise to a variety of outcomes commonly observed in the ecologies of competition and climate change. The fundamental model structure described in Section 2.2.2 and Section 2.2.2 does not only apply to the case of competition, but can be generalized to model different types of interactions such as mutualism or predator-prey by the appropriate selection of growth functions f and g. I believe this approach provides a useful framework for exploring complex ecological systems and processes, and deserves further exploration.

2.6 Note

An edited version of this chapter is currently under review in the journal *Ecological Modelling*.

Chapter 3

INCORPORATING BIOLOGICAL REALISM INTO SPECIES DISTRIBUTION MODELING

3.1 Introduction

Ecological forecasting is a tool that is becoming ever more important as we observe an increase in the number and frequency of global effects of climate change. Understanding how environmental variables such as temperature and rainfall affect species and ecosystems gives us a better ability to anticipate and mitigate the potentially deleterious consequences of climate change. Identifying climate-sensitive species and ecosystems can help resource managers and conservationists design more effective management policies (Stanton et al., 2015).

The difficulty in ecological forecasting lies in the complexity of the ecosystems it attempts to describe. It is no small task to understand how the distribution of a species is shaped by its environment. At larger geographic scales, distributions are largely determined by climate (Pearson and Dawson, 2003); at smaller scales, habitat utilization is more influenced by local processes such as demographic and environmental stochasticity, interaction with other species, and dispersal limitations (Buckley et al., 2010). Many ecological modeling approaches neglect these components completely, which can yield incomplete or inaccurate predictions, especially at finer scales.

One of the most common methods of ecological forecasting is species distribution modeling (also known as climate-envelope modeling or environmental-niche modeling). Species distribution models (SDMs) establish a statistical relationship between the climatic conditions at a given location and species presence or absence at that

location, and use this relationship to predict how population distributions or densities might change over time. These models rely on spatially-explicit climate data and spatially-explicit species occurrence or abundance data, and as such, their results can provide realistic portraits of population distribution across a real landscape. SDMs, however, are often criticized for their simplicity (Araujo and Guisan, 2006; Lawler et al., 2006). In quantifying the climatic niche of a species, they do well in describing *potential* future habitat suitability, but by not accounting for ecological process, they fail to describe how process determines pattern, and, by neglecting process, may inaccurately portray species vulnerability to climate change. Moreover, SDMs most often model species individually, and do not account for the effects of species interaction; this is particularly problematic for specialists that rely strongly on other species.

Integro-difference equations (IDEs), by contrast, can provide a mechanistic understanding of how species traits shape long-term population dynamics. IDEs use a discrete-time, continuous-space framework to model spatially-explicit population density by accounting for two life stages of an organism: growth, where the population grows according to a specified function; and dispersal, where the propagules then disperse to new habitat as determined by a specified dispersal kernel. IDEs are quite flexible and can accommodate a wide variety of models, including stage-structure in populations (Harsch et al., 2014), resource competition by multiple species, changes in habitat quality, density dependence, and environmental and demographic stochasticity (Bouhours and Lewis, 2016). Despite their flexibility, integro-difference models are more theoretical in nature, and typically use an oversimplified notion of species habitat, often reducing it down to a single spatial dimension. While this is useful for understanding population dynamics and processes, it provides little insight to how these processes translate to a physical landscape.

In this chapter, I describe a new modeling framework that bridges the gap between these two approaches by combining the strengths of integro-difference equations and climate-envelope modeling techniques. This framework provides key insight into how

traits such as growth rate and dispersal ability affect long-term population stability in a changing environment.

3.2 Integro-difference equations

IDEs use a spatially-explicit approach to model the growth and dispersal of a population through time. In their simplest form, IDEs are written as

$$N_{t+1}(x) = \int_{\Omega} k(x, y) f[N_t(y)]\, dy, \tag{3.1}$$

with population $N_t(x)$ at location x and time t, growth function f, dispersal kernel $k(x, y)$, and spatial domain Ω. In Chapters 1 and 2, Ω was characterized as a patch of habitat of length L such that $\Omega = [0, L]$, but there are many other possibilities. IDEs are often modeled on an infinite domain (Kot et al., 1996; Veit and Lewis, 1996); (Rinnan, 2018b) found similarities between the invasion speed on an infinite domain and the critical speed for persistence on a finite domain.

To provide a more realistic model of terrestrial habitat, it is necessary to modify (3.1) in two ways. First, we shall generalize (3.1) to two dimensions, so that the spatial domain Ω contains both a latitudinal and longitudinal gradient. Second, we shall incorporate environmental heterogeneity to allow for complex, patchy habitat.

3.2.1 A two-dimensional habitat

Generalizing (3.1) to a two-dimensional habitat yields

$$N_{t+1}(x_1, x_2) = \int_{\Omega}\int_{\Omega} k(x_1 - y_1, x_2 - y_2) f[N_t(y_1, y_2)]\, dy_1\, dy_2, \tag{3.2}$$

which we will abbreviate as

$$N_{t+1}(\mathbf{x}) = \int_{\Omega} k(\mathbf{x}, \mathbf{y}) f[N_t(\mathbf{y})]\, d\mathbf{y}. \tag{3.3}$$

Here, $k(\mathbf{x}, \mathbf{y})$ describes the likelihood of dispersing from the location $\mathbf{y} = (y_1, y_2)$ to the location $\mathbf{x} = (x_1, x_2)$. Phillips and Kot (2015) studied this model in depth, and used a generalized bivariate Gaussian kernel to explore how dispersal affects persistence in two-dimensional moving habitat.

3.2.2 Habitat heterogeneity

Habitat quality functions provide a method of accounting for spatial heterogeneity. A habitat quality function $Q(\mathbf{x})$ (HQF) quantifies habitat quality for each species at a given location $\mathbf{x}$. HQFs are known by many names, and may be encountered as habitat index models, habitat suitability models, or habitat suitability indices. Regardless of name, HQFs act as scaling factors, and can be incorporated into the IDE model in many different ways. In particular, if we assume that the quality of the habitat only affects the establishment of new propagules, we may write

$$N_{t+1}(\mathbf{x}) = Q(\mathbf{x}) \int_{\Omega} k(\mathbf{x}, \mathbf{y}) f[N_t(\mathbf{y})] \, d\mathbf{y}. \tag{3.4}$$

When $Q(\mathbf{x}) = 0$, the location $\mathbf{x}$ is considered inhospitable, and no individuals can survive there. When $Q(\mathbf{x}) = 1$, the location $\mathbf{x}$ is considered ideal habitat, and the population establishes itself at $\mathbf{x}$ as determined by k and f. Habitat heterogeneity affects long-term population persistence, depending on the form of HQF used (Latore et al., 1999).

Equation (3.1) assumes that individuals dispersing inside the habitat patch survive, and those dispersing outside the patch die. This model can be reformulated with a simple HQF by observing that

$$\int_0^L k(x, y) f[N_t(y)] \, dy = Q(x) \int_{-\infty}^{\infty} k(x, y) f[N_t(y)] \, dy \tag{3.5}$$

for

$$Q(x) = \begin{cases} 1, & x \in [0, L], \\ 0, & \text{otherwise.} \end{cases} \tag{3.6}$$

We will later discuss other ways in which $Q(\mathbf{x})$ can be incorporated into IDEs.

3.3 Species distribution models

There are many popular methods and approaches to climate-envelope modeling, which collectively span the spectrum of model complexity. Choosing the right approach is typically guided by the format and quality of the input data, as well as the goals of the modeler. Random Forests, for example, are an excellent choice for habitat suitability classification from presence/absence data (Cutler et al., 2007). Maximum entropy, by contrast, offers a more reliable approach for presence-only data, and has a high degree of predictive accuracy (Phillips et al., 2004). If the modeler's goal is inference rather than prediction, ecological niche factor analysis provides a straightforward characterization of how predictor variables influence habitat suitability (Hirzel et al., 2002). Other common SDM methods include generalized linear models (Guisan and Harrell, 2000), generalized additive models (Guisan et al., 2002), artificial neural networks (Lek and Guégan, 1999), and boosted regression trees (Araújo and New, 2007). Different approaches have been demonstrated to be more reliable than others, and there are several meta-analyses that compare model performance and predictive power.

Let us denote an SDM as $Q(\mathbf{x}, \mathbf{v})$, where $\mathbf{x}$ is a geographic location and $\mathbf{v}$ is a vector of length n representing the values of n predictor variables associated with the location $\mathbf{x}$. $Q(\mathbf{x}, \mathbf{v})$ takes values between 0 and 1, indicating potential habitat

suitability. We may choose a threshold μ such that

$$M(\mathbf{x}, \mathbf{v}, \mu) = \begin{cases} 0, & \text{if } Q(\mathbf{x}, \mathbf{v}) < \mu, \\ 1, & \text{if } Q(\mathbf{x}, \mathbf{v}) \geq \mu, \end{cases}$$

in order to indicate whether habitat is considered suitable (1) or unsuitable (0). A variety of methods are commonly used for threshold selection, and will vary according to the modeler's priorities. In medical tests, for example, it is often more desirable to obtain a high rate of true positives (e.g., correctly detecting cancer), even if it comes at the expense of an increase in false positives (falsely detecting cancer), because the cost of false negatives are so high (failing to detect cancer). In species distribution modeling, a common choice of μ is one that optimizes the sum of model sensitivity (i.e., true positive rate) and specificity (true negative rate).

We denote future SDM predictions for the year t as $Q_t(\mathbf{x}, \tilde{\mathbf{v}}_t, \mu)$, where $\tilde{\mathbf{v}}_t$ signifies the observed or expected values of the predictor variables $\mathbf{v}$ at time t. For the sake of brevity, we will abbreviate the SDM predictions as $Q_t(\mathbf{x})$ for the remainder of the chapter, with an understanding that $Q_t(\mathbf{x})$ is implicitly a function of $\tilde{\mathbf{v}}_t$ and μ.

3.4 Integro-diftribution models

The key step in connecting SDMs and IDEs is to recognize that, in certain cases, the SDMs are conceptually identical to habitat quality functions. Quite simply, we may let $Q(\mathbf{x}) = Q_t(\mathbf{x})$ in (3.4) to get

$$N_{t+1}(\mathbf{x}) = Q_t(\mathbf{x}) \int_\Omega k(\mathbf{x}, \mathbf{y}) f[N_t(\mathbf{y})] \, d\mathbf{y}, \tag{3.7}$$

which we will henceforth unapologetically refer to as an *integro-diftribution model*, or IDM.

Heuristically, the processes described in (3.7) are exactly the same as that of

the traditional IDE in (3.1): at each time step, the population grows according to a specified growth function f, and then disperses according to the kernel k. If propagules disperse into unsuitable habitat, as identified by the habitat quality function Q, they do not survive; if they disperse into suitable habitat, then they survive to the next time step. As the population propagates at each time step, the underlying climate landscape changes incrementally from historical values to projected future values, based on the predictions of the SDM. As we shall see, (3.7) gives us the ability to incorporate observational climate and species data into our IDE population model, and a great deal of flexibility with how the data are incorporated.

A mechanistic modeler might intuitively interpret (3.7) as an IDE that describes how a species will grow and disperse across a real landscape over time, informed by changes in habitat suitability due to climate change. A correlative modeler, by contrast, might interpret (3.7) as an SDM that incorporates the mechanistic processes of population growth and dispersal. These are, in fact, equivalent characterizations of an IDM, but each perspective offers unique insight. IDEs, for example, are often used to estimate invasion speeds of populations or the critical speed of climate change for population persistence. A comparison of the invasion speeds approximated by an IDE and an IDM can illustrate the effects of habitat heterogeneity and topographic complexity. Likewise, SDMs are often used to quantify expected changes in the amount of climatically suitable habitat. Differences between the predicted habitat gains and losses of an SDM and an IDM can be attributed to dispersal and reproduction constraints. These types of model comparisons enable us to address the central question of this chapter: by ignoring important ecological processes, to what extent do traditional SDMs underestimate vulnerability to climate change?

I now provide an illustration of an integro-diftribution model, using the American pika as a case study. Since the primary purpose of this next section is to illustrate the process described above, I will not focus my efforts on fine-tuning a species distribution model to obtain the most predictive accuracy. Instead, I content myself with

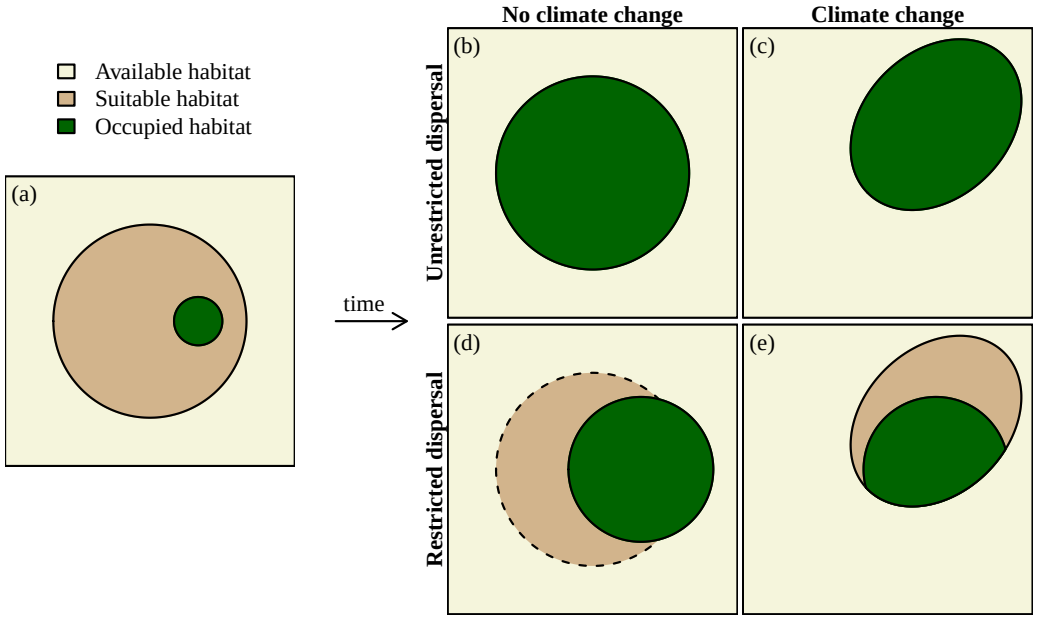

Figure 3.1: A conceptual diagram of differences in model predictions. (a) An initial population inhabiting a small amount of habitat, surrounded by suitable habitat, illustrating the difference between a population's *realized* niche and its *fundamental* niche. Depending on the choice of model, a different outcome will be predicted. (b) Predictions of a typical species distribution model. With no change in climate, the predictions do not change over time. No discernment is made between occupied and suitable habitat. (c) Predictions of the SDM in (b) with a changing climate. The suitable habitat has shifted due to climate change, with no difference between suitable and occupied habitat. (d) Predictions of a typical integro-difference equation. Over time, the population has grown and dispersed into new habitat. The IDE cannot discern between suitable and unsuitable habitat without a habitat quality function. (e) Predictions of a typical integro-diftribution model. The suitable habitat has shifted due to climate change, but the population is limited by dispersal ability and growth rate. Some population is lost due habitat becoming unsuitable. An SDM serves as the habitat quality function of the IDM to identify suitable habitat.

constructing a reasonable SDM, and quantifying its predictive accuracy. Any loss of accuracy should not impact my analysis substantially, since it is the *differences* in predictions between SDMs, IDEs, and IDMs that are of interest.

3.5 An application to the American pika

The American pika (*Ochotona princeps*) is a small mammal that inhabits talus and scree slopes throughout mountain ranges in Western North America. Pika are quite sensitive to high temperatures, and are widely recognized as being threatened by climate change due to loss of habitat associated with warming (Moritz et al., 2008; Erb et al., 2011). Despite evidence of range contraction and declining populations, the IUCN's Red List of Threatened Species database presently categorizes pika as a species of Least Concern (IUCN, 2017).

Pika display remarkably consistent reproductive behavior throughout their range (Smith, 1978). Adult females have two litters per year, but this is generally thought to be an adaptation to threats of predation and the phenological uncertainty associated with spring food availability (Smith and Weston, 1990). The females will produce a second litter regardless of whether the first litter survives to maturity, but will only wean the second litter if the first litter does not survive. As a consequence, only one litter will survive to maturity each year. The average litter size is three, and has not been observed to vary with habitat productivity (Millar and Zwickel, 1972; Smith, 1978).

For my analysis, I used climate data sets consisting of 19 bioclimate variables (see Table 3.1) at a 30 arc-second resolution ($\sim$ 1km), obtained from the WorldClim database (Hijmans et al., 2005). The historical data set was based on climate records averaged from 1960 to 1990. Future projections for 2050 (averages from 2041–2060) were derived from the MIROC5 global climate model for the RCP6.0 representative concentration pathway, representing a scenario of globally increasing greenhouse gas emissions until 2080 (Stocker, 2014). I transformed the historical climate data by

principal component analysis to reduce dimensionality and minimize correlation between variables, resulting in seven PCA factors that collectively accounted for 98.6% of the variance (see Table 3.1). I applied the historical PCA loadings to the future climate data sets to transform them similarly.

Table 3.1: Bioclimate variables obtained from the WorldClim database (Hijmans et al., 2005), derived from monthly measurements of temperature and precipitation. The loadings of the first three PCA factors are shown, with the amount of explained variance in parentheses.

Bioclimate variable		**PCA1** (40.8%)	**PCA2** (35.4%)	**PCA3** (11.7%)
MAT	mean annual temperature (°C)	-0.32	0.13	0.13
HM_{max}	max temp of warmest month (°C)	-0.33		0.13
CM_{min}	min temp of coldest month (°C)	-0.26	0.26	
TAR	temp annual range (HM_{max} - CM_{min})		-0.36	0.11
TS	temp seasonality (sd monthly temp × 100)	0.15	-0.32	0.17
ISO	isothermality (MDR/TAR × 100)	-0.28	0.20	
MTHQ	mean temp of hottest quarter (°C)	-0.31		0.24
MTDQ	mean temp of driest quarter (°C)	-0.23	0.25	-0.15
MTCQ	mean temp of coldest quarter (°C)	-0.29	0.23	
MTWQ	mean temp of wettest quarter (°C)	-0.14	-0.18	0.43
MDR	mean diurnal range (mean of monthly T_{max} - T_{min})	-0.30		
TAP	total annual precipitation (mm)	0.18	0.32	0.18
PWM	precip of wettest month (mm)	0.15	0.29	0.31
PDM	precip of driest month (mm)	0.24	0.22	
PS	precip seasonality (sd/mean monthly precip)			0.55
PWQ	precip of wettest quarter (mm)	0.15	0.30	0.30
PDQ	precip of driest quarter (mm)	0.24	0.24	
PHQ	precip of hottest quarter (mm)	0.25		0.30
PCQ	precip of coldest quarter (mm)	0.11	0.34	0.10

I used two different data sets relating to pika distribution. The first was obtained from the Global Biodiversity Information Facility database (GBIF), which contained 6,802 geographic occurrence records, 1,129 of which corresponded to unique geographic locations at the resolution of the climate data (GBIF, 2017). The second data set was a digital map of historical pika habitat, obtained from the IUCN's Red List of Threatened Species database (IUCN, 2017), which I rasterized to the same resolution as the climate data. I interpreted this habitat raster as presence data with equal utilization weights for all cells in which pika were present (see Figure 3.2).

I fit a MaxEnt species distribution model to the GBIF occurrence records, weighing

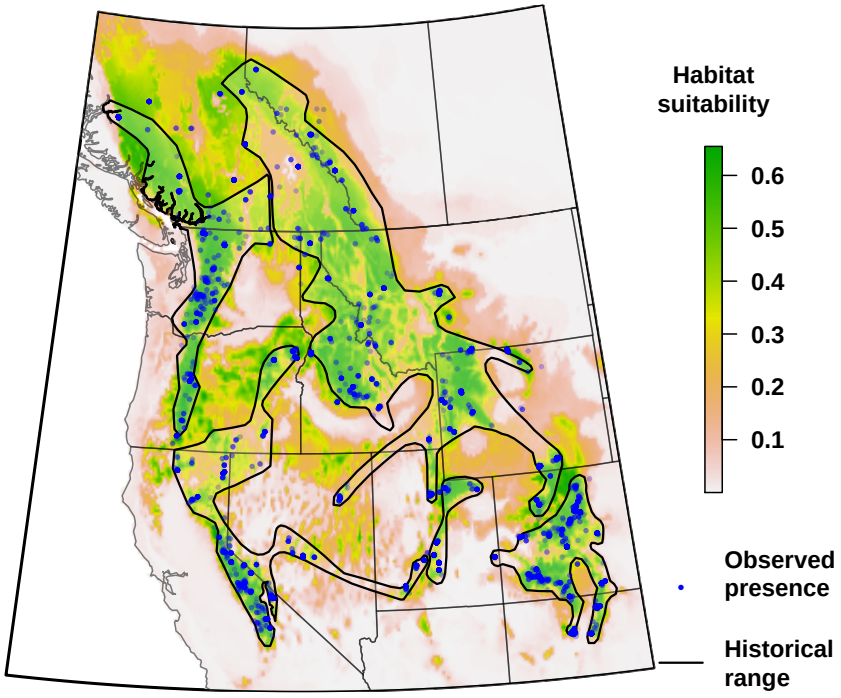

Figure 3.2: Predicted suitability and observed presence of *O. princeps*. The blue points correspond to presence data from the GBIF database (GBIF, 2017). The polygons outlined in black correspond to the historical range of pika from the IUCN database (IUCN, 2017). MaxEnt model predictions of habitat suitability are signified by the underlying raster.

each geographic location of presence equally to account for spatial sampling bias (Beck et al., 2014). I measured model performance in two ways. First, I used 10-fold cross-validation to measure the AUC of the test data (see Figure 3.4). Second, I used the IUCN data to validate the predictions of the MaxEnt model that was trained on the GBIF data by applying different thresholds to the logistic probability predictions of the MaxEnt model, and comparing the binary predictions with the IUCN distribution map.

Adult pika are highly philopatric, and observations of adult dispersal are uncom-

mon (Smith, 1987; Peacock, 1997). There is conflicting information on juvenile pika dispersal behavior. Some studies have stated that juveniles are equally philopatric, with average dispersal distances of less than 100m (Smith and Ivins, 1983, 1987). Several other studies suggest otherwise: Tapper (1973) observed pika dispersal distances of 3km; Hafner (1994) and Hafner and Sullivan (1995) estimated a maximum individual dispersal distance between 10km and 20km; Peacock (1997) found evidence of 2km dispersal events, inferred from measures of genetic similarity of population samples; Robson et al. (2015) theorized restricted pika dispersal from analysis of genetic clustering patterns, but acknowledged that significant migration events may have gone undetected. It seems evident that juvenile pika are certainly *capable* of long-distance dispersal. It is likely that pika are limited more by habitat availability than by intrinsic species vagility (Hafner, 1994), and by habitat fragmentation (Peacock and Smith, 1997).

Unfortunately, I am unaware of any studies that explicitly describe an observed distribution of pika dispersal distances. The absence of such studies are likely due in part to the difficulties associated with direct detection of dispersal events (Koenig et al., 1996). To model pika dispersal, I used a radially symmetric generalized Gaussian dispersal kernel (Phillips and Kot, 2015) of the form

$$k(\mathbf{x},\mathbf{y}) = \frac{\beta}{\pi\Gamma(1/\beta)2^{1/\beta}\sigma^2}\exp\left[-\frac{1}{2}\left(\frac{(x_1-y_1)^2+(x_2-y_2)^2}{\sigma^2}\right)^{\beta}\right], \tag{3.8}$$

with $\sigma = 400$m and $\beta = 0.85$. The parameter β affects the kurtosis of the kernel, allowing for thinner tails when $\beta > 1$ and fatter tails when $\beta < 1$. These parameter values reflect the high site fidelity observed in juvenile pika, as well as occasional long-distance dispersal events of more than 2km. This kernel assumes an equal probability of dispersing in any direction, and does not account for any geographic barriers to dispersal or behavior that targets habitat. I will revisit these assumptions in a later discussion. The kernel is illustrated in Figure 3.3. Please see Appendix III for details

of how this kernel was constructed in R.

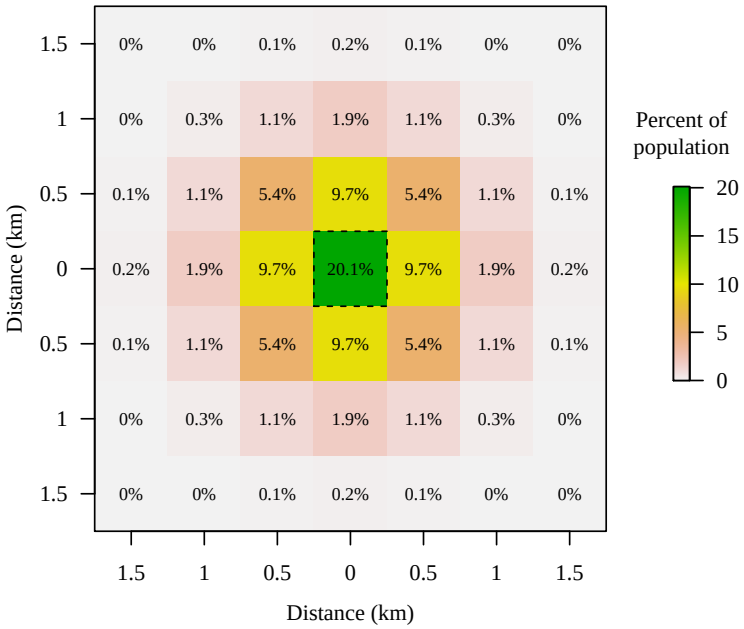

Figure 3.3: The percentage of individuals that settle in each nearby cell after a single dispersal event from a single source cell (dashed outline), assuming a radially symmetric generalized Gaussian dispersal kernel with $\sigma = 400m$ and $\beta = 0.85$. Slightly more than 80% of the pika will remain within one cell's distance of its origin, and slightly less than 2% will disperse more than two cells away.

There is considerable evidence to suggest that pika populations suffer from declining growth rates. Separate studies have estimated the net reproductive growth rate $R_0 \approx 0.996$ (Millar and Zwickel, 1972; Smith, 1974), and this has been supported through observations of shrinking or extirpated pika populations driven by increasing temperatures (Beever et al., 2003; Krajick, 2004; Morrison and Hik, 2007; Calkins et al., 2012; Robson et al., 2015). I modeled density-dependent growth of the population with the Beverton-Holt function

$$f\left[N_t(\mathbf{x})\right] = \frac{R_0 N_t(\mathbf{x})}{1 + \frac{R_0 - 1}{K} N_t(\mathbf{x})}, \tag{3.9}$$

with $R_0 = 1$ and $K = 250$ pika/500m^2. This K reflects estimates of highest population density (Kawamichi, 1982; Smith and Ivins, 1983; Southwick et al., 1986).

Please see Appendix IV for an outline of how I implemented an integro-diftribution model in R using the above data and characterizations of growth and dispersal.

3.5.1 Results

Overall predictive accuracy of the MaxEnt SDM was quite high for both the GBIF presence data and the IUCN range map. The mean AUC for the ten-fold cross-validated GBIF data was 0.913 ($\pm$0.005 sd, $k = 10$; see Figure 3.4). The AUC for the IUCN data was 0.855, with a model sensitivity (true positive rate) of 0.78 and a specificity (true negative rate) of 0.88 at the threshold that maximized the sum of the sensitivity and the specificity.

The SDM predicted moderate decreases in extent of habitat and total habitat area between 1975 and 2050 (see Figure 3.5a and b), with overall total habitat area decreasing 25.1% from 656,000 km^2 to 491,000 km^2. Approximately 174,000 km^2 of habitat was lost due to climate change, and 9,000 km^2 of new habitat was gained. By contrast, a two-dimensional IDE with no habitat quality function suggested substantial increases in total habitat area between 1975 and 2050 (see Figure 3.5c). The total occupied habitat area (i.e., cells with population greater than one) almost doubled from 656,000 km^2 to 1,232,000 km^2. The IDM predicted more habitat loss than either the SDM or the IDE (see Figure 3.5d), with total occupied habitat area (i.e., cells with population greater than one) decreasing by 27.9%, from 656,000 km^2 to 473,000 km^2.

A more detailed portrait of habitat changes can be derived by comparing the differences between historical population density and the SDM, IDE, and IDM predictions of future population density (see Figure 3.6). The IDM suggested that almost half of new suitable habitat will not be utilizable by pika, and a small portion of current habitat will not support future pika populations due to climate-related mortality.

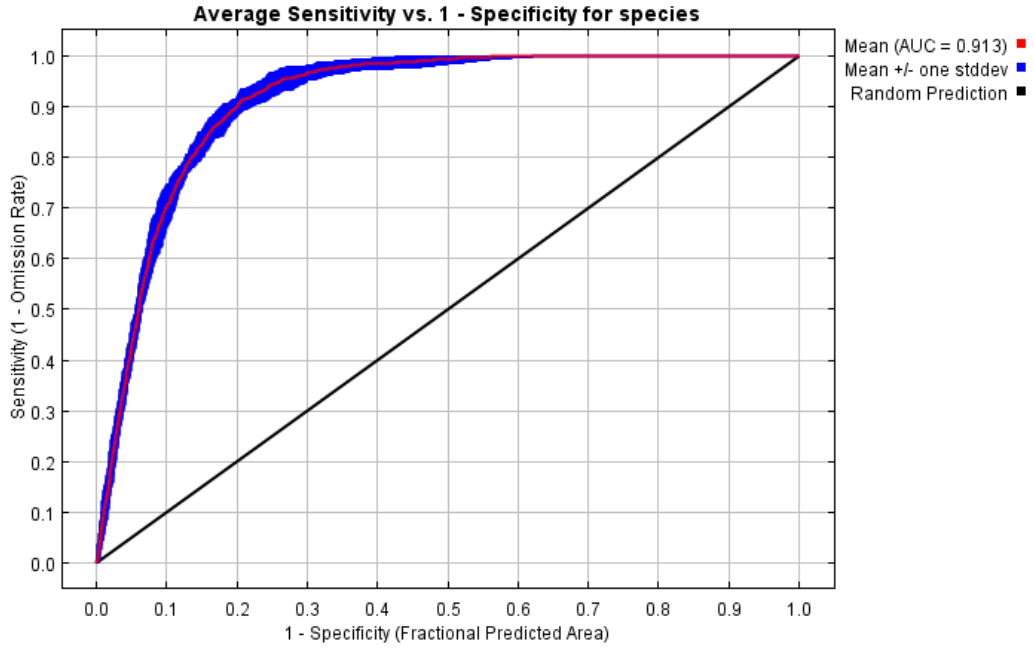

Figure 3.4: The average receiver operating characteristic curve of ten cross-validated test data sets. The area under the curve (AUC) indicates high predictive accuracy for the MaxEnt model, with high rates of sensitivity and specificity simultaneously attainable depending on the threshold chosen.

Differences in model predictions are summarized in Table 3.2.

Comparisons between the population densities $N_0(\mathbf{x})$ and $N_{75}(\mathbf{x})$ reveal further patterns. The IDE predicted no changes in overall population size but a decrease in population density. Over the 75-year period, the mean population density (for cells with population size greater than one) decreased from 128 pika/500m^2 to 68.1 pika/500m^2. By contrast, the IDM predicted a 17% decrease in population density from 128 pika/500m^2 to 106 pika/500m^2, and a concomitant 19% decrease in overall population from 336.4 million individuals to 200.5 million individuals (see Figure 3.7). While the amount of available habitat area predicted by the IDM steadily decreased over time, changes in population density appeared to settle out (see Figure 3.8). The disparity between occupied and available habitat increased over time, which suggests

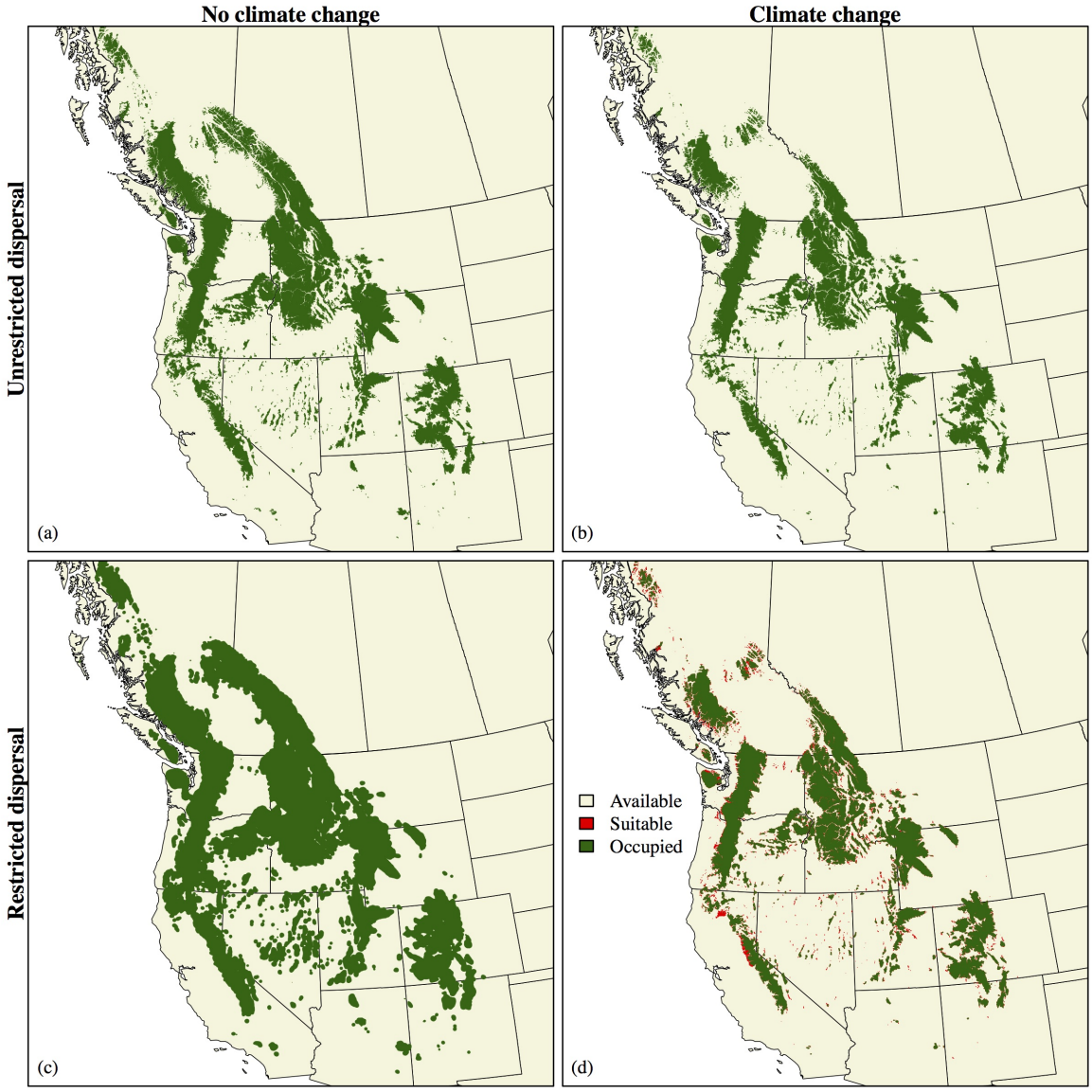

Figure 3.5: Differences in model predictions for *O. princeps*. (a) Historical predictions of the MaxEnt SDM. No discernment is made between occupied and suitable habitat. (b) Future predictions of the SDM in (a). The suitable habitat has shifted due to climate change, with no difference between suitable and occupied habitat. (c) Future predictions of a two-dimensional IDE with no specification of habitat quality. The population has grown and dispersed into new habitat, with an invasion speed determined by the growth rate and dispersal ability. (d) Future predictions of the IDM. The suitable habitat has shifted due to climate change, but the population is limited by dispersal ability and growth rate. Some population is lost due to habitat becoming unsuitable. The SDM in (a) serves as the habitat quality function of the IDM.

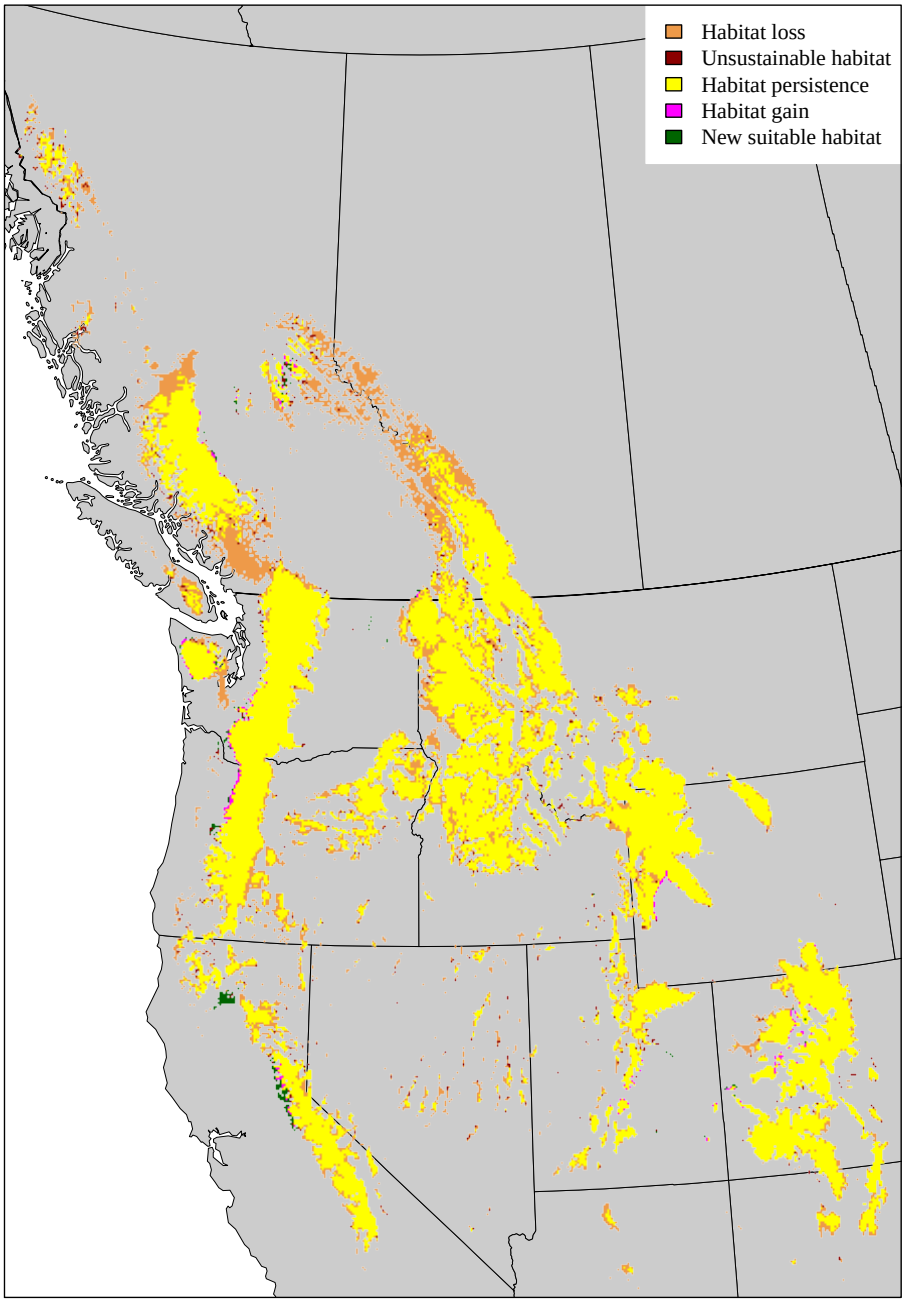

Figure 3.6: Habitat categorization of IDM predictions for *O. princeps*. The majority of habitat remains accessible and viable for the population to persist (yellow). A sizable portion of habitat is lost due to changes in climate (orange). The population is unable to persist in some suitable habitat (maroon), due to the effects of habitat quality on population density. A small amount of new habitat is gained (pink), with more new suitable habitat that is not able to be reached due to dispersal limitations (green).

Table 3.2: A comparison of predicted changes in *O. princeps* habitat. The SDM does not distinguish between suitable and occupied habitat, and cannot identify habitat that is suitable but not able to sustain a population. In the absence of a habitat quality function, the IDE cannot delineate unsuitable habitat, and the amount of suitable but unoccupied habitat is limited only by the extent of the study area.

	SDM	**IDE**	**IDM**
Historical habitat			
- Suitable, occupied	656,388	656,388	656,388
Future habitat			
- No longer suitable	174,137	–	174,137
- Unsustainable	–	46	13,946
- Unchanged	482,251	656,342	468,304
- New suitable, occupied	9,048	575,932	4,766
- New suitable, not occupied	–	∞^*	4,282

that pika may not be able to keep pace with climate change. This is further supported by the IDE model, which, in an infinite homogeneous landscape, has an invasion speed $\hat{c}$ (Phillips and Kot, 2015) of

$$\hat{c} \approx \sqrt{2\sigma^2 \log(R_0)}, \tag{3.10}$$

and thus implies very low spreading speeds when R_0 is very close to 1. The population wave front of the IDE model traveled roughly 10 km over the 75-year period, equating to a rate of spread of approximately 133 m/yr, which is lower than observed and predicted velocities of climate change (Parmesan and Yohe, 2003; Schloss et al., 2012).

The number of discrete habitat patches decreased dramatically from 3,142 in 1975 to 643 by 2050, with a corresponding increase in average patch area from 209 km^2 to 738 km^2 (see Figure 3.9). Most smaller patches of habitat vanished by becoming climatically inhospitable or by failing to sustain an isolated population over time. Habitat connectivity also altered substantially, with two prominent changes: climate change in the Fraser Valley in British Columbia fragmented a continuous habitat patch that connected the Cascade Range in Oregon and Washington with the Coast Mountains in British Columbia, and a similar fragmentation occurred throughout

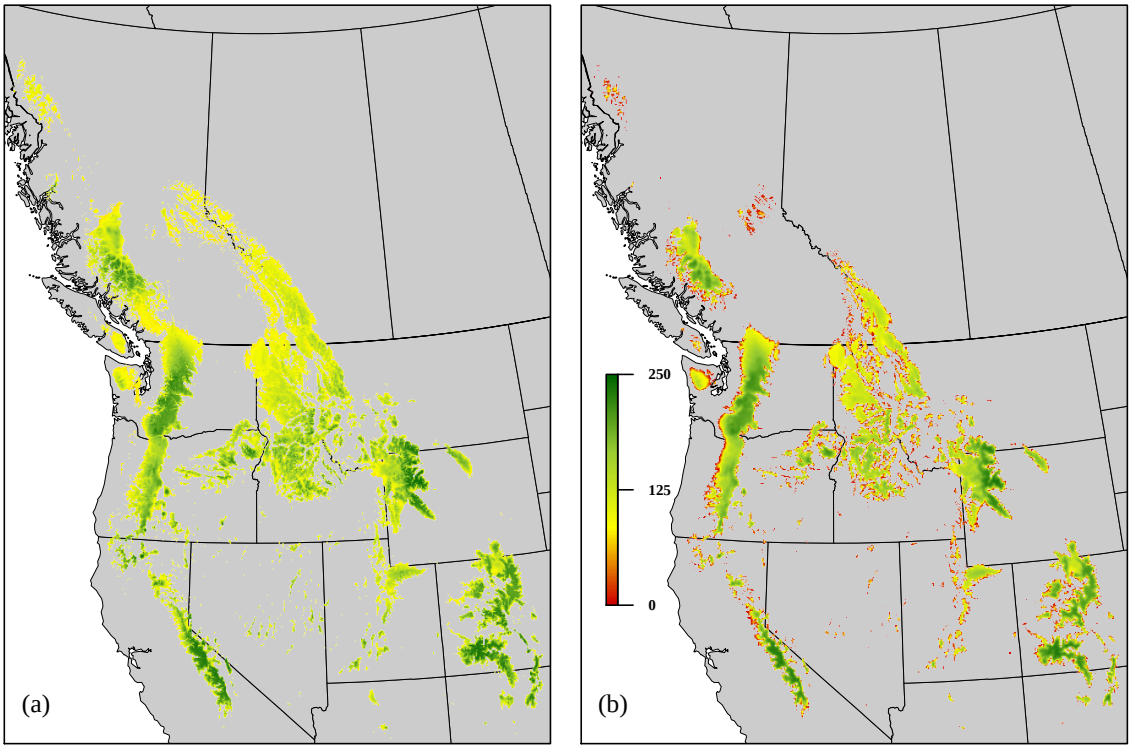

Figure 3.7: (a) Initial historical population density $N_0(\mathbf{x})$ of *O. princeps* for the year 1975. (b) IDM predictions of future population density $N_{75}(\mathbf{x})$ for the year 2050. Population density is given in number of individuals per 500m^2.

Jasper National Park in Alberta, resulting in a geographically isolated subpopulation of pika in British Columbia's Kawka Provincial Park.

A sensitivity analysis of the growth rate and dispersal parameters R_0 and σ suggested that pika populations are more limited by net reproductive rate than by dispersal ability (see Figure 3.10). Higher reproductive rates decreased the amount of unsustainable habitat, and increased the amount of new gained habitat. Average dispersal distance had little effect on the amount of habitat gained. At lower growth rates, average dispersal distance also did not affect the amount of unsustainable habitat. At higher growth rates, increased dispersal distance resulted in increases in unsustainable habitat. This interactive effect between reproductive rate and disper-

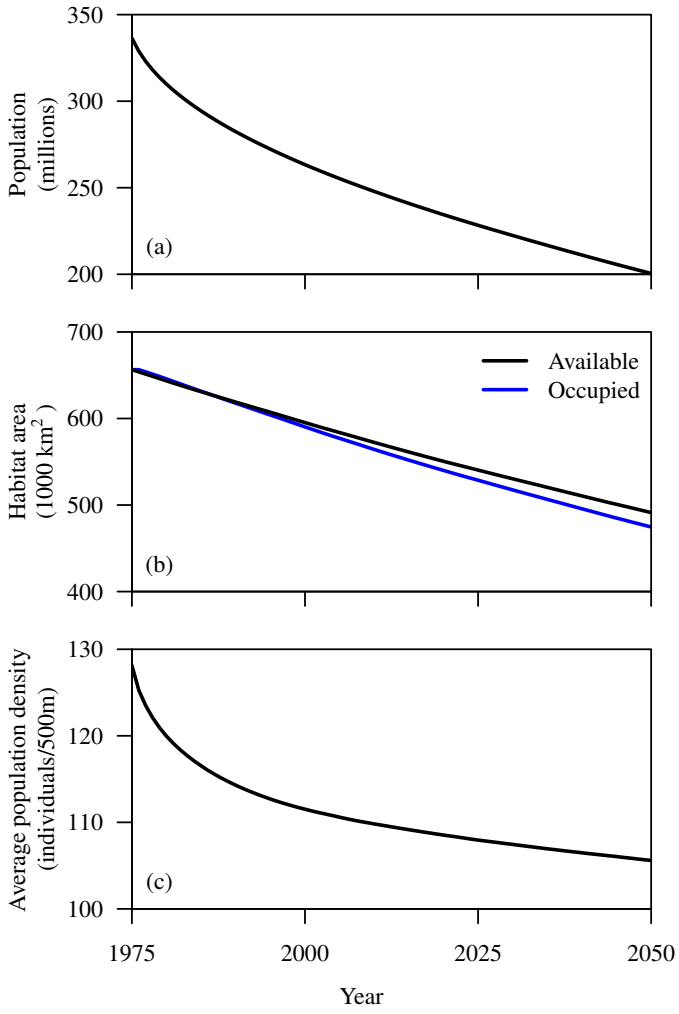

Figure 3.8: Model trends over time in (a) overall pika population, (b) available and occupied habitat area, and (c) mean population density of occupied habitat.

sal distance makes some intuitive sense: a stationary population can persist locally if the rate of reproduction is high enough to offset the population that is lost due to poor habitat quality. As dispersal distance increases, however, more individuals are lost through the dispersal process, further penalizing the local population. It is worth noting, however, that this is in part a consequence of modeling dispersal as a passive process in which individuals make no active effort to disperse toward suitable

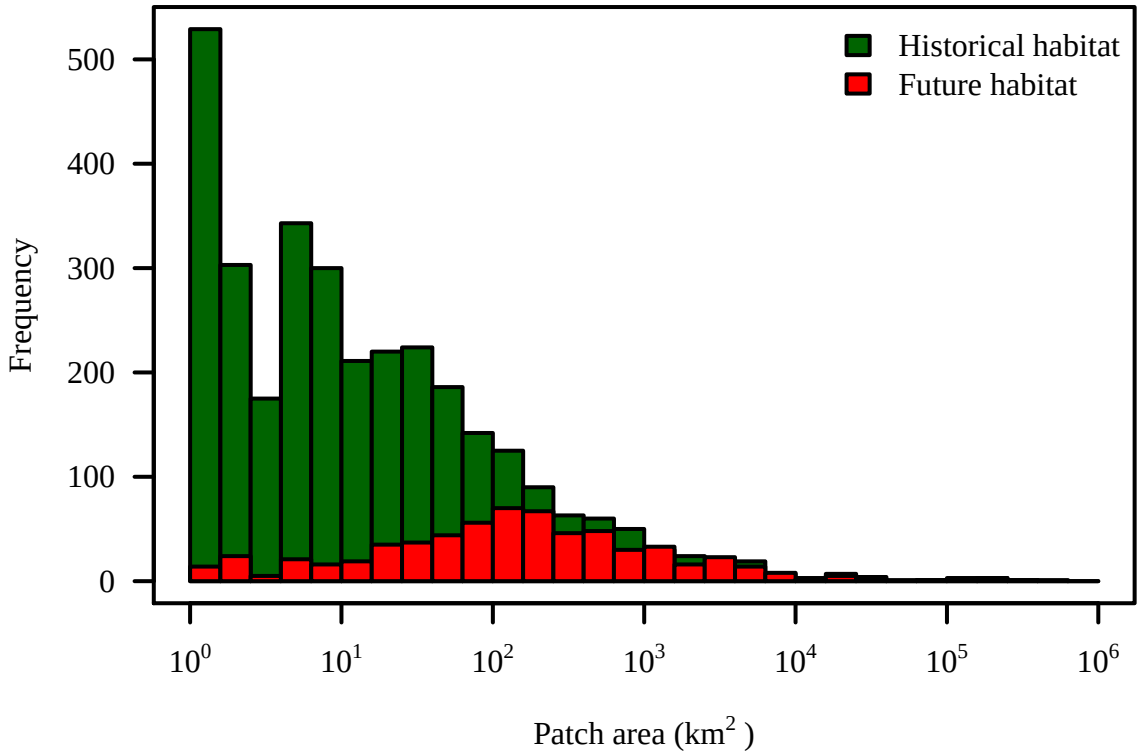

Figure 3.9: Changes in habitat patch size and area of *O. princeps*, as predicted by an IDM. The number of small habitat patches decreased dramatically over time, resulting in a larger mean patch size.

habitat. Dispersal assumptions are discussed in the next section.

Based on these results, I conclude that pika are first and foremost limited by the amount of available habitat. High reproductive rates and an ability to successfully disperse to new habitat will do little to mitigate the effects of climate change, due to the intrinsic physiological limitations of the pika and its consequently narrow climatic niche. Pika populations are further limited by reproductive rate. This is unfortunate because high juvenile mortality rates are strongly correlated with temperature extremes (Morrison and Hik, 2007), which suggests that climate change will further exacerbate this limitation. Longer dispersal events may help individuals reach new habitat, but higher rates of philopatry are generally better for maintaining a stable

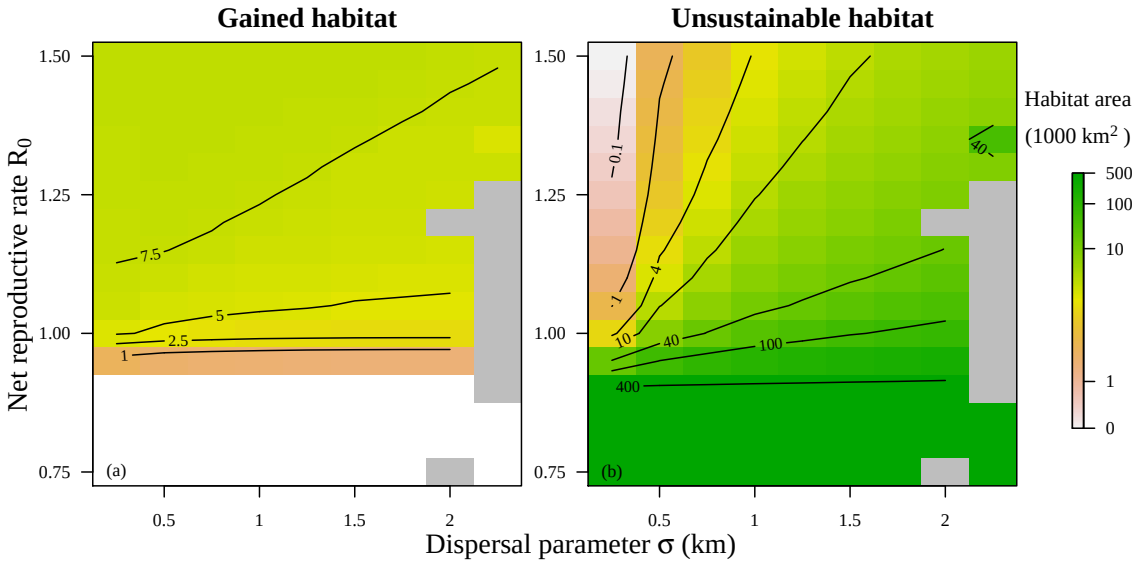

Figure 3.10: A sensitivity analysis of the dispersal parameter σ and the growth rate R_0. (a) For constant R_0, the amount of gained habitat decreases as average dispersal distance increases, and increases for constant σ as R_0 increases. (b) At lower reproductive rates, the amount of unsustainable habitat does not change with increasing dispersal distance. Higher reproduction decreases the amount of unsustainable habitat, but this effect is mitigated at higher dispersal distances.

population. Useful conservation approaches may involve enhancing and maintaining habitat connectivity in strategic locations, assisting the movement of individuals to suitable habitat that is not expected to be reachable by unassisted dispersal, and pursuing further research in promoting juvenile survival.

3.6 Model generalization

Integro-diftribution models provide an enormously flexible and versatile framework, with the ability to accommodate many additional types of ecological processes, as well as more complex representations of the processes I have already discussed. This section outlines some of the possibilities for expanding and generalizing the IDM framework, and suggests many potential future avenues of exploration and research.

3.6.1 More realistic dispersal

IDMs model dispersal with a dispersal kernel $k(\mathbf{x}, \mathbf{y})$ that describes the likelihood of dispersing from the point $\mathbf{y}$ to the point $\mathbf{x}$. In this chapter I assumed that dispersal is both isotropic (equal probability with respect to direction) and homogeneous (not influenced by landscape heterogeneity). This results in a symmetric dispersal kernel that is only a function of the distance between $\mathbf{x}$ and $\mathbf{y}$. As I established in Chapter 1, however, dispersal through a heterogeneous landscape is almost never isotropic.

Compton et al. (2007) combined methods from habitat connectivity modeling and kernel estimation to make what they called a *resistant-kernel estimator*. This resistant-kernel estimator describes the likelihood of dispersing from a focal cell to anywhere else in the landscape, taking into account the "resistance" of the landscape to movement, attributable to differences in land cover, geographical barriers, and human activity. A connectivity analysis is performed to create a landscape resistance layer, whose values are then used as weights for the dispersal kernel. This method has been used to better understand the affect of dispersal ability on connectivity (Cushman and Landguth, 2012).

Resistance kernel modeling provides a potential avenue by which to incorporate a more realistic model of dispersal into the IDM framework. A habitat resistance function $\rho(\mathbf{x}, \mathbf{y})$ can weight the kernel by location-specific landscape resistance with the equation

$$N_{t+1}(\mathbf{x}) = Q_t(\mathbf{x}) \int_{\Omega} \rho(\mathbf{x}, \mathbf{y}) k(\mathbf{x}, \mathbf{y}) f\big[N_t(\mathbf{y})\big]\, d\mathbf{y}. \tag{3.11}$$

Individuals would be more likely to disperse to locations that are easier to reach, and less likely to disperse to locations that are more difficult to reach due to landscape barriers. This approach enables us to model the constraints that landscapes and geography impose on the process of dispersal, in addition to the intrinsic biological limitations of the species.

This approach also resembles methods described by Dewhirst and Lutscher (2009)

for modeling the effects of spatial heterogeneity on dispersal *behavior*, where the kernel $k(x, y)$ is written as a function of habitat quality, such that

$$N_{t+1}(x) = \int_{\Omega} k\big(x, y, Q(y)\big) f[N_t(y)]\, dy. \tag{3.12}$$

In this scenario, individuals in high-quality habitat on average disperse shorter distances than individuals in low-quality habitat. Powell and Zimmermann (2004) described one such application of this formulation, in which seed dispersal is actively assisted by animals that cache food stores. $k\big(x, y, Q(y)\big)$ is a *resource selection function* that describes how habitat quality affects dispersal. A resource selection function can be included in an IDM as

$$N_{t+1}(\mathbf{x}) = Q_t(\mathbf{x}) \int_{\Omega} k\big(\mathbf{x}, \mathbf{y}, Q_t(\mathbf{y})\big) f\big[N_t(\mathbf{y})\big]\, d\mathbf{y}. \tag{3.13}$$

3.6.2 Effects of habitat heterogeneity on growth

Environment has a physiological impact on the growth of individuals, and the long-term consequences of this relationship can be observed in changes in distribution and abundance (Hughes, 2000; Walther et al., 2002; Parmesan, 2006). Temperature has a particularly well documented effect on the growth of several organisms, including trees (Way and Oren, 2010), phytoplankton (Rhee and Gotham, 1981), insects (Thompson, 1978; Krishnaraj and Pritchard, 1995), fish (Pörtner et al., 2001), and mammals (Humphries et al., 2004).

The IDM in (3.7) assumed that habitat quality affects the establishment and survival of new individuals. By contrast, if we assume that habitat quality affects the *growth* stage of the population, we may write

$$N_{t+1}(\mathbf{x}) = Q_t(\mathbf{x}) \int_{\Omega} k(\mathbf{x}, \mathbf{y}) R_t(\mathbf{y}) f\big[N_t(\mathbf{y})\big]\, d\mathbf{y}. \tag{3.14}$$

The function $R(\mathbf{y})f[N_t(\mathbf{y})]$ is the *functional response* curve that describes how habitat quality affects population growth, with $R(\mathbf{y})$ acting as a scaling factor on $f[N_t(\mathbf{y})]$. Ideally, the habitat quality function $Q(\mathbf{x})$ and the functional response $R(\mathbf{y})$ are determined through separate modeling procedures. In the same way that we used SDMs to describe $Q(\mathbf{x})$, so may we use them to describe $R(\mathbf{y})$. Because SDMs offer no mechanistic insight, however, it is impossible to distinguish between an SDM that models $Q(\mathbf{x})$ and one that models $R(\mathbf{y})$, if the same data is used for model training. In the context of IDMs, this becomes a choice of

$$N_{t+1}(\mathbf{x}) = Q_t(\mathbf{x}) \int_\Omega k(\mathbf{x},\mathbf{y}) f\left[N_t(\mathbf{y})\right] d\mathbf{y}, \tag{3.15}$$

if we assume that habitat quality impacts survival of new individuals, and

$$N_{t+1}(\mathbf{x}) = \int_\Omega k(\mathbf{x},\mathbf{y}) R_t(\mathbf{y}) f\left[N_t(\mathbf{y})\right] d\mathbf{y}, \tag{3.16}$$

if we assume that habitat quality affects population growth, with the relationship $Q_t(\mathbf{x}) = R_t(\mathbf{x})$. A comparison between these two models for our case study of American pika shows that (3.16) predicts less sustainability of present habitat than (3.15), but greater accessibility of future habitat (see Table 3.3). This is because all dispersing individuals in (3.16) survive, which likely leads to a higher rate of population spread.

Alternatively, it is possible to represent the individual parameters of the growth function as functions of environmental conditions themselves, rather than simple constants. The Beverton-Holt growth function in (3.9), for example, could be written as

$$f\left[N_t(\mathbf{x})\right] = \frac{R_0(\mathbf{x},\mathbf{v})N_t(\mathbf{x})}{1 + \frac{R_0(\mathbf{x},\mathbf{v})-1}{K(\mathbf{x},\mathbf{v})}N_t(\mathbf{x})} \tag{3.17}$$

where $\mathbf{v}$ again represents the values of the environmental variables at location $\mathbf{x}$. This

Table 3.3: A comparison of predicted changes in *O. princeps* habitat using the models in (3.15) and (3.16). An IDM with functional response $R(\mathbf{y})$ predicts slightly greater losses in habitat than an IDM with habitat quality function $Q(\mathbf{x})$, but slightly more future occupied suitable habitat.

	Habitat quality function $Q(\mathbf{x})$	**Functional response** $R(\mathbf{y})$
Historical habitat		
- Suitable, occupied	656,388	656,388
Future habitat		
- No longer suitable	174,137	174,137
- Unsustainable	13,946	14,312
- Unchanged	468,304	467,939
- New suitable, occupied	4,766	4,832
- New suitable, not occupied	4,282	4,216

could be used to account for spatial and temporal fluctuations in reproductive rates, as observed in a population of collared pika (*O. collaris*), which was attributed to the effect of the Pacific decadal oscillation on snowmelt patterns in the Yukon (Morrison and Hik, 2007).

3.6.3 Multiple species and interactions

Chapter 2 considered a coupled system of IDEs of the form

$$\begin{aligned} M_{t+1}(x) &= \int_{\Omega_m} k_m(x,y) f\big[M_t(y), N_t(y)\big]\, dy, \\ N_{t+1}(x) &= \int_{\Omega_n} k_n(x,y) g\big[M_t(y), N_t(y)\big]\, dy, \end{aligned} \tag{3.18}$$

with functions f and g describing growth in the presence of competition between the two species. This system can easily be adapted to a system of coupled IDMs, written as

$$\begin{aligned} M_{t+1}(\mathbf{x}) &= P_t(\mathbf{x}) \int_{\Omega} k_m(\mathbf{x},\mathbf{y}) f\big[M_t(\mathbf{y}), N_t(\mathbf{y})\big]\, d\mathbf{y}, \\ N_{t+1}(\mathbf{x}) &= Q_t(\mathbf{x}) \int_{\Omega} k_n(\mathbf{x},\mathbf{y}) g\big[M_t(\mathbf{y}), N_t(\mathbf{y})\big]\, d\mathbf{y}, \end{aligned} \tag{3.19}$$

with habitat quality functions $P_t(\mathbf{x})$ and $Q_t(\mathbf{x})$ for species M and N, respectively,

and with $\Omega = \Omega_m \cup \Omega_n$. This model would lead to a better understanding of the extent to which species' geographic distributions are constrained by competition, in addition to the impacts of competition on population density.

Additionally, there is no reason that f and g be restricted to the case of competition. There are many other types of interactive relationships that can be explained mathematically. One example is facultative mutualism, in which each species benefits from the presence of the other (Liu and Elaydi, 2001). This can be written as

$$\begin{aligned} M_{t+1} &= \frac{(\lambda_m - \beta_n N_t)M_t}{1 + \alpha_m M_t}, \\ N_{t+1} &= \frac{(\lambda_n - \beta_m M_t)N_t}{1 + \alpha_n N_t}, \end{aligned} \tag{3.20}$$

where $\lambda_m, \lambda_n, \alpha_m, \alpha_n, \beta_m, \beta_n$ are as defined in Equations (2.1) and (2.2). Another example is the predator-prey system (Leslie, 1958) described by

$$\begin{aligned} N_{t+1} &= \frac{\lambda_n N_t}{1 + \alpha_n N_t + \beta_n P_t}, \\ P_{t+1} &= \frac{\lambda_p P_t}{1 + \alpha_p\left(\frac{P_t}{N_t}\right)}. \end{aligned} \tag{3.21}$$

These types of interactions are readily observable in several high-profile species in the Pacific Northwest, including the endangered greater sage-grouse (*Centrocercus urophasianus*), whose habitat is determined largely by the presence of sagebrush (*Artemisia tridentata*); the Northern spotted owl (*Strix occidentalis caurina*), which experiences strong competition from invasive barred owl (*S. varia*); and the Canada lynx (*Lynx canadensis*), which depends heavily on snowshoe hares (*Lepus americanus*) for food.

We may further generalize the system in (3.19) to n species, written as

$$\mathbf{N}_{t+1}(\mathbf{x}) = \mathbf{Q}_t(\mathbf{x}) \int_\Omega \mathbf{K}(\mathbf{x}, \mathbf{y}) \mathbf{F}\big[\mathbf{N}_t(\mathbf{y})\big]\, d\mathbf{y}, \tag{3.22}$$

where $\mathbf{N}_t(\mathbf{x})$ is a vector of n population densities at time t, $\mathbf{F}$ is a vector of n functions describing the growth for each species as a function of densities $\mathbf{N}_t(\mathbf{y})$, $\mathbf{K}(\mathbf{x}, \mathbf{y})$ is a diagonal $n \times n$ matrix of dispersal kernels, $\mathbf{Q}_t(\mathbf{x})$ is a diagonal $n \times n$ matrix of habitat quality functions, and $\Omega = \bigcup \Omega_i$ the union of all n habitats.

3.6.4 Population structure

Harsch et al. (2014) used a system of coupled IDEs to explore changes in population structure as a consequence of climate change, describing the population with a model of the form

$$\mathbf{N}_{t+1}(x) = \int_{ct}^{L+ct} \big[\mathbf{K}(x-y) \circ \mathbf{A}\big]\mathbf{N}_t(y)\, dy, \tag{3.23}$$

with population projection matrix $\mathbf{A}$, $\mathbf{K}(x-y)$ a matrix of dispersal kernels with element $k_{ij}(x-y)$ describing the dispersal from y to x associated with transition from life stage i to life stage j , and $\mathbf{N}_t(x)$ a vector of population densities at time t. The projection matrix $\mathbf{A}$ accounts for age- or stage-structure in the population. This too lends itself to generalization as a system of IDMs, of the form

$$\mathbf{N}_{t+1}(\mathbf{x}) = \mathbf{Q}_t(\mathbf{x}) \int_{\Omega} \big[\mathbf{K}(\mathbf{x}, \mathbf{y}) \circ \mathbf{A}\big]\mathbf{N}_t(\mathbf{y})\, d\mathbf{y}. \tag{3.24}$$

This system shares many similarities with the multi-species system in (3.22).

Relating this back to our case study, we make the observation that almost all pika dispersal occurs at the juvenile stage (Smith, 1987; Peacock, 1997). A more accurate population model, then, might represent juvenile and adult pika as separate stage classes $J_t(\mathbf{x})$ and $A_t(\mathbf{x})$, as illustrated in Figure 3.11a. The dispersal matrix $\mathbf{K}$ would then be written as

$$\mathbf{K}(\mathbf{x}, \mathbf{y}) = \begin{pmatrix} \delta(\mathbf{x}, \mathbf{y}) & \delta(\mathbf{x}, \mathbf{y}) \\ k(\mathbf{x}, \mathbf{y}) & \delta(\mathbf{x}, \mathbf{y}) \end{pmatrix}, \tag{3.25}$$

with $k(\mathbf{x}, \mathbf{y})$ describing the dispersal associated with the transition from the juvenile to the adult stage, as in (3.8), and with the Dirac delta function $\delta(\mathbf{x}, \mathbf{y})$ representing

transitions that occur without dispersal, given by

$$\delta(\mathbf{x}, \mathbf{y}) = \begin{cases} 0, & \mathbf{x} \neq \mathbf{y}, \\ \infty, & \mathbf{x} = \mathbf{y}, \end{cases} \tag{3.26}$$

so that

$$\int_{\Omega} \delta(\mathbf{x}, \mathbf{y})\, d\mathbf{y} = 1. \tag{3.27}$$

(a)

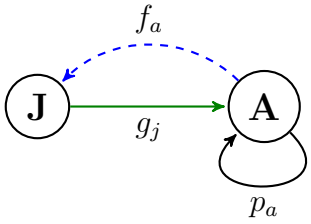

(b)

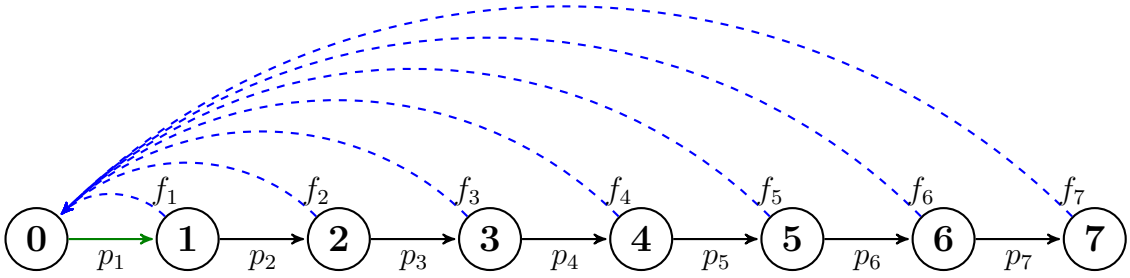

Figure 3.11: Two possible life-cycle diagrams of *O. princeps*. (a) A stage-class population model with juvenile (J) and adult (A) stages. Dispersal (green) takes place between the transition from juvenile to adult. This diagram is represented by the Lefkovitch matrix in (3.28). (b) An age-class model, with dispersal (green) taking place in the transition from the newborn to 1-year age class. This diagram is represented by the Leslie matrix in (3.33).

Similarly, the population projection matrix $\mathbf{A}$ would be written as

$$\mathbf{A} = \begin{pmatrix} 0 & f_a \\ g_j & p_a \end{pmatrix}, \tag{3.28}$$

where p_a is the probability of adult pika surviving to the next time step, and g_j the probability of juveniles surviving to adulthood, and and $f_a = p_a m_a$ is adult fecundity, where m_a is the average number of female offspring produced by adult females (Caswell, 2001). Substituting (3.25) and (3.28) into (3.24) yields

$$\begin{aligned} J_{t+1}(\mathbf{x}) &= Q_{j,t}(\mathbf{x}) \int_\Omega f_a \delta(\mathbf{x},\mathbf{y}) A_t(\mathbf{y})\, d\mathbf{y}, \\ A_{t+1}(\mathbf{x}) &= Q_{a,t}(\mathbf{x}) \int_\Omega \left[g_j k(\mathbf{x},\mathbf{y}) J_t(\mathbf{y}) + p_a \delta(\mathbf{x},\mathbf{y}) A_t(\mathbf{y}) \right] d\mathbf{y}, \end{aligned} \tag{3.29}$$

with habitat quality functions $Q_{j,t}(\mathbf{x})$ and $Q_{a,t}(\mathbf{x})$ for J and A. Using the convenient Dirac delta function property

$$\int_\Omega \delta(\mathbf{x},\mathbf{y}) f(\mathbf{y})\, d\mathbf{y} = f(\mathbf{x}), \tag{3.30}$$

(3.29) may be further simplified to

$$\begin{aligned} J_{t+1}(\mathbf{x}) &= f_a Q_{j,t}(\mathbf{x}) A_t(\mathbf{x}), \\ A_{t+1}(\mathbf{x}) &= p_a Q_{n,t}(\mathbf{x}) A_t(\mathbf{x}) + g_j Q_{a,t}(\mathbf{x}) \int_\Omega k(\mathbf{x},\mathbf{y}) J_t(\mathbf{y})\, d\mathbf{y}. \end{aligned} \tag{3.31}$$

Millar and Zwickel (1972) found similar age structure and mortality rates between two geographically separate pika populations, and estimated $\mathbf{A}$ as

$$\mathbf{A} = \begin{pmatrix} 0 & f_a \\ g_j & p_a \end{pmatrix} = \begin{pmatrix} 0 & 0.698 \\ 0.196 & 0.557 \end{pmatrix}. \tag{3.32}$$

Smith (1974) arrived at comparable estimates for a third population, with slightly

higher adult survival p_a and fecundity f_a. We note that the low probability of surviving to adulthood is largely attributable to the fact that only one of the two litters that females have each year are fully weaned (Smith and Weston, 1990).

Alternatively, a more complex population model might represent each age class individually, as illustrated in Figure 3.11b. Pika attain a maximum age of seven years (Smith, 1974). The matrix $\mathbf{A}$ would thus be written as

$$\mathbf{A} = \begin{pmatrix} 0 & f_1 & f_2 & f_3 & f_4 & f_5 & f_6 & f_7 \\ p_1 & 0 & 0 & 0 & 0 & 0 & 0 & 0 \\ 0 & p_2 & 0 & 0 & 0 & 0 & 0 & 0 \\ 0 & 0 & p_3 & 0 & 0 & 0 & 0 & 0 \\ 0 & 0 & 0 & p_4 & 0 & 0 & 0 & 0 \\ 0 & 0 & 0 & 0 & p_5 & 0 & 0 & 0 \\ 0 & 0 & 0 & 0 & 0 & p_6 & 0 & 0 \\ 0 & 0 & 0 & 0 & 0 & 0 & p_7 & 0 \end{pmatrix}, \tag{3.33}$$

with p_i the probability of survival from age $i-1$ to age i, and $f_i = p_i m_i$ is the fecundity of age class i, where m_i is the average number of female offspring produced by individuals at age i. Millar and Zwickel (1972) estimated the survival probabilities of each age class as $(p_1, p_2, p_3, p_4, p_5, p_6, p_7) = (0.196, 0.628, 0.464, 0.562, 0.561, 0.389, 0.143)$.

Admittedly, the matrix population model in (3.24) has limited practical applicability because it describes unbounded exponential growth. Equation (3.24) may still be used to classify future habitat and compare the predictions with those of an SDM, but the predicted population densities are unlikely to be realistic or meaningful. If the population densities are of primary interest, a further modification of the model is warranted. Jensen (1995) demonstrated how to add logistic density dependence to a traditional Leslie matrix population model with the equation

$$\mathbf{N}_{t+1} = \mathbf{N}_t + D(N)(\mathbf{A} - \mathbf{I})\mathbf{N}_t, \tag{3.34}$$

with identity matrix $\mathbf{I}$ and density-dependent function $D(N) = (K - N)/K$, and with N the sum of the population vector $\mathbf{N}_{t-1}$. Presumably, this model could be incorporated into a stage- or age-structured IDM as

$$\mathbf{N}_{t+1}(\mathbf{x}) = \mathbf{Q}_t(\mathbf{x}) \int_\Omega \Big[\mathbf{K}(\mathbf{x}, \mathbf{y}) \mathbf{N}_t(\mathbf{y}) + D(N) \big[\mathbf{K}(\mathbf{x}, \mathbf{y}) \circ (\mathbf{A} - \mathbf{I}) \big] \mathbf{N}_t(\mathbf{y}) \Big] \, d\mathbf{y}. \quad (3.35)$$

3.6.5 Stochasticity

Bouhours and Lewis (2016) modeled the effects of environmental and demographic stochasticity with a moving habitat model of the form

$$N_{t+1}(x) = \int_{s_t}^{s_t + L} k(x, y) f_{r_t}[N_t(y)] \, dy. \quad (3.36)$$

Here the domain shifts at the rate $s_t = ct + \sigma_t$, and the net reproductive rate is given by $r_t = f'_{r_t}(0)$, where σ_t and r_t are random variables. This approach allows us to relax our assumption of a constant speed of climate change c, as well as the implicit assumption of demographic uniformity in our population of interest. There is a rich body of literature on which to build that explores stochastic dispersal in IDEs (Lewis and Pacala, 2000; Kot et al., 2004; Caswell et al., 2011), and this is clearly a topic that warrants further research efforts in applications to IDMs.

3.7 Discussion

The case study of the American pika illustrates how traditional species distribution models can substantially overestimate the amount of future potential habitat that will be functionally available to a species. This is one of the primary limitations of SDMs (Pearson and Dawson, 2003; Guisan and Thuiller, 2005), and considerable effort has been made in recent years to address this issue with process-based models that account for dispersal limitations. Cellular automaton models have been developed to predict habitat changes, but do not yield predictions of population densities (Carey, 1996;

Collingham and Huntley, 2000). Keith et al. (2008) introduced a model that coupled stochastic population dynamics with SDMs and used it to simulate population persistence under climate change for two different hypothetical varieties of shrubs. Pagel and Schurr (2012) further extended this stochastic model to a Bayesian framework, and explored the impacts of climate change on simulated K- and r-strategist species. By acknowledging the limitations that growth rates and dispersal impose on a population, all of these models yield results that are more informed by biological and ecological constraints, and are thus are likely to present a more accurate portrait of the population's response to climate change.

Integro-difference equations present a useful approach for helping us understand how ecological process shapes ecological pattern. Although IDEs and SDMs are often used to address identical issues in ecology, they represent markedly different approaches, and there appears to be little collaboration between the two disciplines, nor even explicit recognition of one another. Integro-diftribution models attempt to bridge this gap, and in doing so, offer a novel alternative approach to integrating process-based modeling of population traits with correlative methods that quantify the relationship between species and environment.

We may also consider the IDM framework in the context of habitat fragmentation, which poses a substantial threat to population persistence and biodiversity (Wilcove et al., 1998; Pearson et al., 2014). Increasingly, conservation efforts are being guided toward increasing habitat connectivity as a means of strengthening genetic diversity, maintaining biodiversity, increasing resource accessibility, and facilitating movement (Hodgson et al., 2009). Many of these methods focus on *structural* connectivity, which describes the spatial arrangement of habitat (Bunn et al., 2000; McRae et al., 2008). By contrast, (Crooks and Sanjayan, 2006) stressed the importance of *functional* connectivity, which reflects the behavioral responses of populations to the physical structure. Put succinctly, a population whose habitat is structurally connected is not necessarily functionally connected. Climate change is expected to further exacerbate

habitat fragmentation for many species, and an increasing amount of research is focused on more explicitly incorporating climate change into connectivity modeling approaches (Nuñez et al., 2013; Littlefield et al., 2017; Bishop-Taylor et al., 2018). IDMs can be used to describe how changes in habitat connectivity affect population persistence. Furthermore, in modeling the process of dispersal, IDMs address the consequences of functional connectivity, rather than structural.

There are a number of issues that arise in species distribution modeling that equally relevant to the IDM framework. Most of them have been thoroughly discussed elsewhere: Hampe (2004) and Pearson and Dawson (2004) outline the limitations of climate-envelope models; Dormann et al. (2012) offer an excellent overview of the dichotomy between process-based and correlative modeling; and Morin and Thuiller (2009) provide a detailed comparison between the two methods. Rather than rehashing these issues, I will focus my discussion on modeling concerns that are unique to IDMs.

The IDM described in (3.7) is a discrete-time, continuous-space model, but climate data is most often interpolated between the locations of the weather stations that gather the data, and then spatially discretized into raster layers of equal cell size. Strictly speaking, any implementation of an IDM that uses raster data will necessarily discretize space, and thus, would be more accurately described as a type of discrete-time, discrete-space model, similar to cellular automata in the case of single species (Carey, 1996), or coupled-map lattices in the case of multiple species (Zurell et al., 2009). In practice, however, this need not be of great concern, since the same can be said for any implementation of an IDE. Excepting the precious few cases in which IDEs are analytically tractable, numerical analysis is achieved by discretizing space. Examples of this process were seen in Chapters 1 and 2.

It may be tempting, at first glance, for some to categorize IDMs as a type of individual-based model (IBM), but there are two major differences between the two. IBMs track individuals in a population through space and time as they grow and

disperse according to growth and dispersal parameters, subject to stochasticity. By contrast, the IDMs I considered in this chapter were entirely deterministic in nature, and do not track individuals in a population, but rather describe the expected population distribution in each cell, as predicted by the growth and dispersal functions.

Complications may arise from a mismatch between raster cell size and dispersal distance. In particular, if the average dispersal distance is significantly smaller than the cell size, the IDM may not accurately characterize the modeled rate of population spread. In theory, this can be resolved by increasing the resolution of the spatial data; in practice, the computational complexity of the implementation I have described in this chapter will quickly limit the practicality of this solution. For future work, there are several methods to improve model efficiency that may be worth exploring, with a C++ or Python implementation of the IDM algorithm likely to make the most notable difference in runtime. Gilbert et al. (2017) demonstrated several methods for improving the efficiency of simulations of population spread, including the use of adaptive mesh refinement to speed up raster calculations and fast Fourier transforms to model homogeneous dispersal. They used their approach to model a hypothetical species over the entirety of the UK at a 25m resolution, which represents an almost unprecedented improvement in scale.

Although IDMs predicate on several assumptions about population structure and simplify many ecological processes, they nonetheless demonstrate a promising new approach to integrating ecological process with correlative species modeling. To the extent that these simplifications limit the utility of the model, there is, in many cases, a clear path forward for how to relax our assumptions and augment the model with greater ecological complexity. Clearly, the IDM framework is ripe for further exploration in many directions. I believe that many studies on the impacts of climate change could be improved with IDMs, and, as research progresses, the benefits of utilizing this modeling approach will likely increase.

Chapter 4
CONCLUSIONS

The complexity of population dynamics is a natural consequence of multiple environmental pressures and ecological processes acting upon the population simultaneously at different scales. Two of the processes I have considered here, dispersal and interspecific interactions, unfold at the scale of the individual. Population growth, by contrast, often exhibits density dependence, and thus takes place at the scale of a localized population. Additional disparities in temporal scale further complicate the picture. What time scale is meaningful to describe the dispersal of a highly mobile organism? How can we parameterize interaction in a way that captures the interaction effect, and how can this be empirically measured in a population? Acknowledging the unquantifiable gap between a population's fundamental niche and its realized niche, is carrying capacity even a meaningful concept?

There are no easy answers to these questions, nor any answers that, however complicated, are set in stone. With the possible exception of death, the science of ecology does not enjoy any immutable laws. Outcomes in a stochastic environment are, tautologically, uncertain.

Modeling requires compromise; it is simply not possible to capture every nuance of a system. Fortunately, the only occasion in which perfect fidelity is the goal of the modeler is when the modeler is misguided. Instead, we identify the properties of the system that capture our interest and focus our scrutiny on separating the proverbial wheat from the chaff. Underneath the persistent noise and churn of the natural world, how much process can we pare away and still be left with the same outcome?

The notion of population persistence is also scale-dependent. In Chapter 1, I fo-

cused on describing persistence as an emergent property of the overall population. The cumulative effects of individual dispersal and localized population growth were spatially averaged over the population's habitat, which gave a measure of average population density through time, while sacrificing the spatial explicitness of the model. By focusing on the question of whether or not a population *can* survive rather than *where* it survives, I described the outcome of a population model with five independent parameters with a remarkable degree of predictive accuracy using just two simple, directly observable traits. Net reproductive rate R_0 can be inferred without any understanding of the underlying growth process, and average dispersal success GS can be measured by repeated observation of a population over time. In Chapter 2 my characterization of population persistence did not change, but model complexity increased considerably through the coupling of interacting species. Using a similar approach as Chapter 1, I reduced the model from ten or more independent parameters to four parameters p, q, u, and v, each with a direct ecological interpretation, and which together concisely delineated the possible outcomes of survival with little sacrifice in model accuracy.

The complexities of climate change compare with that of population dynamics. Future climate projections are rife with uncertainty. Despite ubiquitous maxims cautioning against statistical extrapolation, many ecologists seem to place a great deal of faith in models that offer portraits of our climate sixty years from now, and there are several examples in the climate change literature where the casual reader might rightly proclaim accusations of authorial hubris. Again, the issue of appropriate temporal scale is also significant: climate change is, by definition, the cumulative change observed in weather events over time, whereas individuals are primarily affected by acute weather events such as droughts, floods, and heat waves. This mismatch in scale compounds our uncertainty.

Chapters 1 and 2 represented climate change in an extremely simplistic way. Rather than attempting to explicitly describe the relationship between population

and habitat, I simply *assumed* the existence of habitat, and that the habitat would shift in space at a constant speed of climate change. Divorcing oneself from these assumptions, it seems much more reasonable to expect the habitat itself to shrink; whether shifting by elevation or latitude, organisms are all bound by the same unfortunate corporeal limitations, and simply cannot run from a changing climate forever. Despite this simplistic (and perhaps optimistic) representation, my portrayal of climate change nonetheless gave valuable insight into how the process of climate change influences persistence. Again, I simply asked if persistence was *possible* in the presence of change, rather than attempting to realistically model the spatio-temporal changes themselves.

At first glance, it may appear as though Chapter 3 took a markedly different approach to the issue of climate change. Rather than the comparably naive one-dimensional representation of habitat, the population instead resided on a real map, with 19 different bioclimatic dimensions associated with each geographic location. This approach, however, was motivated by the same fundamental question: is persistence possible? Rather than attempting to preserve the abundance of climate data, I constructed a climate-envelope model to distill the data down to the information most relevant to our research question. The resulting predictions of habitat suitability defined the geographic distribution of the population's habitat rather than assuming its existence, and future climate projections were used to portray how habitat suitability might realistically change through time, rather than presuming an unbounded ability to shift in space.

A common theme emerges in the modeling process: something lost, something gained. This motif is central to *all* models, from ecology, to physics, to ships in a bottle. If I were to give you a remote-controlled miniature airplane, it would not enable you to fly to Mexico, but you would likely gain a better understanding of the mechanics of flight. Through simplification of population dynamics and habitat, we have gained model tractability, and the ability to hone in on and isolate individual system

components and manipulate them to test the system's robustness to perturbation. We are left with a more complete understanding of the importance and contribution of different ecological processes and a better sense of how these processes enhance or mitigate one another.

In the paper, "Correlation and process in species distribution models: bridging a dichotomy," Dormann et al. (2012) outline "thirteen features common to or different between correlative and process-based models." Many of these features I have already discussed at length, but some are worth revisiting in the broader context of this dissertation.

4.1 Assumptions

Correlative models make several implicit assumptions. An important one is that species are always in equilibrium with their environment, i.e., that their present or historical distribution is an accurate reflection of their habitat niche, and that they will maintain this niche in synchrony with environmental changes over time. In actuality, it is much more reasonable to expect that a species will lag behind habitat changes to some extent, depending on their sensitivity to change, growth rate, and vagility. Fortunately, process-based models do not make this same assumption and can explicitly capture this lag effect. In Chapter 3 the IDM used a correlative SDM to predict the location of future suitable habitat and a process-based IDE to model the extent to which the population is able or unable to keep pace with habitat changes.

Process-based models come with their own set of assumptions as well. The models considered in each of the preceding chapters assumed a thoroughly homogeneous population with physiological traits and habitat requirements that remained constant over time. We need not be beholden to these assumptions, but it is important to recognize that we are making them and to be aware of their potential consequences when interpreting model results.

4.2 Information required

The integro-difference models in each chapter were heavily parameterized. Precision and accuracy are likely less important for some of the parameters than others, such as carrying capacity K. Others, such as the dispersal parameter σ that controls the mean dispersal distance, may display considerably more sensitivity. Although the model results for the American pika in Chapter 3 did not appear to change with dispersal distance, this was likely due to the fact that there was simply not much new habitat for pika to take advantage of. A different picture may emerge for a species with a weaker association with elevation and a better ability to shift latitudinally. Regardless, it should be clear that in order to model ecological process with IDEs, some detailed demographic and physiological information about the species is necessary.

Species distribution models, by contrast, typically make use of a great deal of environmental data and whatever occurrence data is available, but do not depend on any particular knowledge of species traits. For this very reason, SDMs are quite useful as an exploratory tool for determining species sensitivity to different environmental variables.

4.3 Validation

Model validation is accomplished by determining the accuracy of predictions on data that were not used to fit the original model. For this purpose, data sets are often split into "training data" that used to fit and calibrate the model, and "test data" that is used for validation. I demonstrated model validation of the SDM in Chapter 3 in two different ways. The first used cross-validation, also known as *internal* validation, to validate the model on subsets of the occurrence data. The second used *external* validation to confirm model accuracy on a data set entirely separate from the occurrence data. Put together, these exercises give us a sense of the ability of the model to describe the observed data, and the degree to which the model is consistent with

observations outside these data.

Validation for process-based models is more challenging. In order to ascertain that model predictions reflect our observations in Chapters 2 and 3, it would be necessary to have time series of abundance data for each species. At the spatial scale of these models, this is quite a tall order, and I am not aware, unfortunately, of any data sources that meet this specification for these species. Nonetheless, technological advances in remote sensing will continue to improve the temporal and spatial resolution of our data. The ICARUS Initiative (International Cooperation for Animal Research Using Space), for example, has been working assiduously for over a decade to launch a global satellite system dedicated to tracking migratory movements of small animals (Wikelski et al., 2007). This system is presently in construction on the International Space Station with an expected inaugural launch in July 2018. Likewise, the weight of GPS animal tags decreased more than tenfold between 2005 and 2015, and this trend is expected in continue (Kays et al., 2015). Equipped with more data on the temporal and spatial distributions of species, our ability to calibrate and validate models will improve.

4.4 Equifinality

Equifinality describes the non-identifiability problem in parameterized models. Inverse modeling can be used to derive parameter estimations from observation data, but it is entirely possible for multiple parameterizations to describe the data equally well. Kot et al. (1996) provided an excellent illustration of this phenomenon by demonstrating how several different kernels can be used to model dispersal observations of *Drosophila* with equal precision. Despite identical initial conditions, some of the population models exhibited drastically different behavior over time. Another source of equifinality comes from the possibility of several different growth functions that describe the observed population dynamics equally well. These problems are best solved by obtaining more data, but in situations where this is not possible, a sensi-

tivity analysis of parameter estimates or choice of functional form is recommended. In turn, the results of the sensitivity analysis can help guide the collection of more data, to obtain better parameter estimates or to identify sources of uncertainty in the model.

4.5 Extrapolation

The models in each chapter have the ability to extrapolate arbitrarily far into the future, but I urge that any conclusions derived from future projections be approached with an increasing amount of skepticism as the time period between the current and future increases. Population persistence over a specified time frame does not imply indefinite persistence, and it is important to take into account model context. I would argue that the types of models explored here are more useful for predicting extinction times or critical speeds of climate change than they are for describing qualities of a population over time.

4.6 Transferability

In general, an IDE, SDM, or IDM calibrated to suit one species does not demonstrate transferability to other species. As discussed before, the parameters of these models depend heavily on the species. A model calibrated to one species would only be meaningful for a separate species if the two species have similar habitat requirements, niches, physiology, and behavior. The extent to which these models transfer to different geographic locations depends on the location, and the geographic extent of the original model as well; this is an issue of geographic extrapolation rather than temporal. A model that is fit to highly localized data will probably do poorly in making predictions at a significantly larger extent or considerably farther away. A model describing the distribution of American pika only in the Cascade Range, for example, will probably not accurately portray the distribution of pika in the Rockies. In this case, it would be preferable to either fit a model to the entire range and explore the

commonalities in habitat across both locations, or fit different models to each location and acknowledge that each model describes a different subpopulation, which may or may not have similar habitat characteristics.

4.7 Accuracy versus complexity

Increasing model complexity can provide a limited return in model accuracy. This is of less concern for correlative models, which can often be fit in a matter of minutes. The MaxEnt algorithm used for the pika SDM in Chapter 3, for example, converged on 115 estimated coefficients out of possible thousands from the seven PCA variables by considering linear, quadratic, threshold, hinge, and interaction terms. This increase in complexity carried little expense in computation time, and hence was worthwhile for the return in model accuracy.

Process-based models, by contrast, generally require considerably more time to simulate. As a result, the cost of increasing model complexity is much higher. In Section 3.6, I outlined several different possible ways to generalize the IDM framework to add greater model complexity. The practical cost of this complexity is not yet known, but I can comfortably hypothesize that some of the suggested generalizations are likely prohibitively slow in R. The system of n species described in (3.22) is one such example, although this will depend heavily on the extent and resolution of the data, the number of species, and their degree of interaction.

One of the benefits of the analytic approach used in the first two chapters is that it completely sidesteps computational limitation, and focuses on insights that can be derived mathematically. As I have stated previously, IDEs do not typically lend themselves nicely to direct analytic methods, which is why some approximations were necessary to employ before the analysis could proceed. It should be clear, however, that this approach is another example of a situation in which the tradeoff between effort and accuracy determined the complexity of the model that was analyzed.

4.8 Common errors and misuses

The most common mistake of the modeler is to interpret or accept a model as a factual explanation of the relationship it models. This error can often be attributed to fallacious reasoning, such as assuming that correlation implies causation, or affirming the consequent. To paraphrase the Polish philosopher Alfred Korzybski: the map is not the territory. Assuming otherwise invites all kinds of misuse, misapplication, and misinterpretation of the model. This is a frustratingly persistent and pervasive problem in all fields of science, although it is often expressed in a manner subtle enough to fly under the radar. In the pantheon of historically significant scientists, many began their most important work by questioning the fundamental assumptions of their predecessors. To practice science effectively, it is vital to maintain a healthy dose of skepticism and the ability to distinguish narrative from reality.

4.9 Closing thoughts

I believe we are at the beginning of a very exciting era in landscape and population ecology. Moore's Law has accurately described the exponential growth in computing power over the past fifty years, and these technological advances have enabled us to measure patterns, analyze data, ask questions, and work toward answers that were impossible to address until very recently. Continuing progress suggests no end in sight to this trend. We have an increasing ability to validate ecological theory with observations, at finer and finer spatial and temporal resolutions, over increasingly larger spatial extents, and over increasingly longer time horizons. Ecological theory has emphasized the importance of community structure, and advances in modeling have increasingly progressed toward integrated frameworks of species. Step by step, year by year, model complexity becomes less of a practical limitation.

During the seven years I have spent in graduate school at UW, I have witnessed the development of an incredible number of new tools for statistical analysis and

pattern recognition, and some of them have already become outdated. I can scarcely imagine what the field of quantitative ecology will look like over the next fifty years, but I sure look forward to finding out, and, in the process, contributing what I can to the advancement of knowledge.

Yet knowledge alone is not enough. As encouraging as I find the future of the ecological sciences, I find the future of ecological conservation equally discouraging. In those same seven years of graduate school I have seen remarkable steps backward in our cultural awareness of climate, ecological, and conservation issues. Much of that is a consequence of a willful disregard of science and an intentional and strategic dismantling of social infrastructure that was specifically designed to preserve our health, our resources, and our planet. What a fascinating contradiction we are: one of our greatest strengths as a species is to affect positive change when we choose to work together toward a common goal, yet our most consistent failing is the inability to understand the consequences of our choices beyond our own individual lives.

My work is not motivated by a belief that I can bring species back from extinction, that I can stop or reverse climate change, that I can make any kind of a substantial, lasting impact on a global scale. At the most basic level, I am motivated by a desire to help those that struggle to speak for themselves, by a sense of moral obligation to leave this world a better place than when I entered it, and by the belief that I *can* make a positive difference within my sphere of influence. To these ends, I think that science communication and education may be our two most important tools. At the end of my life, I will consider myself successful if I have been able to share my sense of appreciation and reverence for our world with others, and helped them to nurture and instill a similar sense of their own.

The author Stephen Covey stated it thus: "To learn and not to do is really not to learn. To know and not to do is really not to know." *This* is what I look forward to, then, as I transition from graduate school into a career as an ecologist: learning, knowing, doing.

BIBLIOGRAPHY

Google maps. https://goo.gl/maps/M37Mm. Accessed: 2014-09-23.

S. B. Adams. *Mechanisms limiting a vertebrate invasion: Brook trout in mountain streams of the northwestern United States of America*. The University of Montana, 1999.

S. B. Adams, C. A. Frissell, and B. E. Rieman. Movements of nonnative brook trout in relation to stream channel slope. *Transactions of the American Fisheries Society*, 129(3):623–638, 2000.

P. B. Adler, J. HilleRisLambers, and J. M. Levine. A niche for neutrality. *Ecology Letters*, 10(2): 95–104, 2007.

H. Akaike. A new look at the statistical model identification. *IEEE Transactions on Automatic Control*, 19(6):716–723, 1974.

H. R. Akçakaya, S. H. Butchart, G. M. Mace, S. N. Stuart, and C. Hilton-Taylor. Use and misuse of the IUCN Red List Criteria in projecting climate change impacts on biodiversity. *Global Change Biology*, 12(11):2037–2043, 2006.

Y. A. Alpin and J. Merikoski. A simple proof for the inequality between the Perron root of a non-negative matrix and that of its geometric symmetrization. *Lobachevskii Journal of Mathematics*, 31(3):222–223, 2010.

Z. AlSharawi and M. Rhouma. Coexistence and extinction in a competitive exclusion Leslie/Gower model with harvesting and stocking. *Journal of Difference Equations and Applications*, 15(11-12): 1031–1053, 2009.

M. B. Araujo and A. Guisan. Five (or so) challenges for species distribution modelling. *Journal of Biogeography*, 33(10):1677–1688, 2006.

M. B. Araújo and M. Luoto. The importance of biotic interactions for modelling species distributions under climate change. *Global Ecology and Biogeography*, 16(6):743–753, 2007.

M. B. Araújo and M. New. Ensemble forecasting of species distributions. *Trends in Ecology & Evolution*, 22(1):42–47, 2007.

M. B. Araújo, M. Cabeza, W. Thuiller, L. Hannah, and P. H. Williams. Would climate change drive species out of reserves? an assessment of existing reserve-selection methods. *Global Change Biology*, 10(9):1618–1626, 2004.

M. B. Araújo, W. Thuiller, and R. G. Pearson. Climate warming and the decline of amphibians and reptiles in europe. *Journal of Biogeography*, 33(10):1712–1728, 2006.

F. Austerlitz, C. Dutech, P. Smouse, F. Davis, and V. Sork. Estimating anisotropic pollen dispersal: a case study in *Quercus lobata*. *Heredity*, 99(2):193–204, 2007.

M. Baguette, S. Blanchet, D. Legrand, V. M. Stevens, and C. Turlure. Individual dispersal, landscape connectivity and ecological networks. *Biological Reviews*, 88(2):310–326, 2013.

N. Balakrishnan and C. Lai. *Continuous Bivariate Distributions*. Springer, New York, 2009.

M. Basille, C. Calenge, E. Marboutin, R. Andersen, and J.-M. Gaillard. Assessing habitat selection using multivariate statistics: Some refinements of the ecological-niche factor analysis. *Ecological Modelling*, 211(1):233–240, 2008.

M. Basille, I. Herfindal, H. Santin-Janin, J. D. Linnell, J. Odden, R. Andersen, K. Arild Høgda, and J.-M. Gaillard. What shapes Eurasian lynx distribution in human dominated landscapes: selecting prey or avoiding people? *Ecography*, 32(4):683–691, 2009.

M. L. Baskett, J. S. Weitz, and S. A. Levin. The evolution of dispersal in reserve networks. *The American Naturalist*, 170(1):59–78, 2007.

J. Beck, M. Böller, A. Erhardt, and W. Schwanghart. Spatial bias in the GBIF database and its effect on modeling species' geographic distributions. *Ecological Informatics*, 19:10–15, 2014.

E. A. Beever, P. F. Brussard, and J. Berger. Patterns of apparent extirpation among isolated populations of pikas (*Ochotona princeps*) in the Great Basin. *Journal of Mammalogy*, 84(1): 37–54, 2003.

E. A. Beever, C. Ray, J. L. Wilkening, P. F. Brussard, and P. W. Mote. Contemporary climate change alters the pace and drivers of extinction. *Global Change Biology*, 17(6):2054–2070, 2011.

H. Berestycki, O. Diekmann, C. J. Nagelkerke, and P. A. Zegeling. Can a species keep pace with a shifting climate? *Bulletin of Mathematical Biology*, 71(2):399, 2009.

R. J. Beverton and S. J. Holt. On the dynamics of exploited fish populations, Fishery Investigations Series II, Vol. XIX, Ministry of Agriculture. *Fisheries and Food*, 1:957, 1957.

R. Bishop-Taylor, M. G. Tulbure, and M. Broich. Evaluating static and dynamic landscape connectivity modelling using a 25-year remote sensing time series. *Landscape Ecology*, 33(4):625–640, 2018.

R. Bivand and N. Lewin-Koh. maptools: Tools for reading and handling spatial objects. http://CRAN.R-project.org/package=maptools, 2014. R package version 0.8-29.

J. Bouhours and M. A. Lewis. Climate change and integrodifference equations in a stochastic environment. *Bulletin of Mathematical Biology*, 78(9):1866–1903, 2016.

Å. Brännström and D. J. Sumpter. Coupled map lattice approximations for spatially explicit individual-based models of ecology. *Bulletin of Mathematical Biology*, 67(4):663–682, 2005.

B. Broitman, P. Szathmary, K. Mislan, C. Blanchette, and B. Helmuth. Predator–prey interactions under climate change: the importance of habitat vs body temperature. *Oikos*, 118(2):219–224, 2009.

L. Brotons, W. Thuiller, M. B. Araújo, and A. H. Hirzel. Presence-absence versus presence-only modelling methods for predicting bird habitat suitability. *Ecography*, 27(4):437–448, 2004.

J. H. Brown, T. J. Valone, and C. G. Curtin. Reorganization of an arid ecosystem in response to recent climate change. *Proceedings of the National Academy of Sciences*, 94(18):9729–9733, 1997.

T. L. Bryan and A. Metaxas. Predicting suitable habitat for deep-water gorgonian corals on the Atlantic and Pacific continental margins of North America. *Marine Ecology Progress Series*, 330: 113–126, 2007.

L. B. Buckley, M. C. Urban, M. J. Angilletta, L. G. Crozier, L. J. Rissler, and M. W. Sears. Can mechanism inform species distribution models? *Ecology Letters*, 13(8):1041–1054, 2010.

A. G. Bunn, D. Urban, and T. Keitt. Landscape connectivity: a conservation application of graph theory. *Journal of Environmental Management*, 59(4):265–278, 2000.

J. E. Byers and J. M. Pringle. Going against the flow: retention, range limits and invasions in advective environments. *Marine Ecology Progress Series*, 313:27–41, 2006.

C. Calenge. The package adehabitat for the R software: a tool for the analysis of space and habitat use by animals. *Ecological Modelling*, 197(3):516–519, 2006.

C. Calenge and M. Basille. A general framework for the statistical exploration of the ecological niche. *Journal of Theoretical Biology*, 252(4):674–685, 2008.

M. T. Calkins, E. A. Beever, K. G. Boykin, J. K. Frey, and M. C. Andersen. Not-so-splendid isolation: modeling climate-mediated range collapse of a montane mammal *Ochotona princeps* across numerous ecoregions. *Ecography*, 35(9):780–791, 2012.

P. Carey. Disperse: a cellular automaton for predicting the distribution of species in a changed climate. *Global Ecology and Biogeography Letters*, pages 217–226, 1996.

H. Caswell. *Matrix population models*. Wiley Online Library, 2001.

H. Caswell. Sensitivity analysis of transient population dynamics. *Ecology Letters*, 10(1):1–15, 2007.

H. Caswell, M. G. Neubert, and C. M. Hunter. Demography and dispersal: invasion speeds and sensitivity analysis in periodic and stochastic environments. *Theoretical Ecology*, 4(4):407–421, 2011.

I. Chen, J. K. Hill, H.-J. Shiu, J. D. Holloway, S. Benedick, V. K. Chey, H. S. Barlow, C. D. Thomas, et al. Asymmetric boundary shifts of tropical montane lepidoptera over four decades of climate warming. *Global Ecology and Biogeography*, 20(1):34–45, 2011a.

I.-C. Chen, J. K. Hill, R. Ohlemüller, D. B. Roy, and C. D. Thomas. Rapid range shifts of species associated with high levels of climate warming. *Science*, 333(6045):1024–1026, 2011b.

J. S. Clark, C. Fastie, G. Hurtt, S. T. Jackson, C. Johnson, G. A. King, M. Lewis, J. Lynch, S. Pacala, C. Prentice, et al. Reid's paradox of rapid plant migration dispersal theory and interpretation of paleoecological records. *BioScience*, 48(1):13–24, 1998.

J. S. Clark, M. Silman, R. Kern, E. Macklin, and J. HilleRisLambers. Seed dispersal near and far: patterns across temperate and tropical forests. *Ecology*, 80(5):1475–1494, 1999.

J. S. Clark, A. E. Gelfand, C. W. Woodall, and K. Zhu. More than the sum of the parts: forest climate response from joint species distribution models. *Ecological Applications*, 24(5):990–999, 2014.

C. Cobbold, M. Lewis, F. Lutscher, and J. Roland. How parasitism affects critical patch-size in a host–parasitoid model: application to the forest tent caterpillar. *Theoretical Population Biology*, 67(2):109–125, 2005.

Y. C. Collingham and B. Huntley. Impacts of habitat fragmentation and patch size upon migration rates. *Ecological Applications*, 10(1):131–144, 2000.

B. W. Compton, K. McGarigal, S. A. Cushman, and L. R. Gamble. A resistant-kernel model of connectivity for amphibians that breed in vernal pools. *Conservation Biology*, 21(3):788–799, 2007.

J. H. Connell. On the prevalence and relative importance of interspecific competition: evidence from field experiments. *American Naturalist*, pages 661–696, 1983.

L. F. Cook and C. A. Toft. Dynamics of extinction: population decline in the colonially nesting tricolored blackbird *Agelaius tricolor*. *Bird Conservation International*, 15(01):73–88, 2005.

C. Cosner and A. C. Lazer. Stable coexistence states in the Volterra-Lotka competition model with diffusion. *SIAM Journal on Applied Mathematics*, 44(6):1112–1132, 1984.

F. Courchamp, T. Clutton-Brock, and B. Grenfell. Inverse density dependence and the Allee effect. *Trends in Ecology & Evolution*, 14(10):405–410, 1999.

K. R. Crooks and M. Sanjayan. *Connectivity Conservation*, volume 14. Cambridge University Press, 2006.

S. P. Crosbie, W. D. Koenig, W. K. Reisen, V. L. Kramer, L. Marcus, R. Carney, E. Pandolfino, G. M. Bolen, L. R. Crosbie, D. A. Bell, et al. Early impact of West Nile virus on the Yellow-billed Magpie (*Pica nuttalli*). *The Auk*, 125(3):542–550, 2008.

J. Cushing, S. Levarge, N. Chitnis, and S. M. Henson. Some discrete competition models and the competitive exclusion principle. *Journal of Difference Equations and Applications*, 10(13-15): 1139–1151, 2004.

S. A. Cushman. Effects of habitat loss and fragmentation on amphibians: a review and prospectus. *Biological Conservation*, 128(2):231–240, 2006.

S. A. Cushman and E. L. Landguth. Multi-taxa population connectivity in the Northern Rocky Mountains. *Ecological Modelling*, 231:101–112, 2012.

D. R. Cutler, T. C. Edwards, K. H. Beard, A. Cutler, K. T. Hess, J. Gibson, and J. J. Lawler. Random forests for classification in ecology. *Ecology*, 88(11):2783–2792, 2007.

C. Daly, W. P. Gibson, G. H. Taylor, G. L. Johnson, and P. Pasteris. A knowledge-based approach to the statistical mapping of climate. *Climate Research*, 22(2):99–113, 2002.

A. J. Davis, L. S. Jenkinson, J. H. Lawton, B. Shorrocks, and S. Wood. Making mistakes when predicting shifts in species range in response to global warming. *Nature*, 391(6669):783–786, 1998.

T. P. Dawson, S. T. Jackson, J. I. House, I. C. Prentice, and G. M. Mace. Beyond predictions: biodiversity conservation in a changing climate. *Science*, 332(6025):53–58, 2011.

H. J. De Knegt, F. Van Langevelde, A. K. Skidmore, A. Delsink, R. Slotow, S. Henley, G. Bucini, W. F. De Boer, M. B. Coughenour, C. C. Grant, et al. The spatial scaling of habitat selection by African elephants. *Journal of Animal Ecology*, 80(1):270–281, 2011.

S. Dewhirst and F. Lutscher. Dispersal in heterogeneous habitats: thresholds, spatial scales, and approximate rates of spread. *Ecology*, 90(5):1338–1345, 2009.

N. Dolgener, L. Freudenberger, M. Schluck, N. Schneeweiss, P. Ibisch, and R. Tiedemann. Environmental niche factor analysis (ENFA) relates environmental parameters to abundance and genetic diversity in an endangered amphibian, the fire-bellied-toad (*Bombina bombina*). *Conservation Genetics*, 15(1):11–21, 2014.

D. L. Donoho and P. J. Huber. The notion of breakdown point. *A Festschrift for Erich L. Lehmann*, pages 157–184, 1983.

C. F. Dormann, J. M. McPherson, M. B. Araújo, R. Bivand, J. Bolliger, G. Carl, R. G. Davies, A. Hirzel, W. Jetz, W. D. Kissling, et al. Methods to account for spatial autocorrelation in the analysis of species distributional data: a review. *Ecography*, 30(5):609–628, 2007.

C. F. Dormann, S. J. Schymanski, J. Cabral, I. Chuine, C. Graham, F. Hartig, M. Kearney, X. Morin, C. Römermann, B. Schröder, et al. Correlation and process in species distribution models: bridging a dichotomy. *Journal of Biogeography*, 39(12):2119–2131, 2012.

J. B. Dunham, S. B. Adams, R. E. Schroeter, and D. C. Novinger. Alien invasions in aquatic ecosystems: toward an understanding of brook trout invasions and potential impacts on inland cutthroat trout in western North America. *Reviews in Fish Biology and Fisheries*, 12(4):373–391, 2002.

W. A. Dunson and J. Travis. The role of abiotic factors in community organization. *American Naturalist*, pages 1067–1091, 1991.

J. Elith, J. R. Leathwick, and T. Hastie. A working guide to boosted regression trees. *Journal of Animal Ecology*, 77(4):802–813, 2008.

J. Elith, S. J. Phillips, T. Hastie, M. Dudík, Y. E. Chee, and C. J. Yates. A statistical explanation of MaxEnt for ecologists. *Diversity and Distributions*, 17(1):43–57, 2011.

R. Engler, A. Guisan, and L. Rechsteiner. An improved approach for predicting the distribution of rare and endangered species from occurrence and pseudo-absence data. *Journal of Applied Ecology*, 41(2):263–274, 2004.

L. P. Erb, C. Ray, and R. Guralnick. On the generality of a climate-mediated shift in the distribution of the American pika (*Ochotona princeps*). *Ecology*, 92(9):1730–1735, 2011.

J. S. Evans, M. A. Murphy, Z. A. Holden, and S. A. Cushman. Modeling species distribution and change using random forest. In *Predictive species and habitat modeling in landscape ecology*, pages 139–159. Springer, 2011.

W. F. Fagan and F. Lutscher. Average dispersal success: linking home range, dispersal, and metapopulation dynamics to reserve design. *Ecological Applications*, 16(2):820–828, 2006.

A. Farashi, M. Kaboli, and M. Karami. Predicting range expansion of invasive raccoons in northern Iran using ENFA model at two different scales. *Ecological Informatics*, 15:96–102, 2013.

C. B. Field, V. R. Barros, K. Mach, and M. Mastrandrea. Climate change 2014: impacts, adaptation, and vulnerability. *Contribution of Working Group II to the IPCC 5th Assessment Report of the Intergovernmental Panel on Climate Change*, 2014.

W. B. Foden, S. H. Butchart, S. N. Stuart, J.-C. Vié, H. R. Akçakaya, A. Angulo, L. M. DeVantier, A. Gutsche, E. Turak, L. Cao, et al. Identifying the world's most climate change vulnerable species: a systematic trait-based assessment of all birds, amphibians and corals. *PLoS One*, 8(6): e65427, 2013a.

W. B. Foden, G. M. Mace, and S. H. Butchart. Indicators of climate change impacts on biodiversity. *Biodiversity Monitoring and Conservation: Bridging the Gap between Global Commitment and Local Action*, pages 120–137, 2013b.

B. J. Fox and J. Luo. Estimating competition coefficients from census data: a re-examination of the regression technique. *Oikos*, pages 291–300, 1996.

S. Frontier. Étude de la décroissance des valeurs propres dans une analyse en composantes principales: Comparaison avec le modéle du bâton brisé. *Journal of Experimental Marine Biology and Ecology*, 25(1):67–75, 1976.

B. Gaylord and S. D. Gaines. Temperature or transport? Range limits in marine species mediated solely by flow. *The American Naturalist*, 155(6):769–789, 2000.

GBIF. *Ochotona princeps* (Richardson, 1828) in GBIF Secretariat. GBIF Backbone Taxonomy. Checklist Dataset https://doi.org/10.15468/39omei, 2017. Accessed via GBIF.org: 2018-02-27.

M. A. Gilbert, S. M. White, J. M. Bullock, and E. A. Gaffney. Speeding up the simulation of population spread models. *Methods in Ecology and Evolution*, 8(4):501–510, 2017.

S. E. Gilman, M. C. Urban, J. Tewksbury, G. W. Gilchrist, and R. D. Holt. A framework for community interactions under climate change. *Trends in Ecology & Evolution*, 25(6):325–331, 2010.

D. Goodman. The demography of chance extinction. *Viable Populations for Conservation*, 11:34, 1987.

A. Guisan and F. E. Harrell. Ordinal response regression models in ecology. *Journal of Vegetation Science*, 11(5):617–626, 2000.

A. Guisan and C. Rahbek. SESAM–a new framework integrating macroecological and species distribution models for predicting spatio-temporal patterns of species assemblages. *Journal of Biogeography*, 38(8):1433–1444, 2011.

A. Guisan and W. Thuiller. Predicting species distribution: offering more than simple habitat models. *Ecology Letters*, 8(9):993–1009, 2005.

A. Guisan, T. C. Edwards Jr, and T. Hastie. Generalized linear and generalized additive models in studies of species distributions: setting the scene. *Ecological Modelling*, 157(2):89–100, 2002.

S. L. Gunckel, A. R. Hemmingsen, and J. L. Li. Effect of bull trout and brook trout interactions on foraging habitat, feeding behavior, and growth. *Transactions of the American Fisheries Society*, 131(6):1119–1130, 2002.

D. J. Hafner. Pikas and permafrost: post-Wisconsin historical zoogeography of Ochotona in the southern Rocky Mountains, USA. *Arctic and Alpine Research*, pages 375–382, 1994.

D. J. Hafner and R. M. Sullivan. Historical and ecological biogeography of Nearctic pikas (Lagomorpha: Ochotonidae). *Journal of Mammalogy*, 76(2):302–321, 1995.

S. M. Haig, T. D. Mullins, and E. D. Forsman. Subspecific relationships and genetic structure in the spotted owl. *Conservation Genetics*, 5(5):683–705, 2004.

D. B. Hall. Zero-inflated Poisson and binomial regression with random effects: a case study. *Biometrics*, 56(4):1030–1039, 2000.

J. G. Hallett and S. L. Pimm. Direct estimation of competition. *American Naturalist*, pages 593–600, 1979.

A. Hampe. Bioclimate envelope models: what they detect and what they hide. *Global Ecology and Biogeography*, 13(5):469–471, 2004.

T. Hance, J. Van Baaren, P. Vernon, and G. Boivin. Impact of extreme temperatures on parasitoids in a climate change perspective. *Annual Review of Entomology*, 52(1):107, 2006.

L. Hannah. Are a million species at risk? In *Saving a million species: extinction risk from climate change*, pages 3–9. Island Press, 2011.

R. Harrington, I. Woiwod, and T. Sparks. Climate change and trophic interactions. *Trends in Ecology & Evolution*, 14(4):146–150, 1999.

D. J. Harris. Generating realistic assemblages with a joint species distribution model. *Methods in Ecology and Evolution*, 6(4):465–473, 2015.

M. A. Harsch, Y. Zhou, J. HilleRisLambers, and M. Kot. Keeping pace with climate change: stage-structured moving-habitat models. *The American Naturalist*, 184(1):25–37, 2014.

M. A. Harsch, A. Phillips, Y. Zhou, M.-R. Leung, D. S. Rinnan, and M. Kot. Moving forward: insights and applications of moving-habitat models for climate change ecology. *Journal of Ecology*, 105(5):1169–1181, 2017.

M. P. Hassell, H. N. Comins, and R. M. Mayt. Spatial structure and chaos in insect population dynamics. *Nature*, 353(6341):255, 1991.

R. Hickling, D. B. Roy, J. K. Hill, R. Fox, and C. D. Thomas. The distributions of a wide range of taxonomic groups are expanding polewards. *Global Change Biology*, 12(3):450–455, 2006.

B. High, K. A. Meyer, D. J. Schill, and E. R. Mamer. Distribution, abundance, and population trends of bull trout in Idaho. *North American Journal of Fisheries Management*, 28(6):1687–1701, 2008.

R. J. Hijmans. raster: Geographic data analysis and modeling. http://CRAN.R-project.org/package=raster, 2014. R package version 2.2-31.

R. J. Hijmans and C. H. Graham. The ability of climate envelope models to predict the effect of climate change on species distributions. *Global Change Biology*, 12(12):2272–2281, 2006.

R. J. Hijmans, S. E. Cameron, J. L. Parra, P. G. Jones, and A. Jarvis. Very high resolution interpolated climate surfaces for global land areas. *International Journal of Climatology*, 25(15): 1965–1978, 2005.

R. J. Hijmans, S. Phillips, J. Leathwick, and J. Elith. dismo: Species distribution modeling. https://CRAN.R-project.org/package=dismo, 2017. R package version 1.1-4.

R. Hilborn, D. J. Hively, O. P. Jensen, and T. A. Branch. The dynamics of fish populations at low abundance and prospects for rebuilding and recovery. *ICES Journal of Marine Science*, 71(8): 2141–2151, 2014.

J. HilleRisLambers, M. A. Harsch, A. K. Ettinger, K. R. Ford, and E. J. Theobald. How will biotic interactions influence climate change–induced range shifts? *Annals of the New York Academy of Sciences*, 1297(1):112–125, 2013.

A. Hirzel, J. Hausser, and N. Perrin. Biomapper 3.1. *Lab. of Conservation Biology, Department of Ecology and Evolution, University of Lausanne*, 2004. URL http://www.unil.ch/biomapper.

A. H. Hirzel. *Linking landscape and population ecology for large population management modelling: the case of Ibex (Capra ibex) in Switzerland*. PhD thesis, Université de Lausanne, 2001. URL http://www.2.unil.ch/biomapper/Download/hirzel-2001-phd.zip.

A. H. Hirzel, J. Hausser, D. Chessel, and N. Perrin. Ecological-niche factor analysis: how to compute habitat-suitability maps without absence data? *Ecology*, 83(7):2027–2036, 2002.

J. A. Hodgson, C. D. Thomas, B. A. Wintle, and A. Moilanen. Climate change, connectivity and conservation decision making: back to basics. *Journal of Applied Ecology*, 46(5):964–969, 2009.

E. E. Holmes, M. A. Lewis, J. Banks, and R. Veit. Partial differential equations in ecology: spatial interactions and population dynamics. *Ecology*, pages 17–29, 1994.

T. Horiguchi and Y. Fukui. A variation of the Jentzsch theorem for a symmetric integral kernel and its application. *Interdisciplinary Information Sciences*, 2(2):139–144, 1996.

Y. Hosono. The minimal speed of traveling fronts for a diffusive Lotka-Volterra competition model. *Bulletin of Mathematical Biology*, 60(3):435–448, 1998.

J. S. Hughes, C. A. Cobbold, K. Haynes, and G. Dwyer. Effects of forest spatial structure on insect outbreaks: insights from a host-parasitoid model. *The American Naturalist*, 185(5):E130–E152, 2015.

L. Hughes. Biological consequences of global warming: is the signal already apparent? *Trends in Ecology & Evolution*, 15(2):56–61, 2000.

M. M. Humphries, J. Umbanhowar, and K. S. McCann. Bioenergetic prediction of climate change impacts on northern mammals. *Integrative and Comparative Biology*, 44(2):152–162, 2004.

A. H. Hurlbert and W. Jetz. Species richness, hotspots, and the scale dependence of range maps in ecology and conservation. *Proceedings of the National Academy of Sciences*, 104(33):13384–13389, 2007.

A. H. Hurlbert and E. P. White. Disparity between range map-and survey-based analyses of species richness: patterns, processes and implications. *Ecology Letters*, 8(3):319–327, 2005.

J. A. Hutchings and L. Gerber. Sex–biased dispersal in a salmonid fish. *Proceedings of the Royal Society of London. Series B: Biological Sciences*, 269(1508):2487–2493, 2002.

G. E. Hutchinson. Concluding remarks. *Cold Spring Harbor Symposium on Quantitative Biology*, 22:415–427, 1957.

D. Isaak, S. Wenger, E. Peterson, J. Ver Hoef, S. Hostetler, C. Luce, J. Dunham, J. Kershner, B. Roper, D. Nagel, et al. NorWeST: an interagency stream temperature database and model for the Northwest United States. *US Fish and Wildlife Service, Great Northern Landscape Conservation Cooperative Grant*, 2011. URL www.fs.fed.us/rm/boise/AWAE/projects/NorWeST.html.

D. J. Isaak, C. H. Luce, B. E. Rieman, D. E. Nagel, E. E. Peterson, D. L. Horan, S. Parkes, and G. L. Chandler. Effects of climate change and wildfire on stream temperatures and salmonid thermal habitat in a mountain river network. *Ecological Applications*, 20(5):1350–1371, 2010.

D. J. Isaak, M. K. Young, D. E. Nagel, D. L. Horan, and M. C. Groce. The cold-water climate shield: delineating refugia for preserving salmonid fishes through the 21st century. *Global Change Biology*, 2015.

IUCN. IUCN Red List categories and criteria: version 3.1. *IUCN Species Survival Commission*, 2001.

IUCN. The IUCN Red List of Threatened Species, Version 2017-3. http://www.iucnredlist.org, 2017. Accessed: 2017-12-01.

D. A. Jackson. Stopping rules in principal components analysis: a comparison of heuristical and statistical approaches. *Ecology*, pages 2204–2214, 1993.

A. Jensen. Simple density-dependent matrix model for population projection. *Ecological modelling*, 77(1):43–48, 1995.

R. Jentzsch. Über Integralgleichungen mit positivem Kern. *Journal für die reine und angewandte Mathematik*, 141:235–244, 1912.

K. J. Jesse. Modelling of a diffusive Lotka-Volterra-System: the climate-induced shifting of tundra and forest realms in North-America. *Ecological Modelling*, 123(2):53–64, 1999.

W. Jetz, D. S. Wilcove, and A. P. Dobson. Projected impacts of climate and land-use change on the global diversity of birds. *PLoS Biology*, 5(6):e157, 2007.

I. Jolliffe. *Principal component analysis*. Wiley Online Library, 2005.

Y. Kan-On. Fisher wave fronts for the Lotka-Volterra competition model with diffusion. *Nonlinear Analysis: Theory, Methods & Applications*, 28(1):145–164, 1997.

P. Kareiva. Experimental and mathematical analyses of herbivore movement: quantifying the influence of plant spacing and quality on foraging discrimination. *Ecological Monographs*, pages 261–282, 1982.

T. Kawamichi. Factors affecting sizes of home range and territory in pikas. *Japanese Journal of Ecology*, 32(1):21–27, 1982.

R. Kays, M. C. Crofoot, W. Jetz, and M. Wikelski. Terrestrial animal tracking as an eye on life and planet. *Science*, 348(6240):aaa2478, 2015.

M. Kearney and W. Porter. Mechanistic niche modelling: combining physiological and spatial data to predict species ranges. *Ecology Letters*, 12(4):334–350, 2009.

E. R. Keeley. Demographic responses to food and space competition by juvenile steelhead trout. *Ecology*, 82(5):1247–1259, 2001.

D. A. Keith, H. R. Akçakaya, W. Thuiller, G. F. Midgley, R. G. Pearson, S. J. Phillips, H. M. Regan, M. B. Araújo, and T. G. Rebelo. Predicting extinction risks under climate change: coupling stochastic population models with dynamic bioclimatic habitat models. *Biology Letters*, 4(5): 560–563, 2008.

W. D. Koenig, D. Van Vuren, and P. N. Hooge. Detectability, philopatry, and the distribution of dispersal distances in vertebrates. *Trends in Ecology & Evolution*, 11(12):514–517, 1996.

L. Y. Kolotilina. Lower bounds for the Perron root of a nonnegative matrix. *Linear Algebra and its Applications*, 180:133–151, 1993.

M. Kot and A. Phillips. Bounds for the critical speed of climate-driven moving-habitat models. *Mathematical Biosciences*, 262:65–72, 2015.

M. Kot and W. M. Schaffer. Discrete-time growth-dispersal models. *Mathematical Biosciences*, 80 (1):109–136, 1986.

M. Kot, M. A. Lewis, and P. van den Driessche. Dispersal data and the spread of invading organisms. *Ecology*, 77(7):2027–2042, 1996.

M. Kot, J. Medlock, T. Reluga, and D. B. Walton. Stochasticity, invasions, and branching random walks. *Theoretical Population Biology*, 66(3):175–184, 2004.

K. Krajick. All downhill from here? *Science*, 303(5664):1600–1602, 2004. doi: 10.1126/science.303.5664.1600.

R. Krishnaraj and G. Pritchard. The influence of larval size, temperature, and components of the functional response to prey density on growth rates of the dragonflies *Lestes disjunctus* and *Coenagrion resolutum* (Insecta: Odonata). *Canadian Journal of Zoology*, 73(9):1672–1680, 1995.

J. Latore, P. Gould, and A. Mortimer. Spatial dynamics and critical patch size of annual plant populations. *Journal of Theoretical Biology*, 190(3):277–285, 1998.

J. Latore, P. Gould, and A. Mortimer. Effects of habitat heterogeneity and dispersal strategies on population persistence in annual plants. *Ecological Modelling*, 123(2-3):127–139, 1999.

J. J. Lawler, D. White, R. P. Neilson, and A. R. Blaustein. Predicting climate-induced range shifts: model differences and model reliability. *Global Change Biology*, 12(8):1568–1584, 2006.

J. J. Lawler, S. L. Shafer, D. White, P. Kareiva, E. P. Maurer, A. R. Blaustein, and P. J. Bartlein. Projected climate-induced faunal change in the Western Hemisphere. *Ecology*, 90(3):588–597, 2009.

J. Leathwick, J. Elith, and T. Hastie. Comparative performance of generalized additive models and multivariate adaptive regression splines for statistical modelling of species distributions. *Ecological Modelling*, 199(2):188–196, 2006.

S. Lek and J.-F. Guégan. Artificial neural networks as a tool in ecological modelling, an introduction. *Ecological Modelling*, 120(2-3):65–73, 1999.

M. S. Lenarz, M. E. Nelson, M. W. Schrage, and A. J. Edwards. Temperature mediated moose survival in northeastern Minnesota. *Journal of Wildlife Management*, 73(4):503–510, 2009.

S. J. Leroux, M. Larrivée, V. Boucher-Lalonde, A. Hurford, J. Zuloaga, J. T. Kerr, and F. Lutscher. Mechanistic models for the spatial spread of species under climate change. *Ecological Applications*, 23(4):815–828, 2013.

P. Leslie. A stochastic model for studying the properties of certain biological systems by numerical methods. *Biometrika*, 45(1/2):16–31, 1958.

P. Leslie and J. Gower. The properties of a stochastic model for two competing species. *Biometrika*, pages 316–330, 1958.

P. H. Leslie. On the use of matrices in certain population mathematics. *Biometrika*, 33(3):183–212, 1945.

P. S. Levin, S. Achord, B. E. Feist, and R. W. Zabel. Non–indigenous brook trout and the demise of pacific salmon: a forgotten threat? *Proceedings of the Royal Society of London B: Biological Sciences*, 269(1501):1663–1670, 2002.

S. A. Levin, H. C. Muller-Landau, R. Nathan, and J. Chave. The ecology and evolution of seed dispersal: a theoretical perspective. *Annual Review of Ecology, Evolution, and Systematics*, pages 575–604, 2003.

J. M. Levine and D. J. Murrell. The community-level consequences of seed dispersal patterns. *Annual Review of Ecology, Evolution, and Systematics*, pages 549–574, 2003.

J. M. Levine and M. Rees. Coexistence and relative abundance in annual plant assemblages: the roles of competition and colonization. *The American Naturalist*, 160(4):452–467, 2002.

R. Levins. *Evolution in changing environments: some theoretical explorations*. Number 2. Princeton University Press, 1968.

M. Lewis and S. Pacala. Modeling and analysis of stochastic invasion processes. *Journal of Mathematical Biology*, 41(5):387–429, 2000.

M. A. Lewis, B. Li, and H. F. Weinberger. Spreading speed and linear determinacy for two-species competition models. *Journal of Mathematical Biology*, 45(3):219–233, 2002.

E. L. Little, Jr et al. Atlas of United States trees. Conifers and important hardwoods. *Miscellaneous Publications. United States Department of Agriculture*, 1(1146), 1971.

C. E. Littlefield, B. H. McRae, J. L. Michalak, J. J. Lawler, and C. Carroll. Connecting today's climates to future climate analogs to facilitate movement of species under climate change. *Conservation Biology*, 31(6):1397–1408, 2017.

P. Liu and S. N. Elaydi. Discrete competitive and cooperative models of Lotka–Volterra type. *Journal of Computational Analysis and Applications*, 3(1):53–73, 2001.

B. A. Loiselle, C. H. Graham, J. M. Goerck, and M. C. Ribeiro. Assessing the impact of deforestation and climate change on the range size and environmental niche of bird species in the Atlantic forests, Brazil. *Journal of Biogeography*, 37(7):1288–1301, 2010.

F. Lutscher and M. A. Lewis. Spatially-explicit matrix models. *Journal of Mathematical Biology*, 48(3):293–324, 2004.

F. Lutscher, E. Pachepsky, and M. A. Lewis. The effect of dispersal patterns on stream populations. *Siam Review*, 47(4):749–772, 2005.

F. Lutscher, R. M. Nisbet, and E. Pachepsky. Population persistence in the face of advection. *Theoretical Ecology*, 3(4):271–284, 2010.

R. MacArthur and R. Levins. The limiting similarity, convergence, and divergence of coexisting species. *American Naturalist*, pages 377–385, 1967.

S. Manel, H. C. Williams, and S. J. Ormerod. Evaluating presence–absence models in ecology: the need to account for prevalence. *Journal of Applied Ecology*, 38(5):921–931, 2001.

R. M. May and G. F. Oster. Bifurcations and dynamic complexity in simple ecological models. *American Naturalist*, pages 573–599, 1976.

R. M. May et al. Simple mathematical models with very complicated dynamics. *Nature*, 261(5560): 459–467, 1976.

J. H. McCormick, K. E. Hokanson, and B. R. Jones. Effects of temperature on growth and survival of young brook trout, *Salvelinus fontinalis*. *Journal of the Fisheries Board of Canada*, 29(8): 1107–1112, 1972.

B. H. McRae, B. G. Dickson, T. H. Keitt, and V. B. Shah. Using circuit theory to model connectivity in ecology, evolution, and conservation. *Ecology*, 89(10):2712–2724, 2008.

C. Merow, M. J. Smith, and J. A. Silander. A practical guide to MaxEnt for modeling species distributions: what it does, and why inputs and settings matter. *Ecography*, 36(10):1058–1069, 2013.

G. Midgley, G. Hughes, W. Thuiller, and A. Rebelo. Migration rate limitations on climate change-induced range shifts in Cape Proteaceae. *Diversity and Distributions*, 12(5):555–562, 2006.

J. S. Millar and F. C. Zwickel. Determination of age, age structure, and mortality of the pika, *Ochotona princeps* (Richardson). *Canadian Journal of Zoology*, 50(2):229–232, 1972.

R. F. Miller and J. A. Rose. Fire history and western juniper encroachment in sagebrush steppe. *Journal of Range Management*, pages 550–559, 1999.

R. F. Miller et al. Biology, ecology, and management of western juniper (*Juniperus occidentalis*). Technical report, Corvallis, Or.: Agricultural Experiment Station, Oregon State University, 2005.

X. Morin and M. J. Lechowicz. Niche breadth and range area in North American trees. *Ecography*, 36(3):300–312, 2013.

X. Morin and W. Thuiller. Comparing niche-and process-based models to reduce prediction uncertainty in species range shifts under climate change. *Ecology*, 90(5):1301–1313, 2009.

C. Moritz, J. L. Patton, C. J. Conroy, J. L. Parra, G. C. White, and S. R. Beissinger. Impact of a century of climate change on small-mammal communities in Yosemite National Park, USA. *Science*, 322(5899):261–264, 2008.

S. F. Morrison and D. S. Hik. Demographic analysis of a declining pika *Ochotona collaris* population: linking survival to broad-scale climate patterns via spring snowmelt patterns. *Journal of Animal Ecology*, 76(5):899–907, 2007.

J. Muñoz, Á. M. Felicísimo, F. Cabezas, A. R. Burgaz, and I. Martínez. Wind as a long-distance dispersal vehicle in the Southern Hemisphere. *Science*, 304(5674):1144–1147, 2004.

S. Nakano, S. Kitano, K. Nakai, and K. D. Fausch. Competitive interactions for foraging microhabitat among introduced brook charr, *Salvelinus fontinalis*, and native bull charr, *S. confluentus*, and westslope cutthroat trout, *Oncorhynchus clarki lewisi*, in a Montana stream. *Environmental Biology of Fishes*, 52(1-3):345–355, 1998.

R. Nathan. Long-distance dispersal of plants. *Science*, 313(5788):786–788, 2006.

R. Nathan and H. C. Muller-Landau. Spatial patterns of seed dispersal, their determinants and consequences for recruitment. *Trends in Ecology & Evolution*, 15(7):278–285, 2000.

R. Nathan, G. Perry, J. T. Cronin, A. E. Strand, and M. L. Cain. Methods for estimating long-distance dispersal. *Oikos*, 103(2):261–273, 2003.

T. A. Nuñez, J. J. Lawler, B. H. McRae, D. J. Pierce, M. B. Krosby, D. M. Kavanagh, P. H. Singleton, and J. J. Tewksbury. Connectivity planning to address climate change. *Conservation Biology*, 27(2):407–416, 2013.

J. D. Olden and D. A. Jackson. Illuminating the black box: a randomization approach for understanding variable contributions in artificial neural networks. *Ecological Modelling*, 154(1-2): 135–150, 2002.

A. Ostrowski. On the convergence of the Rayleigh quotient iteration for the computation of the characteristic roots and vectors. *Archive for Rational Mechanics and Analysis*, 3(1):325–340, 1959.

E. Pachepsky, F. Lutscher, R. Nisbet, and M. Lewis. Persistence, spread and the drift paradox. *Theoretical Population Biology*, 67(1):61–73, 2005.

J. Pagel and F. M. Schurr. Forecasting species ranges by statistical estimation of ecological niches and spatial population dynamics. *Global Ecology and Biogeography*, 21(2):293–304, 2012.

T. Park. Experimental studies of interspecies competition. I. Competition between populations of the flour beetles, *Tribolium confusum* (Duval) and *Tribolium castaneum* (Herbst). *Ecological Monographs*, 18:265–308, 1948.

C. Parmesan. Ecological and evolutionary responses to recent climate change. *Annual Review of Ecology, Evolution, and Systematics*, 37:637–669, 2006.

C. Parmesan and G. Yohe. A globally coherent fingerprint of climate change impacts across natural systems. *Nature*, 421(6918):37, 2003.

C. Parmesan, N. Ryrholm, C. Stefanescu, J. K. Hill, C. D. Thomas, H. Descimon, B. Huntley, L. Kaila, J. Kullberg, T. Tammaru, et al. Poleward shifts in geographical ranges of butterfly species associated with regional warming. *Nature*, 399(6736):579–583, 1999.

M. L. Parry. *Climate Change 2007: impacts, adaptation and vulnerability: contribution of Working Group II to the fourth assessment report of the Intergovernmental Panel on Climate Change*, volume 4. Cambridge University Press, 2007.

M. M. Peacock. Determining natal dispersal patterns in a population of North American pikas (*Ochotona princeps*) using direct mark-resight and indirect genetic methods. *Behavioral Ecology*, 8(3):340–350, 1997.

M. M. Peacock and A. T. Smith. The effect of habitat fragmentation on dispersal patterns, mating behavior, and genetic variation in a pika (*Ochotona princeps*) metapopulation. *Oecologia*, 112(4): 524–533, 1997.

R. G. Pearson. Climate change and the migration capacity of species. *Trends in Ecology & Evolution*, 21(3):111–113, 2006.

R. G. Pearson and T. P. Dawson. Predicting the impacts of climate change on the distribution of species: are bioclimate envelope models useful? *Global Ecology and Biogeography*, 12(5):361–371, 2003.

R. G. Pearson and T. P. Dawson. Bioclimate envelope models: what they detect and what they hide — response to Hampe (2004). *Global Ecology and Biogeography*, 13(5):471–473, 2004.

R. G. Pearson, W. Thuiller, M. B. Araújo, E. Martinez-Meyer, L. Brotons, C. McClean, L. Miles, P. Segurado, T. P. Dawson, and D. C. Lees. Model-based uncertainty in species range prediction. *Journal of Biogeography*, 33(10):1704–1711, 2006.

R. G. Pearson, J. C. Stanton, K. T. Shoemaker, M. E. Aiello-Lammens, P. J. Ersts, N. Horning, D. A. Fordham, C. J. Raxworthy, H. Y. Ryu, J. McNees, et al. Life history and spatial traits predict extinction risk due to climate change. *Nature Climate Change*, 4(3):217–221, 2014.

C. M. Pease, R. Lande, and J. Bull. A model of population growth, dispersal and evolution in a changing environment. *Ecology*, 70(6):1657–1664, 1989.

A. L. Perry, P. J. Low, J. R. Ellis, and J. D. Reynolds. Climate change and distribution shifts in marine fishes. *Science*, 308(5730):1912–1915, 2005.

C. A. Pfister. Estimating competition coefficients from census data: a test with field manipulations of tidepool fishes. *American Naturalist*, pages 271–291, 1995.

A. Phillips and M. Kot. Persistence in a two-dimensional moving-habitat model. *Bulletin of Mathematical Biology*, 77(11):2125–2159, 2015.

B. L. Phillips, G. P. Brown, M. Greenlees, J. K. Webb, and R. Shine. Rapid expansion of the cane toad (*Bufo marinus*) invasion front in tropical Australia. *Austral Ecology*, 32(2):169–176, 2007.

S. J. Phillips, M. Dudík, and R. E. Schapire. A maximum entropy approach to species distribution modeling. In *Proceedings of the Twenty-First International Conference on Machine Learning*, page 83. ACM, 2004.

E. R. Pianka. *Competition and niche theory*. Ariel Oxford, UK, 1981.

M. L. Pinsky, B. Worm, M. J. Fogarty, J. L. Sarmiento, and S. A. Levin. Marine taxa track local climate velocities. *Science*, 341(6151):1239–1242, 2013.

L. J. Pollock, R. Tingley, W. K. Morris, N. Golding, R. B. O'Hara, K. M. Parris, P. A. Vesk, and M. A. McCarthy. Understanding co-occurrence by modelling species simultaneously with a Joint Species Distribution Model (JSDM). *Methods in Ecology and Evolution*, 5(5):397–406, 2014.

H.-O. Pörtner, B. Berdal, R. Blust, O. Brix, A. Colosimo, B. De Wachter, A. Giuliani, T. Johansen, T. Fischer, R. Knust, et al. Climate induced temperature effects on growth performance, fecundity and recruitment in marine fish: developing a hypothesis for cause and effect relationships in Atlantic cod (*Gadus morhua*) and common eelpout (*Zoarces viviparus*). *Continental Shelf Research*, 21(18-19):1975–1997, 2001.

H. P. Possingham and J. Roughgarden. Spatial population dynamics of a marine organism with a complex life cycle. *Ecology*, 71(3):973–985, 1990.

E. Post and C. Pedersen. Opposing plant community responses to warming with and without herbivores. *Proceedings of the National Academy of Sciences*, 105(34):12353–12358, 2008.

A. Potapov and M. Lewis. Climate and competition: the effect of moving range boundaries on habitat invasibility. *Bulletin of Mathematical Biology*, 66(5):975–1008, 2004.

J. A. Pounds, M. R. Bustamante, L. A. Coloma, J. A. Consuegra, M. P. Fogden, P. N. Foster, E. La Marca, K. L. Masters, A. Merino-Viteri, R. Puschendorf, et al. Widespread amphibian extinctions from epidemic disease driven by global warming. *Nature*, 439(7073):161–167, 2006.

J. A. Powell and N. E. Zimmermann. Multiscale analysis of active seed dispersal contributes to resolving Reid's paradox. *Ecology*, 85(2):490–506, 2004.

A. M. Prasad, L. R. Iverson, and A. Liaw. Newer classification and regression tree techniques: bagging and random forests for ecological prediction. *Ecosystems*, 9(2):181–199, 2006.

R Core Team. *R: A Language and Environment for Statistical Computing*. R Foundation for Statistical Computing, Vienna, Austria, 2017. URL https://www.R-project.org/.

F. J. Rahel and J. D. Olden. Assessing the effects of climate change on aquatic invasive species. *Conservation Biology*, 22(3):521–533, 2008.

H. Rahmandad and J. Sterman. Heterogeneity and network structure in the dynamics of diffusion: comparing agent-based and differential equation models. *Management Science*, 54(5):998–1014, 2008.

L. A. Real and S. A. Levin. *Theoretical advances: the role of theory in the rise of modern ecology*. University of Chicago Press, Chicago, Illinois, USA, 1991.

J. R. Reimer, M. B. Bonsall, and P. K. Maini. Approximating the critical domain size of integrodifference equations. *Bulletin of Mathematical Biology*, pages 1–38, 2015.

G.-Y. Rhee and I. J. Gotham. The effect of environmental factors on phytoplankton growth: temperature and the interactions of temperature with nutrient limitation. *Limnology and Oceanography*, 26(4):635–648, 1981.

S. Rickebusch, W. Thuiller, T. Hickler, M. B. Araujo, M. T. Sykes, O. Schweiger, and B. Lafourcade. Incorporating the effects of changes in vegetation functioning and CO2 on water availability in plant habitat models. *Biology Letters*, 4(5):556–559, 2008.

W. E. Ricker. Stock and recruitment. *Journal of the Fisheries Board of Canada*, 11(5):559–623, 1954.

A. Rieux, S. Soubeyrand, F. Bonnot, E. K. Klein, J. E. Ngando, A. Mehl, V. Ravigne, J. Carlier, and L. d. L. de Bellaire. Long-distance wind-dispersal of spores in a fungal plant pathogen: estimation of anisotropic dispersal kernels from an extensive field experiment. *PLoS One*, 9(8):e103225, 2014.

D. S. Rinnan. CENFA: Climate and ecological niche factor analysis. https://CRAN.R-project.org/package=CENFA, 2018a. R package version 0.1.0.

D. S. Rinnan. The dispersal success and persistence of populations with asymmetric dispersal. *Theoretical Ecology*, 11(1):55–69, 2018b.

E. G. Ritchie, J. K. Martin, C. N. Johnson, and B. J. Fox. Separating the influences of environment and species interactions on patterns of distribution and abundance: competition between large herbivores. *Journal of Animal Ecology*, 78(4):724–731, 2009.

K. M. Robson, C. T. Lamb, and M. A. Russello. Low genetic diversity, restricted dispersal, and elevation-specific patterns of population decline in American pikas in an atypical environment. *Journal of Mammalogy*, 97(2):464–472, 2015.

A. S. Rodrigues, J. D. Pilgrim, J. F. Lamoreux, M. Hoffmann, and T. M. Brooks. The value of the IUCN Red List for conservation. *Trends in Ecology & Evolution*, 21(2):71–76, 2006.

M. A. Rodríguez. A modeling framework for assessing long-distance dispersal and loss of connectivity in stream fish. In *American Fisheries Society Symposium*, volume 73, pages 263–279, 2010.

P. J. Rousseeuw and C. Croux. Alternatives to the median absolute deviation. *Journal of the American Statistical Association*, 88(424):1273–1283, 1993.

R. D. Sagarin, J. P. Barry, S. E. Gilman, and C. H. Baxter. Climate-related change in an intertidal community over short and long time scales. *Ecological Monographs*, 69(4):465–490, 1999.

T. Sattler, F. Bontadina, A. H. Hirzel, and R. Arlettaz. Ecological niche modelling of two cryptic bat species calls for a reassessment of their conservation status. *Journal of Applied Ecology*, 44 (6):1188–1199, 2007.

C. A. Schloss, T. A. Nuñez, and J. J. Lawler. Dispersal will limit ability of mammals to track climate change in the Western Hemisphere. *Proceedings of the National Academy of Sciences*, 109(22): 8606–8611, 2012.

T. W. Schoener. Competition and the form of habitat shift. *Theoretical Population Biology*, 6(3): 265–307, 1974.

N. Schtickzelle, G. Mennechez, and M. Baguette. Dispersal depression with habitat fragmentation in the bog fritillary butterfly. *Ecology*, 87(4):1057–1065, 2006.

A. J. Schwenk. Tight bounds on the spectral radius of asymmetric nonnegative matrices. *Linear Algebra and its Applications*, 75:257–265, 1986.

J. H. Selong, T. E. McMahon, A. V. Zale, and F. T. Barrows. Effect of temperature on growth and survival of bull trout, with application of an improved method for determining thermal tolerance in fishes. *Transactions of the American Fisheries Society*, 130(6):1026–1037, 2001.

S. J. Sinclair, M. D. White, and G. R. Newell. How useful are species distribution models for managing biodiversity under future climates? *Ecology and Society*, 15(1), 2010.

G. T. Skalski and J. F. Gilliam. Modeling diffusive spread in a heterogeneous population: a movement study with stream fish. *Ecology*, 81(6):1685–1700, 2000.

A. T. Smith. The distribution and dispersal of pikas: consequences of insular population structure. *Ecology*, 55(5):1112–1119, 1974.

A. T. Smith. Comparative demography of pikas (*Ochotona*): effect of spatial and temporal age-specific mortality. *Ecology*, 59(1):133–139, 1978.

A. T. Smith. Population structure of pikas: dispersal versus philopatry. In *Mammalian dispersal patterns: the effects of social structure on population genetics*, pages 128–142. University of Chicago Press Chicago, Illinois, 1987.

A. T. Smith and B. L. Ivins. Colonization in a pika population: dispersal vs philopatry. *Behavioral Ecology and Sociobiology*, 13(1):37–47, 1983.

A. T. Smith and B. L. Ivins. Temporal separation between philopatric juvenile pikas and their parents limits behavioural conflict. *Animal Behaviour*, 35(4):1210–1214, 1987.

A. T. Smith and M. L. Weston. *Ochotona princeps*. *Mammalian Species*, (352):1–8, 1990.

R. E. Snyder. How demographic stochasticity can slow biological invasions. *Ecology*, 84(5):1333–1339, 2003.

C. Soares and J. C. Brito. Environmental correlates for species richness among amphibians and reptiles in a climate transition area. In *Vertebrate Conservation and Biodiversity*, pages 261–276. Springer, 2006.

S. Solomon. *Climate change 2007-the physical science basis: Working group I contribution to the fourth assessment report of the IPCC*, volume 4. Cambridge University Press, 2007.

F. A. L. Sorte and F. R. Thompson, III. Poleward shifts in winter ranges of North American birds. *Ecology*, 88(7):1803–1812, 2007.

S. Soubeyrand, J. Enjalbert, A. Sanchez, and I. Sache. Anisotropy, in density and in distance, of the dispersal of yellow rust of wheat: experiments in large field plots and estimation. *Phytopathology*, 97(10):1315–1324, 2007.

M. E. Soule and B. A. Wilcox. *Conservation biology: an evolutionary-ecological perspective*. Number 333.95 C755. Sinauer, 1980.

C. H. Southwick, S. C. Golian, M. R. Whitworth, J. C. Halfpenny, and R. Brown. Population density and fluctuations of pikas (*Ochotona princeps*) in Colorado. *Journal of Mammalogy*, 67 (1):149–153, 1986.

J. C. Stanton, K. T. Shoemaker, R. G. Pearson, and H. R. Akçakaya. Warning times for species extinctions due to climate change. *Global Change Biology*, 21(3):1066–1077, 2015.

F. M. Steiner, B. C. Schlick-Steiner, J. VanDerWal, K. D. Reuther, E. Christian, C. Stauffer, A. V. Suarez, S. E. Williams, and R. H. Crozier. Combined modelling of distribution and niche in invasion biology: a case study of two invasive *Tetramorium* ant species. *Diversity and Distributions*, 14(3):538–545, 2008.

T. Stocker. *Climate change 2013: the physical science basis: Working Group I contribution to the Fifth assessment report of the Intergovernmental Panel on Climate Change*. Cambridge University Press, 2014.

B. K. Sullivan, R. W. Bowker, K. B. Malmos, and E. W. Gergus. Arizona distribution of three Sonoran Desert anurans: *Bufo retiformis*, *Gastrophryne olivacea*, and *Pternohyla fodiens*. *Western North American Naturalist*, 56(1):38–47, 1996.

Y. Svirezhev. Lotka–Volterra models and the global vegetation pattern. *Ecological Modelling*, 135 (2):135–146, 2000.

S. Tapper. *The Spatial Organisation of Pikas, Ochotona and Its Effect on Population Recruitment*. PhD thesis, University of Alberta, 1973. URL https://books.google.com/books?id=JLwUtAEACAAJ.

C. D. Thomas, A. Cameron, R. E. Green, M. Bakkenes, L. J. Beaumont, Y. C. Collingham, B. F. Erasmus, M. F. De Siqueira, A. Grainger, L. Hannah, et al. Extinction risk from climate change. *Nature*, 427(6970):145–148, 2004.

C. D. Thomas, J. K. Hill, B. J. Anderson, S. Bailey, C. M. Beale, R. B. Bradbury, C. R. Bulman, H. Q. Crick, F. Eigenbrod, H. M. Griffiths, et al. A framework for assessing threats and benefits to species responding to climate change. *Methods in Ecology and Evolution*, 2(2):125–142, 2011.

D. J. Thompson. Towards a realistic predator-prey model: the effect of temperature on the functional response and life history of larvae of the damselfly, *Ischnura elegans*. *The Journal of Animal Ecology*, pages 757–767, 1978.

J. T. Thorson, M. D. Scheuerell, A. O. Shelton, K. E. See, H. J. Skaug, and K. Kristensen. Spatial factor analysis: a new tool for estimating joint species distributions and correlations in species range. *Methods in Ecology and Evolution*, 6(6):627–637, 2015.

W. Thuiller, S. Lavorel, M. B. Araújo, M. T. Sykes, and I. C. Prentice. Climate change threats to plant diversity in Europe. *Proceedings of the National Academy of Sciences of the United States of America*, 102(23):8245–8250, 2005.

W. Thuiller, D. M. Richardson, and G. F. Midgley. Will climate change promote alien plant invasions? In *Biological Invasions*, pages 197–211. Springer, 2007.

D. Tilman. Niche tradeoffs, neutrality, and community structure: a stochastic theory of resource competition, invasion, and community assembly. *Proceedings of the National Academy of Sciences of the United States of America*, 101(30):10854–10861, 2004.

L. W. Traill, C. J. Bradshaw, and B. W. Brook. Minimum viable population size: a meta-analysis of 30 years of published estimates. *Biological Conservation*, 139(1-2):159–166, 2007.

L. W. Traill, M. L. Lim, N. S. Sodhi, and C. J. Bradshaw. Mechanisms driving change: altered species interactions and ecosystem function through global warming. *Journal of Animal Ecology*, 79(5):937–947, 2010.

A. Trakhtenbrot, R. Nathan, G. Perry, and D. M. Richardson. The importance of long-distance dispersal in biodiversity conservation. *Diversity and Distributions*, 11(2):173–181, 2005.

M. C. Urban, J. J. Tewksbury, and K. S. Sheldon. On a collision course: competition and dispersal differences create no-analogue communities and cause extinctions during climate change. *Proceedings of the Royal Society of London B: Biological Sciences*, 279(1735):2072–2080, 2012.

US Fish and Wildlife Service and others. Bull trout recovery: Monitoring and evaluation guidance. Technical report, US Fish and Wildlife Service, 2008.

U.S. Geological Survey. Digital representation of "Atlas of United States Trees" by Elbert L. Little, Jr. http://gec.cr.usgs.gov/data/little. Accessed: 2014-08-01.

W. H. Van der Putten, M. Macel, and M. E. Visser. Predicting species distribution and abundance responses to climate change: why it is essential to include biotic interactions across trophic levels. *Philosophical Transactions of the Royal Society B: Biological Sciences*, 365(1549):2025–2034, 2010.

R. W. Van Kirk and M. A. Lewis. Integrodifference models for persistence in fragmented habitats. *Bulletin of Mathematical Biology*, 59(1):107–137, 1997.

O. Vasilyeva, F. Lutscher, and M. Lewis. Analysis of spread and persistence for stream insects with winged adult stages. *Journal of Mathematical Biology*, 72(4):851–875, 2016.

R. R. Veit and M. A. Lewis. Dispersal, population growth, and the Allee effect: dynamics of the house finch invasion of eastern North America. *American Naturalist*, pages 255–274, 1996.

M. Vilà, J. D. Corbin, J. S. Dukes, J. Pino, and S. D. Smith. Linking plant invasions to global environmental change. In *Terrestrial ecosystems in a changing world*, pages 93–102. Springer, 2007.

S. Vuilleumier and H. P. Possingham. Does colonization asymmetry matter in metapopulations? *Proceedings of the Royal Society of London B: Biological Sciences*, 273(1594):1637–1642, 2006.

S. Wagner, K. Wälder, E. Ribbens, and A. Zeibig. Directionality in fruit dispersal models for anemochorous forest trees. *Ecological Modelling*, 179(4):487–498, 2004.

G.-R. Walther, E. Post, P. Convey, A. Menzel, C. Parmesan, T. J. Beebee, J.-M. Fromentin, O. Hoegh-Guldberg, and F. Bairlein. Ecological responses to recent climate change. *Nature*, 416(6879):389–395, 2002.

M.-H. Wang, M. Kot, and M. G. Neubert. Integrodifference equations, Allee effects, and invasions. *Journal of Mathematical Biology*, 44(2):150–168, 2002.

T. Wang, A. Hamann, D. L. Spittlehouse, and T. Q. Murdock. ClimateWNA-high-resolution spatial climate data for Western North America. *Journal of Applied Meteorology & Climatology*, 51(1), 2012.

D. A. Way and R. Oren. Differential responses to changes in growth temperature between trees from different functional groups and biomes: a review and synthesis of data. *Tree Physiology*, 30(6): 669–688, 2010.

S. Werth, H. H. Wagner, F. Gugerli, R. Holderegger, D. Csencsics, J. M. Kalwij, and C. Scheidegger. Quantifying dispersal and establishment limitation in a population of an epiphytic lichen. *Ecology*, 87(8):2037–2046, 2006.

M. Wikelski, R. W. Kays, N. J. Kasdin, K. Thorup, J. A. Smith, and G. W. Swenson. Going wild: what a global small-animal tracking system could do for experimental biologists. *Journal of Experimental Biology*, 210(2):181–186, 2007.

D. S. Wilcove, D. Rothstein, J. Dubow, A. Phillips, and E. Losos. Quantifying threats to imperiled species in the United States. *BioScience*, 48(8):607–615, 1998.

S. E. Williams, L. P. Shoo, J. L. Isaac, A. A. Hoffmann, and G. Langham. Towards an integrated framework for assessing the vulnerability of species to climate change. *PLoS Biology*, 6(12):e325, 2008.

M. Willson. Dispersal mode, seed shadows, and colonization patterns. In *Frugivory and seed dispersal: ecological and evolutionary aspects*, pages 261–280. Springer, 1993.

M. F. Willson and A. Traveset. The ecology of seed dispersal. *Seeds: The ecology of regeneration in plant communities*, 2:85–110, 2000.

R. J. Wilson, D. Gutiérrez, J. Gutiérrez, D. Martínez, R. Agudo, and V. J. Monserrat. Changes to the elevational limits and extent of species ranges associated with climate change. *Ecology Letters*, 8(11):1138–1146, 2005.

M. S. Wisz, J. Pottier, W. D. Kissling, L. Pellissier, J. Lenoir, C. F. Damgaard, C. F. Dormann, M. C. Forchhammer, J.-A. Grytnes, A. Guisan, et al. The role of biotic interactions in shaping distributions and realised assemblages of species: implications for species distribution modelling. *Biological Reviews*, 88(1):15–30, 2013.

R. Wolmarans, M. P. Robertson, and B. J. van Rensburg. Predicting invasive alien plant distributions: how geographical bias in occurrence records influences model performance. *Journal of Biogeography*, 37(9):1797–1810, 2010.

C. Xu, B. Letcher, and K. Nislow. Size-dependent survival of brook trout *Salvelinus fontinalis* in summer: effects of water temperature and stream flow. *Journal of Fish Biology*, 76(10):2342–2369, 2010.

B. E. Young, K. R. Hall, E. Byers, K. Gravuer, G. Hammerson, A. Redder, and K. Szabo. Rapid assessment of plant and animal vulnerability to climate change. *Wildlife Conservation in a Changing Climate*, page 129, 2012.

P. P. Zabreyko, A. Koshelev, M. Krasnoselskii, S. Mikhlin, L. Rakovshchik, and V. Y. Stetsenko. *Integral equations: A reference text*. Springer, 2013.

J. Zhang and S. Li. A review of machine learning based species' distribution modelling. In *2017 International Conference on Industrial Informatics-Computing Technology, Intelligent Technology, Industrial Information Integration (ICIICII)*, pages 199–206. IEEE, 2017.

Y. Zhou and M. Kot. Discrete-time growth-dispersal models with shifting species ranges. *Theoretical Ecology*, 4(1):13–25, 2011.

D. Zurell, F. Jeltsch, C. F. Dormann, and B. Schröder. Static species distribution models in dynamically changing systems: how good can predictions really be? *Ecography*, 32(5):733–744, 2009.

Appendix I

A PROOF OF STABILITY OF THE COMPETITIVE IDE EQUILIBRIUM SOLUTION (M^*, N^*)

The stability of the nontrivial coexistence equilibrium

$$L_B = \Bigg(\frac{\alpha_n(\lambda_m - 1) - \beta_m(\lambda_n - 1)}{\alpha_m\alpha_n - \beta_m\beta_n} \, , \tag{I.1}$$

$$\frac{\alpha_m(\lambda_n - 1) - \beta_n(\lambda_m - 1)}{\alpha_m\alpha_n - \beta_m\beta_n} \Bigg) \tag{I.2}$$

has long been established (Leslie and Gower, 1958), but I have not yet demonstrated the stability of our estimate of the mean population density at equilibrium. I provide a proof here.

Represent the approximated average populations by

$$f(M, N) = \frac{S_m\lambda_m M}{1 + \alpha_m M + \beta_m N}, \tag{I.3}$$

$$g(M, N) = \frac{S_n\lambda_n N}{1 + \alpha_n N + \beta_n M}, \tag{I.4}$$

with nontrivial fixed point $P_B = (M^*, N^*)$, where

$$M^* = \frac{\alpha_n(S_m\lambda_m - 1) - \beta_m(S_n\lambda_n - 1)}{\alpha_m\alpha_n - \beta_m\beta_n}, \tag{I.5}$$

$$N^* = \frac{\alpha_m(S_n\lambda_n - 1) - \beta_n(S_m\lambda_m - 1)}{\alpha_m\alpha_n - \beta_m\beta_n}. \tag{I.6}$$

Defining

$$p = \frac{S_m\lambda_m - 1}{\alpha_m}, \tag{I.7}$$

$$q = \frac{S_n\lambda_n - 1}{\alpha_n}, \tag{I.8}$$

and noting that

$$\alpha_m M^* + \beta_m N^* = \alpha_m p, \tag{I.9}$$

$$\alpha_n N^* + \beta_n M^* = \alpha_n q, \tag{I.10}$$

we write the Jacobian matrix J as

$$J = \begin{pmatrix} \frac{\partial f}{\partial M} & \frac{\partial f}{\partial N} \\ \\ \frac{\partial g}{\partial M} & \frac{\partial g}{\partial N} \end{pmatrix} \tag{I.11}$$

$$= \begin{pmatrix} \frac{1+\beta_m N}{1+\alpha_m p} & -\frac{\beta_m M}{1+\alpha_m p} \\ \\ -\frac{\beta_n N}{1+\alpha_n q} & \frac{1+\beta_n M}{1+\alpha_n q} \end{pmatrix}. \tag{I.12}$$

(M^*, N^*) is stable when

$$|\mathrm{Tr}(J)| - 1 < \mathrm{Det}(J) < 1. \tag{I.13}$$

We first show that $\mathrm{Det}(J) < 1$. Assuming $p > 0$, $q > 0$, it follows that

$$\mathrm{Det}(J) = \frac{1 + \beta_m N + \beta_n M}{(\alpha_m p + 1)(\alpha_n q + 1)} \tag{I.14}$$

$$< \frac{1 + \alpha_m M + \beta_m N + \alpha_n N + \beta_n M}{(\alpha_m p + 1)(\alpha_n q + 1)} \tag{I.15}$$

$$= \frac{1 + \alpha_m p + \alpha_n q}{(\alpha_m p + 1)(\alpha_n q + 1)} \tag{I.16}$$

$$= \frac{1 + \alpha_m p + \alpha_n q}{1 + \alpha_m p + \alpha_n q + \alpha_m \alpha_n p q} \tag{I.17}$$

$$< 1. \tag{I.18}$$

Next we show that $\mathrm{Tr}(J) - 1 < \mathrm{Det}(J)$. Defining u, v as

$$u = \frac{\beta_m \beta_n}{\alpha_m \alpha_n}, \qquad v = \frac{\beta_m (S_n \lambda_n - 1)}{\alpha_n (S_m \lambda_m - 1)}, \tag{I.19}$$

and assuming that $u < v < 1$, then

$$\begin{aligned}
\mathrm{Tr}(J) - 1 =& \frac{1+\beta_m N}{1+\alpha_m p} + \frac{1+\beta_n M}{1+\alpha_n q} - 1 && \text{(I.20)}\\
=& \frac{(1+\beta_m N)(1+\alpha_n q) + (1+\beta_n M)(1+\alpha_m p)}{(1+\alpha_m p)(1+\alpha_n q)} - 1 && \text{(I.21)}\\
=& \frac{1+\beta_m N+\beta_n M}{(1+\alpha_m p)(1+\alpha_n q)} + && \text{(I.22)}\\
& \frac{1+\alpha_n q+\alpha_m p+\alpha_n\beta_m qN+\alpha_m\beta_n pM}{(1+\alpha_m p)(1+\alpha_n q)} - 1 && \text{(I.23)}\\
=& \mathrm{Det}(J) + \frac{\alpha_n\beta_m qN+\alpha_m\beta_n pM-\alpha_m\alpha_n pq}{(1+\alpha_m p)(1+\alpha_n q)}. && \text{(I.24)}
\end{aligned}$$

Since $u < v < 1$ implies that $\beta_n p < \alpha_n q$ and $\beta_m q < \alpha_m p$, (A.24) implies that

$$\mathrm{Tr}(J) - 1 < \mathrm{Det}(J) + \frac{\alpha_n\alpha_m pN+\alpha_m\alpha_n qM-\alpha_m\alpha_n pq}{(1+\alpha_m p)(1+\alpha_n q)}. \quad \text{(I.25)}$$

In order to show that $\mathrm{Tr}(J) - 1 < \mathrm{Det}(J)$, we must have

$$\begin{aligned}
\alpha_m\alpha_n pN+\alpha_m\alpha_n qM &< \alpha_m\alpha_n pq && \text{(I.26)}\\
pN+qM &< pq && \text{(I.27)}\\
pq\frac{1-u/v}{1-u} + qp\frac{1-v}{1-u} &< pq && \text{(I.28)}\\
1-u/v+1-v &> 1-u && \text{(I.29)}\\
u-u/v &> v-1 && \text{(I.30)}\\
u(v-1) &> v(v-1) && \text{(I.31)}\\
u &< v\frac{(v-1)}{(v-1)} && \text{(I.32)}\\
u &< v. && \text{(I.33)}
\end{aligned}$$

Thus, if $u < v < 1$ and $p > 0$, $q > 0$, the fixed point $P_B = (M^*, N^*)$ is asymptotically stable. I note that this proof also demonstrates the stability of the coexistence equilibrium $G_B = (M^*, N^*)$ in a

shifting habitat, where

$$M^* = \frac{\alpha_n(GS_m\lambda_m - 1) - \beta_m(GS_n\lambda_n - 1)}{\alpha_m\alpha_n - \beta_m\beta_n}, \tag{I.34}$$

$$N^* = \frac{\alpha_m(GS_n\lambda_n - 1) - \beta_n(GS_m\lambda_m - 1)}{\alpha_m\alpha_n - \beta_m\beta_n}. \tag{I.35}$$

Simply substitute GS_m, GS_n for S_m, S_n, respectively, and proceed through the proof as before.

Appendix II

R CODE FOR A TWO-SPECIES IDE COMPETITION MODEL

R code for the simulation of the two-species competition model in Section 2.3.4.

```
library(expm) # for matrix exponentiation


# Laplace dispersal kernel
dlaplace <- function(x, location = 0, scale = 1){
  .5/scale * exp(-abs(x - location)/scale)
}


# geometric symmetrization of average dispersal success GnS
GnS <- function(L, sigma, c, kernel = "normal", n = 0, p = 101){
  if(kernel == "normal") func <- dnorm
  if(kernel=="Cauchy") func <- dcauchy
  if(kernel=="Laplace") func <- dlaplace
  loc <- seq(from = 0, to = L, length.out = p)
  dif <- round(loc[2] - loc[1], 5)
  pmat <- matrix(0, ncol = p, nrow = p)
  for(i in 1:p){
    for(j in 1:p){
      pmat[i,j] <- func(loc[i] + c, loc[j], sigma) * dif
    }
  }
  pmat <- pmat %^% (2^n)
  smat <- matrix(0, ncol = p, nrow = p)
  for(i in 1:p){
    for(j in 1:p){
      smat[i,j] <- sqrt(pmat[i,j] * pmat[j,i])
    }
  }
  return((sum(smat)/p)^(2^-n))
```

```
}

# draw random parameter values
k <- 100
set.seed(50)
parameters <- data.frame(L = rep(10, k))
parameters$lambda.m <- rexp(k, 2) + 1
parameters$lambda.n <- rexp(k, 2) + 1
parameters$sig.m <- rlnorm(k, .5, .5)
parameters$sig.n <- rlnorm(k, .5, .5)
parameters$c <- rexp(k, 1)
parameters$alpha.m <- rlnorm(k, -2, .5)
parameters$alpha.n <- rlnorm(k, -2, .5)
parameters$beta.m <- rexp(k, 1/parameters$alpha.m)
parameters$beta.n <- rexp(k, 1/parameters$alpha.n)
parameters$K.m <- with(parameters, (lambda.m - 1)/alpha.m)
parameters$K.n <- with(parameters, (lambda.n - 1)/alpha.n)
parameters$G2S.m <- mapply(GnS, L = 10, sigma = parameters$sig.m, c = parameters$c, n = 2)
parameters$G2S.n <- mapply(GnS, L = 10, sigma = parameters$sig.n, c = parameters$c, n = 2)

# derived parameters to predict outcome
parameters$p <- with(parameters, (G2S.m*lambda.m - 1)/alpha.m)
parameters$q <- with(parameters, (G2S.n*lambda.n - 1)/alpha.n)
parameters$u <- with(parameters, (beta.m*beta.n)/(alpha.m*alpha.n))
parameters$v <- with(parameters, beta.m*(G2S.n*lambda.n - 1)/(alpha.n*(G2S.m*lambda.m - 1)))

# model predictions
parameters$Predicted <- with(parameters,
                             ifelse(p <= 0 & q <= 0, "None",
                                    ifelse(p <= 0 & q > 0, "N",
                                           ifelse(p > 0 & q <= 0, "M",
                                                  ifelse(u < v & v < 1, "Both",
                                                         ifelse(u < v & v > 1, "N",
                                                                ifelse(u > v & v < 1, "M",
                                                                       "M.or.N")))))))

# function to calculate numerical results given a set of parameter values
simulator <- function(pars, kernel = "normal", p = 101, nogens = 100){
```

```
if(kernel == "normal") func <- dnorm
if(kernel=="Cauchy") func <- dcauchy
if(kernel=="Laplace") func <- dlaplace

dat <- pars
locs <- seq(from = 0, to = dat$L, length.out = p)
dif <- round(locs[2] - locs[1], 5)
p <- 101

# initial population vectors
x <- rep(dat$K.m, p)
y <- rep(dat$K.n, p)

# dispersal matrix for M
pmat.m <- matrix(0, ncol = p, nrow = p)
for(i in 1:p){
  for(j in 1:p){
    pmat.m[i,j] <- func(locs[i] + dat$c, locs[j], dat$sig.m) * dif
  }
}

# Dispersal matrix for N
pmat.n <- matrix(0, ncol = p, nrow = p)
for(i in 1:p){
  for(j in 1:p){
    pmat.n[i,j] <- func(locs[i] + dat$c, locs[j], dat$sig.n) * dif
  }
}

# numerical IDE function
ide <- function(x, y){
  x1 <- (dat$lambda.m*x)/(1 + dat$alpha.m*x + dat$beta.m*y)  # Leslie-Gower growth of M
  y1 <- (dat$lambda.n*y)/(1 + dat$alpha.n*y + dat$beta.n*x)  # Leslie-Gower growth of N
  x1 <- c(pmat.m %*% x1)  # dispersal of M
  y1 <- c(pmat.n %*% y1)  # dispersal of N
  list(x = x1, y = y1)
}
```

```
  tmat_x <- matrix(NA, nrow = nogens, ncol = p)
  tmat_x[1,] <- ide(x, y)$x
  tmat_y <- matrix(NA, nrow = nogens, ncol = p)
  tmat_y[1,] <- ide(x, y)$y

  for(j in 2:nogens){
    temp <- ide(x = tmat_x[j-1,], y = tmat_y[j-1,])
    tmat_x[j,] <- temp$x
    tmat_y[j,] <- temp$y
  }

  # mean population densities of last generation
  Mmean <- mean(tmat_x[nogens,])
  Nmean <- mean(tmat_y[nogens,])

  # if mean of M or N is less than 10% of carrying capacity,
  # record how many generations species survived before dying out
  Mgen <- ifelse(Mmean > .1*dat$K.m, nogens, {
    temp <- rowMeans(tmat_x)
    which.min(abs(temp - .1*dat$K.m)) })
  Ngen <- ifelse(Nmean > .1*dat$K.n, nogens, {
    temp <- rowMeans(tmat_y)
    which.min(abs(temp - .1*dat$K.n)) })

  return(list(Mmean = Mmean, Nmean = Nmean, Mgen = Mgen, Ngen = Ngen))
}

# numerical simulations of IDEs using the random parameter values
for(i in 1:k){
  dat <- parameters[i,]
  temp <- simulator(pars = dat)
  parameters$Observed[i] <- with(temp,
                                 ifelse(Mmean > .1*dat$K.m & Nmean > .1*dat$K.n, "Both",
                                        ifelse(Mmean < .1*dat$K.m & Nmean > .1*dat$K.n, "N",
                                               ifelse(Mmean > .1*dat$K.m & Nmean < .1*dat$K.n, "M",
                                                      "None"))))
  parameters$Mmean[i] <- temp$Mmean
  parameters$Nmean[i] <- temp$Nmean
```

```
  parameters$Mgen[i] <- temp$Mgen
  parameters$Ngen[i] <- temp$Ngen
  print(i)
}

# results
obs <- factor(parameters$Observed, levels = c("None", "M", "N", "Both", "M.or.N"))
pred <- factor(parameters$Predicted, levels = c("None", "M", "N", "Both", "M.or.N"))
table(pred, obs, deparse.level = 2)

confusionMatrix(pred, reference = obs)
```

Appendix III

R CODE FOR A GENERALIZED 2D GAUSSIAN DISPERSAL KERNEL

The `raster` package in R provides many useful functions that were utilized in the implementation of the integro-diftribution model algorithm described in Chapter **??**. In particular, the `focalWeight` function enabled the construction of a two-dimensional kernel, which could then be used as an argument in the `focal` function to simulate the dispersal process. The `focalWeight` function provides a fairly limited choice of kernels, however; the 2D Gaussian is the only choice suitable for our modeling purposes.

I wrote a new function that allows the user to specify a generalized 2D Gaussian kernel, which gives control over the kurtosis of the distribution, in addition to the dispersal parameter. The argument `x` should be a Raster* object. The argument `sigma` specifies the dispersal parameter, in units of the CRS projection of `x`. `sigma` can optionally be a vector of length two, with the second value specifying the size of the matrix returned. The default size is 3 times `sigma`. The argument `beta` is the additional parameter that controls the kurtosis.

```
focalWeightGen <- function (x, sigma, beta = 1) {
  x <- res(x)
  #genGauss.weight(x, sigma, beta = beta)
  if (length(sigma) == 1) {
    d <- 3 * sigma
  } else {
    d <- sigma[2]
    sigma <- sigma[1]
  }
  nx <- 1 + 2 * floor(d/x[1])
  ny <- 1 + 2 * floor(d/x[2])
  m <- matrix(ncol = nx, nrow = ny)
  xr <- (nx * x[1])/2
  yr <- (ny * x[2])/2
  r <- raster(m, xmn = -xr[1], xmx = xr[1], ymn = -yr[1], ymx = yr[1],
       crs = "+proj=utm +zone=1 +datum=WGS84")
  p <- xyFromCell(r, 1:ncell(r))^2
  m <- beta/(pi * gamma(1/beta) * 2^(1/beta) * sigma^2) *
       exp(-.5 * ((p[, 1] + p[, 2])/(sigma^2)) ^ beta)
  m <- matrix(m, ncol = nx, nrow = ny, byrow = TRUE)
  m/sum(m)
}
```

This function may then be used in place of the `focalWeight` function to simulate the dispersal process:

```
gf <- focalWeightGen(ras.growth, sigma = 400, beta = 0.6)
ras.disp <- focal(ras.growth, w = gf)
```

Appendix IV

AN OUTLINE OF IDM IMPLEMENTATION IN R

Here I outline the process of implementing an IDM in R, interspersed with examples of pseudo-code to help guide the reader. The code in this section utilizes the `raster` package for reading, writing, and manipulation of raster datasets (Hijmans, 2014), and the `dismo` package for the construction of a MaxEnt SDM (Hijmans et al., 2017).

Initialization

I begin with a raster brick comprised of layers of historical climate data, and a raster brick comprised of layers of future climate data. In this example, the historical climate data represent values from 1975, and the future values represent climate projections made for the year 2050.

```
climdat.1975 <- brick("Climate_data_1975.grd")
climdat.2050 <- brick("Climate_data_2050.grd")
```

From these I wish to interpolate climate data for each year between the historical and future periods. I write a loop that interpolates linearly between the two, with the assumption that the rate of climate change is constant over the time period of interest.

```
diffs <- climdat.2050 - climdat.1975
for(i in 1:75){
    tempdat <- climdat.1975 + diffs * i / 75
    tempname <- paste0("Climate_data_", i + 1975, ".grd")
    writeRaster(tempdat, filename = tempname)
}
```

I now construct an SDM to serve as the habitat quality function $Q_0(\mathbf{x})$, using the historical data and the geographic locations of species occurrence. In this example, I create a MaxEnt SDM with the `dismo::maxent` function. The occurrence data are provided as latitute and longitude coordinates.

```
pres <- read.csv("Occurrences.csv")
mod <- maxent(x = climdat.1975, p = pres, ...)
```

Using this model, I create a binary raster of historical predicted habitat suitability, using a specified threshold `lambda` that optimizes the model fit.

```
t <- "Maximum.training.sensitivity.plus.specificity.logistic.threshold"
lambda <- mod@results[t, ]
pr.0 <- predict(mod, x = climdat.1975)
pr.0[pr.0 >= lambda] <- 1
pr.0[pr.0 < lambda] <- 0
```

Similarly, I create binary rasters of future predicted habitat suitability for each time step, based on our annually interpolated future climate values. I use a loop to make a prediction for each year.

```
pr.br <- brick(pr.0)
for(i in 1:75){
    tempname <- paste0("Climate_data_", i + 1975, ".grd")
    climdat <- brick(tempname)
    pr <- predict(mod, x = climdat)
    pr[pr >= lambda] <- 1
    pr[pr < lambda] <- 0
    pr.br[[i + 1]] <- pr
}
```

I now have a raster of predicted habitat suitability $Q_t(\mathbf{x})$ for each time step t, concluding the necessary initial preparation of our climate data.

Turning now to the population data, I desire the initial population $N_0(\mathbf{y})$ to be described by a raster with abundances in each cell. Ideally, this would be based on direct observational data of population abundance, but these data are not always available (e.g., if our occurrence data is limited to presence/absence records). In this situation, I can use the SDM to approximate the population density if I assume that habitat suitability is strongly correlated with population density. To do so, I simply take the predictions of habitat suitability, set any habitat below a certain threshold to 0, and then multiply the remaining logistic probabilities by the carrying capacity K of the species.

```
pr.0 <- predict(mod, x = climdat.1975)
pr.0[pr.0 < lambda] <- 0
ras.0 <- pr.0 * K
```

This yields a raster of population densities, with higher densities in locations of more suitable habitat, and no individuals in locations that are considered unsuitable. I now begin modeling the processes of growth and dispersal.

Growth

The population $N_0(\mathbf{y})$ grows according to the growth function f, resulting in the population $f[N_0(\mathbf{y})]$. In practice, this is accomplished by applying the growth function `f` to the values of the raster using the `raster::calc` function. The following code illustrates this step for a Beverton-Holt growth function with $R_0 = 2$ and $K = 100$.

```
K <- 100
R0 <- 2
f <- function(x){
    R0 * x / (1 + (R0 - 1) * x / K)
}
ras.growth <- calc(ras.0, fun = f)
```

Dispersal

The population $f\big(N_0(\mathbf{y})\big)$ disperses according to the dispersal kernel $k(\mathbf{x}, \mathbf{y})$. I implement this in two steps, beginning with the assumption that dispersal is only a function of distance, i.e., $k(\mathbf{x}, \mathbf{y}) = k(\mathbf{x} - \mathbf{y})$. First, the kernel is specified with the `raster::focalWeight` function. A Gaussian kernel with $\sigma = 2$, for example, would be constructed by

```
gf <- focalWeight(ras.growth, 2, 'Gauss')
```

This returns a matrix of dispersal weights at a resolution that matches the `ras.growth` raster. Second, the dispersal process is implemented via a moving window with the `raster::focal` function.

```
ras.disp <- focal(ras.growth, w = gf)
```

The resulting raster describes the population density given by

$$\sum_{\mathbf{y}} k(\mathbf{x}, \mathbf{y}) f[N_0(\mathbf{y})]. \tag{IV.1}$$

Habitat selection

The preceding dispersal process was "unconstrained", in that individuals dispersed without regard to the suitability of the habitat to which they moved. In this final step, the habitat quality function penalizes all the individuals that dispersed to unsuitable habitat. The raster that resulted from the dispersal step is simply multiplied by the appropriate binary suitability raster created during the initialization step. The "*" operator multiplies the rasters together on a location-by-location basis, similar to a Hadamard product, which represents element-wise matrix multiplication.

```
ras.1 <- pr.0 * ras.disp
```

The end result is a raster that describes population density at the next time step, given by

$$N_1(\mathbf{x}) = Q_0(\mathbf{x}) \sum_{\mathbf{y}} k(\mathbf{x} - \mathbf{y}) f[N_0(\mathbf{y})], \tag{IV.2}$$

which converges to the IDM formula in (3.7) as the resolution of the climate data rasters (and hence, all the subsequently generated rasters) increase.

Iteration

I then repeat the processes of growth, dispersal, and habitat selection using a loop to iterate through time steps, based on the growth function `f` and dispersal matrix `gf` created previously, and reading in the appropriate interpolated climate data and the corresponding predictions of habitat suitability $Q_t(\mathbf{x})$ for each time step t.

```
ras.br <- brick(ras.0)
for(i in 1:75){
    temp.growth <- calc(ras.br[[i]], fun = f)
    temp.disp <- focal(temp.growth, w = gf)
    ras.br[[i + 1]] <- pr.br[[i]] * temp.disp
}
```

This gives me the brick `ras.br` of raster layers, with layer $t + 1$ representing the population density $N_t(\mathbf{x})$ at time step t.